# Evaluation of metakaolin-based geopolymer for the treatment of simulant radionuclides: Analysis of surface chemistry and immobilisation behaviour

(模擬放射性核種処理におけるメタカオリン系ジオポリマーの評価: 表面化学と取り込み挙動の分析)

by

**Xiaobo Niu**
B.Sc. Eng. (2017), M.Sc. Eng. (2020)

**DISSERTATION**
Presented in Partial Fulfillment of the Requirements for the Degree of

**DOCTOR OF PHILOSOPHY**

in
Graduate School of Engineering
of the

HOKKAIDO
UNIVERSITY

**Japan**

Approved by the committee in charge,
Yogarajah Elakneswaran, *Chair*
Naoki Hiroyoshi
Tsutomu Sato
Kiyofumi Kurumisawa
**September 2023**

“There is no law except the law that there is no law.”

– John Archibald Wheeler

# ABSTRACT

The development of nuclear power has significantly contributed to the progress of productivity in modern society. However, it has also brought forth formidable challenges. Issues such as nuclear fuel back-end disposal, radioactive waste management, and nuclear accident response pose inevitable hurdles, resulting in the generation of numerous radionuclides. Effectively containing these radionuclides is crucial to prevent environmental pollution and ensure a safe ecosystem for living organisms. Certain radionuclides, both cationic (e.g., $^{137}Cs$, $^{90}Sr$, and $^{60}Co$) and anionic (e.g., $^{131}I$ and $^{79}Se$), present significant environmental risks when it comes to the storage or disposal of nuclear waste. This is primarily due to their relatively long half-life and high mobility in soil and aqueous systems.

Geopolymer materials, emerging as a potential alternative to conventional Portland cement, have garnered widespread attention as a potential waste form for immobilising radionuclides. However, research in the field of radionuclides immobilisation within geopolymers is still in its early stages, necessitating further systematic and in-depth studies. This thesis focuses on investigating the adsorption behaviour of alkali-activated metakaolin geopolymers on both cationic and anionic radionuclides. Predictive models based on thermodynamics are developed to better understand and forecast this behaviour. Moreover, efforts are made to address the lack of anionic radionuclide immobilisation capacity in alkali-activated metakaolin geopolymers. By tailoring the materials, their capability to immobilize anionic radionuclides is enhanced. Additionally, the study explores the immobilisation of anions

using phosphoric acid-activated metakaolin geopolymers, providing valuable insights into the surface chemistry and electrostatic properties of acid-activated geopolymer materials.

In **Chapter 1**, background information of the study was presented, including the stages of nuclear power development, opportunities, and challenges. In addition, the application scenarios of geopolymer materials in the disposal of radionuclides methods are presented. Finally, based on the presented background, the research objectives and structural organization of this thesis are discussed.

In **Chapter 2**, a literature review of geopolymer materials was presented, including basic properties, different activation pathways, and their hydration processes. In addition, basic information on radionuclides is presented, including chemical properties, toxicity, isotopic properties of radionuclides, and their general disposal methods.

In **Chapter 3**, two types of metakaolin-based geopolymers (Metastar501 and Sobueclay) were synthesized. They were evaluated for their binding capacity and interaction with $Cs^{+}$, $Sr^{2+}$, $Co^{2+}$, $I^{-}$, $IO_3^{-}$, $SeO_3^{2-}$, and $SeO_4^{2-}$. Results showed that both geopolymers effectively immobilized cationic radionuclides, while neither of the geopolymers could effectively incorporate anionic radionuclides. $Cs^{+}$ uptake involved a one-to-one exchange with $K^{+}$, while $Sr^{2+}$ and $Co^{2+}$ exhibited one-to-two and one-to-one exchanges with $K^{+}$. $Co^{2+}$ binding was influenced by the formation of cobalt blue ($CoAl_2O_4$). Thermodynamic modelling predicted low-concentration binding of $Cs^{+}$ and $Sr^{2+}$ based on the ion exchange mechanism.

In **Chapter 4**, a modification to metakaolin-based geopolymers to enhance their uptake capabilities for selenium oxyanions was proposed. Through co-precipitation experiments, binding analysis, and structural analysis, it was discovered that the in-situ formation of ettringite enables effective uptake of $SeO_3^{2-}$ and $SeO_4^{2-}$. The modified geopolymer, with its in-situ ettringite, not only retains its capacity to uptake cationic radionuclides but also acquires the ability to uptake $SeO_3^{2-}$. In addition, the developed thermodynamic modelling accurately predicts the uptake of $SeO_3^{2-}$ at low concentrations.

In **Chapter 5**, the study explored the electrostatic properties and anion immobilisation potential of PGPs. Results indicate that acid activation triggers geopolymerisation, forming $Al_x$-PO units that control surface charge. PGPs exhibit extreme zeta potential values in water. In acidic conditions, leaching of $Al_{VI}$-PO units decreases zeta potential, while loss of a proton from $Al_{VI}$/Si-OH group decreases zeta potential in alkaline conditions. PGPs effectively immobilize $SeO_3^{2-}$, $SeO_4^{2-}$, $I^-$, and $IO_3^-$ anions through stabilization/solidification.

Finally, **Chapter 6** presents the key findings and conclusions of this thesis. It offered valuable insights into the immobilisation of $Cs^+$, $Sr^{2+}$, $Co^{2+}$, $I^-$, $IO_3^-$, $SeO_3^{2-}$, and $SeO_4^{2-}$ in both alkaline-activated and acid-activated metakaolin geopolymers. Additionally, a summary of the surface chemistry and electrostatic properties of the newly proposed acid-activated geopolymers was provided. Furthermore, suggestions are made for future in-depth studies on geopolymers for radionuclide immobilisation.

# 概要

原子力発電は、現代社会の生産性向上に大きく寄与してきたが、核燃料の後処理や放射性廃棄物の管理、原発事故への対応など、解決すべき課題も多く抱えている。原子力利用に伴って発生する放射性核種を効果的に制御することは、環境汚染を防ぎ、生物にとって安全な生態系を確保するために極めて重要である。特に、放射性廃棄物の貯蔵や処理においては、半減期が比較的長く、土壌や水系での移動性が高い $^{137}Cs$、$^{90}Sr$、$^{60}Co$ などの陽性核種や $^{131}I$、$^{79}Se$ などの陰性核種の固定化法を確立することが重要である。

ジオポリマーは、ポルトランドセメントの代替材料として注目されており、廃棄物中の放射性核種の固定化にも利用できる可能性があるものと期待されている。しかし、ジオポリマー中の放射性核種の固定化に関する研究はまだ初期段階で、より体系的かつ詳細な研究が必要である。本研究は、アルカリ活性化メタカオリンジオポリマーに対する陽性および陰性放射性核種の吸着挙動に焦点を当てて検討している。また、これらの核種の吸着挙動をよりよく理解するため、熱力学に基づく予測モデルを開発している。さらに、アルカリ活性化メタカオリンジオポリマーの陰性放射性核種の固定化能力を向上させることに取り組み、調製方法の工夫により陰性放射性核種の固定化能力を向上させることができることを見出している。また、リン酸活性化メタカオリンジオポリマーを用いた陰イオンの固定化についても検討し、本材料の表面化学と静電特性に関する貴重な知見を得ている。

第1章では、原子力発電の開発プロセスや課題など、本研究の背景に関する情報をまとめている。また、放射性核種の処分にジオポリマー材料を適用する際のシナリオや方法について紹介している。最後に、本論文の研究目的と構成を述べている。

第2章では、ジオポリマー材料の基本的な特性、さまざまな活性化経路、およびそれらの水和プロセスを含む先行研究の成果をまとめている。また、放射性核種に関する化学的性質、毒性、同位体特性、一般的な処分方法などの基本情報を紹介している。

第 3 章では，2 種類のメタカオリン系ジオポリマー（Metastar501 と Sobueclay）を合成し、$Cs^{+}$, $Sr^{2+}$, $Co^{2+}$, $I^{-}$, $IO_3^{-}$, $SeO_3^{2-}$, $SeO_4^{2-}$との結合能力および相互作用を評価している。いずれのジオポリマーもカチオン性放射性核種を効果的に固定化することができたが、アニオン性放射性核種を効果的に取り込むことはできなかった。$Cs^{+}$は $K^{+}$と 1 対 1 の交換により、また，$Sr^{2+}$と $Co^{2+}$ は $K^{+}$と 1 対 2 および 1 対 1 のイオン交換により取り込まれるが、$Co^{2+}$の結合にはコバルトブルー（$CoAl_2O_4$）の形成も関わっていることを示している。熱力学モデリングにより、$Cs^{+}$と $Sr^{2+}$は、イオン交換メカニズムに基づき、低濃度で固定化できることを示している。

第4章では、メタカオリン系ジオポリマーの陰性核種に対する取り込み能力を向上させる新たな方法を提案している。提案された方法では，ジオポリマー形成時にエトリンガイトをその場生成させる。共沈実験、結合解析、構造解析により、この改質ジオポリマーは、陽性核種の取り込み能力を維持するだけでなく、陰性の $SeO_3^{2-}$や $SeO_4^{2-}$に対する取り込み能力も獲得していることを確認している。また，熱力学モデリングにより低濃度での $SeO_3^{2-}$の取り込みを正確に予測できることも確かめている。

第5章では、陰性核種の取り込みに有効な別の方法としてリン酸活性化ジオポリマー（PGP）の利用について検討している。リン酸による活性化でポリマー化を開始させると、表面電荷を支配する Alx-PO ユニットが形成された。PGP のゼータ電

位は、ｐＨ４付近で最大となり，酸性条件下では $Al_{VI}$-PO ユニットが溶出してゼータ電位が低下し、アルカリ性条件下では $Al_{VI}$/Si-OH 基からのプロトン乖離によりゼータ電位が低下する。PGP のゼータ電位は pH0-6 の領域では正の値を取り，種々の陰性核種（$SeO_3^{2-}$、$SeO_4^{2-}$、$I^-$、$IO_3^-$）を効果的に固定できた。

第 6 章では、本論文の主要な成果と結論をまとめ、アルカリ活性化およびリン酸活性化メタカオリンジオポリマーにおける $Cs^+$、$Sr^{2+}$、$Co^{2+}$、$I^-$、$IO_3^-$、$SeO_3^{2-}$および$SeO_4^{2-}$の固定化に関する知見を要約している。また、ジオポリマーを利用した放射性核種の固定化に関する今後の研究への提案も行っている。

# ACKNOWLEDGEMENTS

Time flies like an arrow. I can still vividly remember the scent of the air in Hokkaido during the autumn of 2018. Since then, I embarked on the most significant and precious journey of my life at Hokkaido University. Throughout these five years of my academic pursuit, the person I am most grateful to is my supervisor, Prof. Yogarajah Elakneswaran. It is his patient guidance that has transformed me from an ignorant novice in scientific research into a capable and independent researcher. His unique academic pursuits and noble taste for scientific inquiry have influenced me to constantly surpass myself, gradually evolving into the person I aspired to become years ago. I will also inherit the spirit and passion for research from my supervisor, Prof. Yogarajah Elakneswaran, and pass it on to more young individuals in the future. It is my honour to be his student.

I am deeply grateful to Prof. Naoki Hiroyoshi, Prof. Tsutomu Sato, and Prof. Kiyofumi Kurumisawa for serving as members of my annual degree examination and final dissertation evaluation committee during my doctoral studies. Their extensive knowledge and academic experience in their respective fields undoubtedly helped me refine my research work and improve the quality of my dissertation. I sincerely appreciate the time they dedicated and the thoughtful feedback they provided throughout the entire process.

I would like to express my gratitude to the research team at the Laboratory of Chemical Resources. Their presence has made the past years truly remarkable, as they have provided an engaging and supportive environment. I am particularly thankful to Mr. Chaerun Raudhatul Islam from the Environmental Geology Laboratory, who has been my companion

and supporter in the field for many years. Furthermore, I extend my appreciation to Prof. John L. Provis from the University of Sheffield, UK. Through our collaboration on projects and co-authoring articles, I have learned invaluable qualities and enthusiasm from him as a dedicated researcher. His guidance and assistance have been exceptionally generous. I would also like to acknowledge Mr. Naoya Nakagawa from the FCC Machine Analysis and Management Support Office, as well as Ms. Reina Ishikawa from the Technical Center Technology Department of the Faculty of Engineering for training me the intricacies of operating various experimental instruments.

I am immensely grateful to JST SPRING (Grant Number JPMJSP2119) for granting me valuable research opportunities and providing financial support throughout my PhD journey. Their full grant and research funding have played a crucial role in the successful completion of my work. I would also like to thank the JAEA Nuclear Energy S&T and Human Resource Development Project for supporting part of this work through concentrating wisdom Grant Number JPJA20P12345678 and EPSRC (UK) under grants EP/T013524/1.

Last but not least, I would like to express my heartfelt gratitude to my extraordinary parents for granting me the incredible privilege of being their cherished child throughout the remarkable voyage of my life. They are the reason for my existence, my motivation to move forward, and my pillar of strength. I want to thank my parents for teaching me how to persevere and pursue my dreams; they never doubted that I could succeed. Their support and trust allowed me to face challenges and surpass my limits. They taught me to persevere in my efforts, to never give up, and to always remain humble and grateful. I want to express my

deep love and gratitude to my parents. They are the most important people in my life, and their hard work and selflessness have provided me with the best conditions to pursue my dreams. Without them, I would not have reached where I am today. I am forever grateful for rising me up.

# CONTENTS

# LIST OF FIGURES

# LIST OF TABLES

# CHAPTER 1

# INTRODUCTION

## General background

Nuclear power generation has emerged as a significant source of clean energy, with the potential to meet increasing global energy demands while reducing greenhouse gas emissions [1,2]. The development of nuclear power has presented both opportunities and challenges for the industry [3,4]. On the one hand, it offers a low-carbon alternative to fossil fuels, which is particularly crucial as the world seeks to transition to renewable energy sources. Moreover, nuclear power plants have a long lifespan and can provide a stable and reliable source of energy, making them particularly attractive for countries with high energy demand.

However, nuclear power also poses significant challenges, particularly with regards to the handling of radioactive waste [5]. The safe handling and disposal of radioactive waste is a crucial aspect of nuclear power generation. Radioactive isotopes emitted by nuclear reactors can have harmful effects on human health and the environment. Exposure to radiation can cause radiation sickness, cancer, and other illnesses. Radioactive waste also poses a long-term threat to the environment, as it can contaminate soil, water, and air for thousands of years [6]. The risk of nuclear accidents is another significant challenge associated with nuclear power. While the probability of such accidents is relatively low, the consequences can be devastating. The Fukushima Daiichi disaster in 2011 was a stark reminder of the potential risks associated with nuclear power generation [7]. The disaster was caused by a massive earthquake and tsunami, which damaged the plant's cooling system, leading to multiple reactor meltdowns and the release of radioactive material into the surrounding environment [8]. The disaster resulted in widespread contamination and forced the

evacuation of tens of thousands of people. Given the significant challenges associated with the handling and disposal of radioactive waste, there has been ongoing research and development of new technologies for the safe and effective management of nuclear waste [9, 10]. When it comes to the disposal of nuclear waste, one of the key considerations is the need for long-term isolation and containment of radioactive materials [11, 12]. Several strategies have been proposed for achieving this, including space isolation, glacier isolation, deep-sea isolation, and geological disposal [13]. Among these selections, geological disposal has emerged as the most promising option [14].

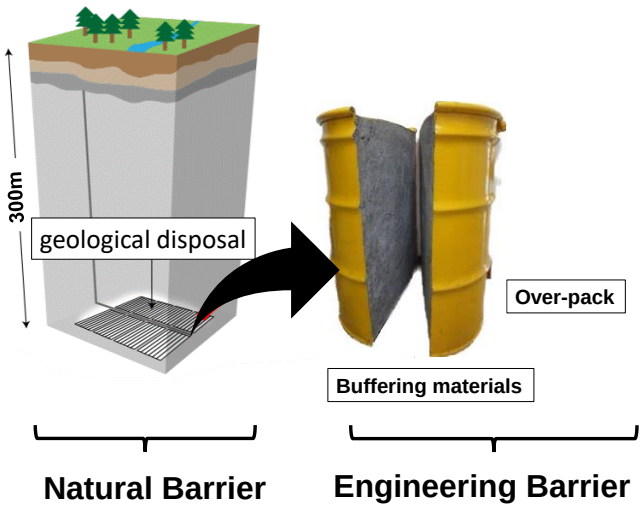


**Figure 1-1.** Schematic diagram of the geological disposal of radioactive waste [22].

Geological disposal involves the placement of nuclear waste in deep geological formations, where it is isolated from the surface environment by layers of rock and other materials [15]. The geological formation must be stable, geologically isolated, and have a low potential for water flow, in order to ensure that the waste is contained and isolated over the long term. One

of the most promising options for geological disposal is deep borehole disposal [16]. This involves drilling a deep borehole into suitable geological formations and placing the waste in canisters at the bottom of the borehole [17]. The borehole is then sealed with a series of barriers, including a cement plug, a bentonite clay buffer, and a steel casing. The waste canisters are surrounded by additional layers of clay and rock, providing additional barriers against water flow and potential contamination. Deep borehole disposal offers several advantages over other disposal options [18]. It allows for the disposal of waste in a relatively small footprint, making it ideal for densely populated areas. It also minimizes the risk of human intrusion, as the waste is placed at a depth of several kilometers and can only be accessed using specialized equipment. Finally, deep borehole disposal is a highly engineered and monitored process, ensuring that the waste is safely and securely contained over the long term. Indeed, the success of geological disposal of nuclear waste hinges on the effectiveness of the engineered barriers used to contain the waste and prevent its release into the environment [19]. These barriers must be designed to prevent the migration of radionuclides into the surrounding geological environment and to protect against potential exposure to humans and ecosystems. Effective buffer materials for nuclear waste disposal must possess properties such as low aqueous solubility, stable phases, reasonable mechanical properties, and chemical resistance to ensure long-term containment and prevent environmental contamination [20, 21].

Glass and ceramic materials have been widely used for the immobilisation of high-level radioactive waste, such as spent nuclear fuel [23]. These materials are highly durable and can provide excellent long-term stability for nuclear waste [24]. However, their production

process can be complex and expensive, making them less attractive for low-level waste management [25]. On the other hand, cement-based materials, such as Portland cement, are often used for immobilising low-level radioactive waste due to their accessibility and relatively low cost [26, 27]. Portland cement is widely available and can be easily produced, making it a practical option for waste management [28]. However, it should be noted that cement-based materials may not provide the same level of long-term stability as glass or ceramic materials [29, 30]. This is because cement can degrade over time due to factors such as radiation exposure, chemical reactions, physical stress and even the high free water content, which may cause problematic hydrogen generation, potentially leading to the release of radioactive materials into the environment [31, 32, 33]. As such, it is important to carefully consider the specific properties and requirements of the waste being immobilized when selecting a suitable buffering material for waste management purposes.

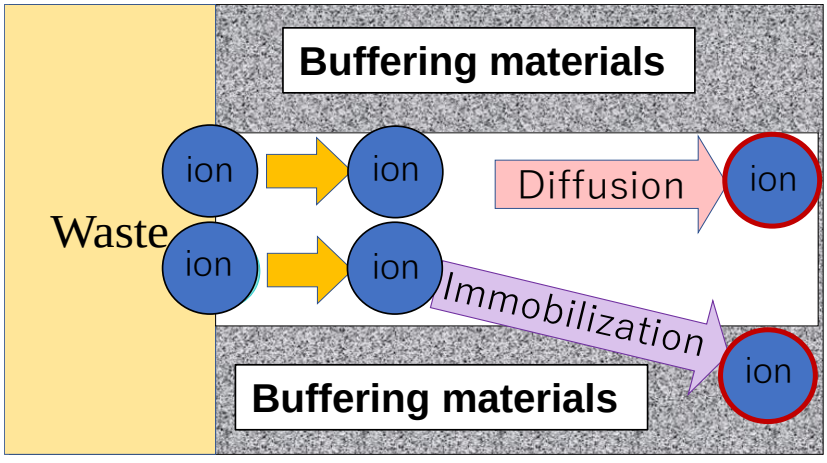


**Figure 1-2.** Diffusion and immobilisation of radionuclides in buffer materials.

One promising approach is the use of geopolymer materials for the immobilisation of radionuclides. Geopolymers are a class of eco-friendly type of inorganic polymer that are widely regarded as sustainable [34, 35]. They are synthesized by activating aluminosilicate precursors with an activator solution at specific temperatures [36]. Geopolymers can be produced from a range of aluminosilicate precursors, including clays [37, 38], as well as industrial by-products like fly ash [39], concrete waste [40], and blast furnace slag [41], among others. The activator solution used for synthesis can be either alkaline (such as sodium/potassium hydroxide or silicate) or acidic (such as aluminium phosphate/phosphoric acid), which determines the two main routes for geopolymer production, as shown in **Figure 1-3** [42, 43, 44]. The resulting slurry, comprising precursors and activators, is then poured into molds, and cured in a suitable environment. The properties of obtained geopolymers are highly dependent on the selection of the aluminosilicate precursor, activator solution, and curing temperature, and should be optimized for the intended application [46, 47, 48]. Additionally, geopolymer composites have been demonstrated to be more environmentally sustainable than cement-based composites, due to their lower energy requirements and reduced carbon emissions [49]. Industrial waste-based geopolymer composites, such as those made from fly ash, slag, and other aluminosilicate materials, have been reported to reduce carbon emissions by up to 80%, making geopolymers a greener alternative to cement [50, 51].

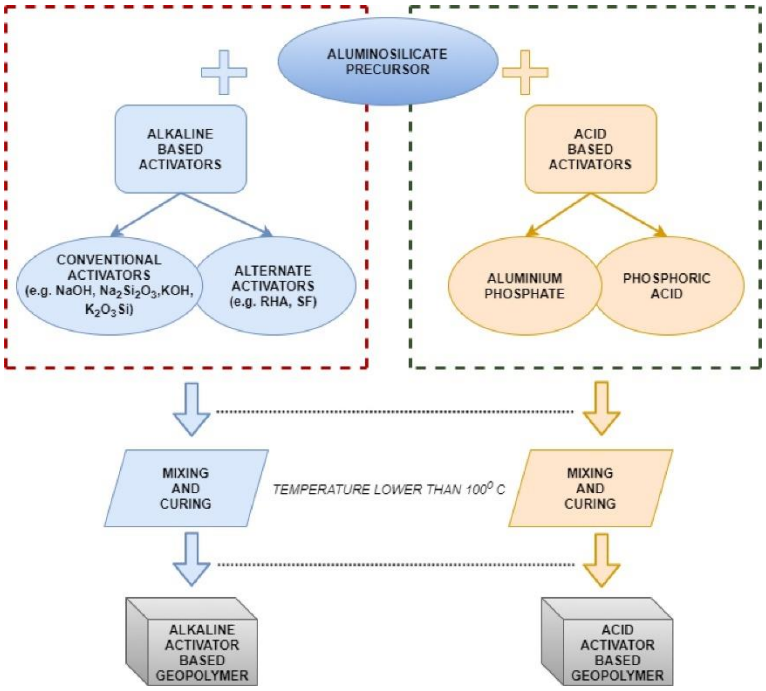


**Figure 1-3.** Synthesis of geopolymers by different types of activators [45].

Compared to other candidate materials, geopolymer materials offer several advantages for the immobilisation of radionuclides. Geopolymer materials can be produced from a wide range of industrial waste materials, making them a more sustainable and cost-effective option for waste management [52]. They also offer excellent chemical and thermal stability and can effectively encapsulate radioactive isotopes, preventing their release into the environment [53, 54, 55]. Furthermore, geopolymer materials can be tailored to specific waste types, making them a versatile option for nuclear waste management [56]. Therefore, the use of geopolymer materials for the immobilisation of radionuclides presents a promising solution to the challenges associated with nuclear waste management.

Recent research has focused on the development of geopolymer-based waste forms for the immobilisation of various types of nuclear waste, including spent nuclear fuel, high-level waste, and low-level waste [57, 58]. These waste forms have shown promising results in laboratory and field tests [59], and their potential application in nuclear waste management has been the subject of ongoing investigation.

## 1.1 Scope and objectives of the research

The overarching objective of this thesis is to comprehensively evaluate and investigate the application of geopolymer materials in the nuclear safety field of radionuclide adsorption and solidification, utilizing a multifaceted perspective of thermodynamics and surface chemistry. From a material science perspective, a range of geopolymer materials have been synthesized through alkali activation, acid activation, and admixture addition, with significant efforts focused on comprehending the synthesis, hydration, and other fundamental aspects of geopolymers. Moreover, diverse types of geopolymers have been evaluated for their adsorption and solidification capacities for different radionuclides, resulting in an extensive understanding of the underlying mechanisms, and predictive thermodynamic models have been developed to explain and forecast these processes.

**Figure 1-4** summarises the specific scope of this research work. Initially, the study explores the adsorption and immobilisation capacity and mechanism of alkali-activated geopolymers, which currently receive widespread attention. Both cationic and anionic radionuclides are evaluated, and their ion exchange processes are explained and predicted by thermodynamic modelling. Next, the research focuses on addressing the lack of immobilisation capacity for anionic radionuclides of alkali-activated geopolymers by generating in-situ ettringite with sufficient immobilisation capacity. This is accomplished by adjusting the composition and controlling the maintenance conditions, and it effectively modifies alkali-activated geopolymers. Finally, the study delves into understanding the structure, surface chemistry, and electrostatic properties of acid-activated geopolymers, which have great potential for

immobilising anionic radionuclides. This is the first time that these properties have been thoroughly explored and understood.

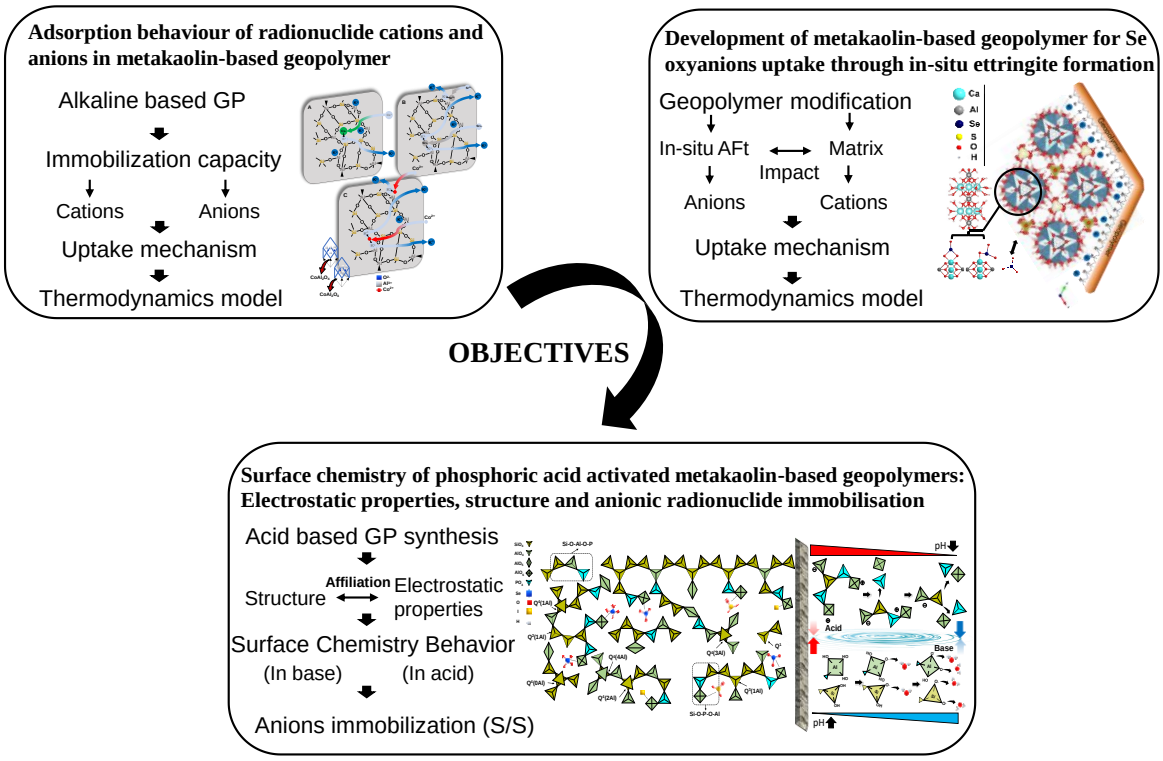


**Figure 1-4.** Outline of the scope of this research work.

## 1.2 Originality and significance of the work

With the development of technology level, society will inevitably enter the 5.0 era. The revolution in productivity and the awakening of people's environmental awareness will lead to a significant optimization of the energy structure. Nuclear energy as an efficient energy in the new era takes an important role in saving energy. This technology can help reduce $CO_2$ emissions and prevent environmental pollution. Thus, it is generally considered to be of great strategic importance in terms of national development. However, the accident of FDNPS has had a profound impact on the nuclear power sector in Japan and the world. Concerns on nuclear safety and discussions about how to perfect the radioactive waste generated by the nuclear industry have held back the development and application of nuclear energy. Further nuclear energy development in the future should take this accident as a starting point and cooperate with many parties to carry out professional assessment and control from different disciplines to ensure that the highly radioactive waste generated in this accident is effectively disposed of, providing valuable practical experience for the future upgrading of the energy structure and optimization of the nuclear power industry.

Geopolymers have been proven to be effective in adsorbing and immobilising heavy metals, making them a promising alternative to traditional materials like cement. However, there is a lack of research on the immobilisation of high-content cationic radionuclides such as $Cs^+$, $Sr^{2+}$, and $Co^{2+}$ from the FDNPS accident. The limited understanding of the incorporation mechanisms for $Cs^+$ and $Sr^{2+}$ further highlights the need for more research in this area. Furthermore, it is important to explore the interaction of alkali-activated geopolymer with

anionic radionuclides, including $I^-$, $IO_3^-$, $SeO_3^{2-}$, and $SeO_4^{2-}$. This has been largely ignored in previous studies, despite the urgency and importance of this issue. The permanent negative surface potential of geopolymers makes them less favorable for the adsorption and immobilisation of anionic radionuclides. Therefore, research should be conducted to modify the structure and composition of geopolymer materials to develop their adsorption capacity for anionic radionuclides. In addition, a more promising solution may be the development of geopolymer materials with positive surface charges. Another important issue is the lack of sufficient development in thermodynamic modeling of radionuclide adsorption by geopolymers. This hinders both the deeper understanding of the underlying mechanisms of radionuclide adsorption and immobilisation by geopolymers and limits the efficiency and economy of safe radionuclide disposal. Therefore, more research in this area is needed to improve the understanding of the processes involved and to develop more efficient and economical methods for the safe disposal of radionuclides.

The present research, under this circumstance, is endeavouring to fulfill the following points of significance:

1) Thoroughly understanding of the mechanism of radionuclides uptake by alkaline based geopolymers provides a theoretical basis for the application of alkaline based geopolymers in the treatment of nuclear waste.

2) The composition and preparation conditions of metakaolin-based geopolymers are proposed to be modified so as to form in-situ ettringite to develop its absorption capacity for anionic radionuclides (selenium oxyanions).

3) The thermodynamic model of geopolymer-radionuclide interaction based on ion exchange mechanism was developed, which can explain and predict the adsorption behaviour and ensure the safety of long-term radioactive waste disposal.

4) For the first time, the structural and environmental factors leading to the surface charge properties of phosphate activated metakaolin geopolymer materials are revealed. And its positively charged surface in a specific pH range has great potential for the immobilisation of anionic radionuclides.

## 1.3 Organization of Dissertation

This dissertation is organized into a total of six chapters.

**Chapter 1** describes the objective, scope and significance of this study.

**Chapter 2** presents a review of relevant literature on various aspects. Early sections of this chapter discuss the fundamentals of geopolymer materials, microstructure and hydration products for the basic understanding. Latter sections discuss the chemistry properties of multiple radionuclides and methods of disposing of them by applying geopolymers. Finally, the details and limitation of the previously developed approach of adsorption and immobilisation for radionuclides through the geopolymer and other potential materials are discussed.

**Chapter 3** analyzes the immobilisation capacities of alkaline metakaolin-based geopolymers to cationic radionuclides ($Cs^{+}$, $Sr^{2+}$, and $Co^{2+}$) and anionic radionuclides ($I^{-}$, $IO_3^{-}$, $SeO_3^{2-}$, and $SeO_4^{2-}$). The uptake mechanism is evaluated using zeta potential, binding of radionuclides, and leaching of alkalis. Additionally, a thermodynamic model is developed to predict the binding of $Cs^{+}$ and $Sr^{2+}$ in the geopolymer.

**Chapter 4** proposes compositions and sets of preparation conditions to modify the alkaline metakaolin-based geopolymers with the aim of enhancing its uptake capabilities for anionic radionuclides (Se oxyanions) through the in-situ ettringite formation. The uptake behaviour and mechanism of ettringite, and geopolymer with in-situ ettringite, are evaluated through co-precipitation experiments, binding investigation, and structural analysis. Finally, the

thermodynamic modelling is developed according to the ion exchange mechanism which effectively predicts the uptake of $SeO_3^{2-}$ at low concentrations.

**Chapter 5** aims to analyze the surface chemical properties of phosphoric acid activated metakaolin-based geopolymers, which possesses a positively charged surface in a certain pH range. This chapter investigates the structure-related surface electrostatic properties and the behaviour of structural and surface electrical properties under various pH conditions. Furthermore, this study demonstrates, for the first time, the potential of using phosphoric acid activated metakaolin-based geopolymers as a waste form for immobilising anionic radionuclides ($SeO_3^{2-}$, $SeO_4^{2-}$, $I^-$ and $IO_3^-$) in solidification/stabilization (S/S) processes.

**Chapter 6** presents the overview of the findings and conclusions drawn in this work, along with the recommendations for the future works.

## References

[1] S. Sadekin, S. Zaman, M. Mahfuz, R. Sarkar, Nuclear power as foundation of a clean energy future: A review, Energy Procedia, 160(2019) 513-518.

[2] P. Moriarty, D. Honnery, What is the global potential for renewable energy?, Renew. Sust. Energ. Rev., 16(2012) 244-252.

[3] J.D. Jenkins, Z. Zhou, R. Ponciroli, R.B. Vilim, F. Ganda, F. de Sisternes, A. Botterud, The benefits of nuclear flexibility in power system operations with renewable energy, Applied Energy, 222(2018) 872-884.

[4] S. Zhou, X. Zhang, Nuclear energy development in China: A study of opportunities and challenges, Energy, 35(2010) 4282-4288.

[5] S. Adams, S. Odonkor, Status, opportunities, and challenges of nuclear power development in Sub-Saharan Africa: The case of Ghana, Prog. Nucl. Energy, 138(2021).

[6] S. M. Landon, Energy: Yesterday, Today, and the Opportunities and Challenges of Tomorrow, International Geology Review, 44:12(2002) 1105-1114.

[7] TEPCO, 2013. Basic Policy for the Contaminated Water Issue at the TEPCO's Fukushima Daiichi Nu-clear Power Station.

[8] TEPCO, n.d. Contaminated Water Treatment.

[9] M. Alwaeli, V. Mannheim, Investigation into the Current State of Nuclear Energy and Nuclear Waste Management—A State-of-the-Art Review, Energies, 15(2022).

[10] T. A. Kurniawan, M. H. D. Othman, D. Singh, R. Avtar, G. H. Hwang, T. Setiadi, W. Lo, Technological solutions for long-term storage of partially used nuclear waste: A critical review, Annals of Nuclear Energy, 166(2022) 108736.

[11] F. Boris, B. Jens, S. David, S. Peter, International Approaches for Nuclear Waste Disposal in Geological Formations: Geological Challenges in Radioactive Waste Isolation—Fifth Worldwide Review, United States, N. p., 2017.

[12] J. Cuevas, A. I. Ruiz, R. Fernández, E. Torres, A. Escribano, M. Regadío, M. J. Turrero, Lime mortar-compacted bentonite–magnetite interfaces: An experimental study focused on the understanding of the EBS long-term performance for high-level nuclear waste isolation DGR concept, Appl. Clay Sci., 124–125(2016) 79-93.

[13] S. Bachu, T. McEwen. Geological Media and Factors for the Long-Term Emplacement and Isolation of Carbon Dioxide and Radioactive Waste. In: Toth, F. (eds) Geological Disposal of Carbon Dioxide and Radioactive Waste: A Comparative Assessment. Advances in Global Change Research, 44(2011).

[14] B. Grambow; Geological Disposal of Radioactive Waste in Clay, Elements, 12(2016) 239–245.

[15] N. Chapman, A. Hooper, The disposal of radioactive wastes underground, Proc. Geol. Assoc., 123(2012) 46-63.

[16] R. C. Ewing, R. A. Whittleston, B. W.D. Yardley, Geological Disposal of Nuclear Waste: a Primer, Elements, 12(2016) 233–237.

[17] M. Dirk, K. Travis, N. Chapman, P. V. Brady, H. Griffiths, The State of the Science and Technology in Deep Borehole Disposal of Nuclear Waste, Energies, 13(2020) 833.

[18] B. Kochkin, V. Malkovsky, S. Yudintsev, V. Petrov, M. Ojovan, Problems and perspectives of borehole disposal of radioactive waste, Prog. Nucl. Energy, 139(2021).

[19] L. Trotignon, V. Devallois, H. Peycelon, C. Tiffreau, X. Bourbon, Predicting the long term durability of concrete engineered barriers in a geological repository for radioactive waste, Phys. Chem. Earth Parts A/B/C, 32(2007) 259-274.

[20] Y. Xiong, Y. Wang, G. Roselle, S. Kim, Lead/lead-alloy as a corrosion-resistant outer layer packaging material for high level nuclear waste disposal, Nucl. Eng. Des., 380(2021).

[21] C.M. Jantzen, W.E. Lee, M.I. Ojovan, 6 - Radioactive waste (RAW) conditioning, immobilisation, and encapsulation processes and technologies: overview and advances, Radioactive Waste Management and Contaminated Site Clean-Up, Woodhead Publishing, (2013) 171-272.

[22] Japan Atomic Energy Agency. (n.d.). Overview of the Geological Disposal of High-Level Radioactive Waste.

[23] D. Caurant, P. Loiseau, O. Majérus, V. A. Chevaldonnet, I. Bardez, A. Quintas, Glasses, glass-ceramics and ceramics for immobilisation of highly radioactive nuclear wastes[M]. Hauppauge: Nova Science, 2007.

[24] W. J. Weber, A. Navrotsky, S. Stefanovsky, E. R. Vance, E.. Vernaz. Materials Science of High-Level Nuclear Waste Immobilisation, MRS Bulletin, 34(2009) 46–53.

[25] R. C. Ewing, W. Lutze, High-level nuclear waste immobilisation with ceramics, Ceram. Int., 17(1991) 287-293.

[26] F.P. Glasser, M. Atkins, Cements in Radioactive Waste Disposal. MRS Bulletin, 19(1994) 33-38.

[27] J. Koťátková, J. Zatloukal, P. Reiterman, K. Kolář, Concrete and cement composites used for radioactive waste deposition, J. Environ. Radioact., 178-179(2017) 147-155.

[28] C. M. Jantzen, F.P. Glasser, E.E. Lachowske, Radioactive Waste-Portland Cement Systems: I, Radionuclide Distribution, 84th Annual Meeting, The American Ceramic Society, Cincinnati, 67(1982) 668-673.

[29] K. G. Papadokostaki, A. Savidou, Study of leaching mechanisms of caesium ions incorporated in Ordinary Portland Cement, J. Hazard. Mater., 171(2009) 1024-1031.

[30] J. Davidovits, D. Comrie, Long Term Durability of Hazardous Toxic and Nuclear Waste Disposals, Proceedings of Geopolymer, 88(1988) 125-134.

[31] K. Volchek, M. Y. Miah, W. Kuang, Z. DeMaleki, F. H. Tezel, Adsorption of cesium on cement mortar from aqueous solutions, J. Hazard. Mater., 194(2011) 331-337.

[32] M. A. Haddad, E. Ofer-Rozovsky, G. Bar-Nes, E.J.C. Borojovich, A. Nikolski, D. Mogiliansky, A. Katz, Formation of zeolites in metakaolin-based geopolymers and their potential application for Cs immobilisation, J. Nucl. Mater., 493(2017) 168-179.

[33] R.M. Cornell, Adsorption of cesium on minerals: A review. J. Radioanal. Nucl. Chem., 171(1993), 483–500.

[34] J. Davidovits, Geopolymers: Inorganic polymeric new materials, J. Therm. Anal. 37 (1991) 1633–1656

[35] N.B. Singh, B. Middendorf, Geopolymers as an alternative to Portland cement: An overview, Constr. Build Mater., 237(2020) 117455.

[36] J. Davidovits, Geopolymer Chemistry and Applications, 2nd Ed., Geopolymer Institute, 2008

[37] N. Essaidi, B. Samet, S. Baklouti, S. Rossignol, Feasibility of producing geopolymers from two different Tunisian clays before and after calcination at various temperatures, Appl. Clay Sci. 88-89 (2014) 221–227.

[38] H. Xu, J.S. van Deventer, Geopolymerisation of multiple minerals, Miner. Eng. 15(2002) 1131–1139

[39] I. Ismail, S.A. Bernal, J.L. Provis, R. San Nicolas, S. Hamdan, J.S. van Deventer, Modication of phase evolution in alkali-activated blast furnace slag by the incorporation of fly ash, Cem. Concr. Compos. 45 (2014) 125–135.

[40] K. Komnitsas, D. Zaharaki, Geopolymerisation: a review and prospects for the minerals industry, Miner. Eng. 20 (2007) 1261–1277.

[41] H. Xu, W. Gong, L. Syltebo, K. Izzo, W. Lutze, I.L. Pegg, Effect of blast furnace slag grades on fly ash based geopolymer waste forms, Fuel, 133 (2014) 332–340.

[42] R.S. Krishna, J. Mishra, S. Meher, S.K. Das, S.M. Mustakim, S.K. Singh, Industrial solid waste management through sustainable green technology: case study insights from steel and mining industry in Keonjhar, India, Mater. Today Proc., 33(2020) 5243–5249.

[43] M. Zribi, B. Samet, S. Baklouti, Effect of curing temperature on the synthesis, structure and mechanical properties of phosphate-based geopolymers, J. Non Cryst. Solids, 511 (2019) 62–67.

[44] M. Zribi, B. Samet, S. Baklouti, F. Chaari, et al., Screening of factors influencing phosphate-based geopolymers consolidation time, using Plackett-Burman design, in: Advances in Materials, Mechanics and Manufacturing. LectureNotes in Mechanical Engineering, Springer, Cham, 2020 115–122.

[45] R.S. Krishna, J. Mishra, M. Zribi, F. Adeniyi, S. Saha, S. Baklouti, F. U. A. Shaikh, H.S. Gökçe, A review on developments of environmentally friendly geopolymer technology, Materialia, 20(2021) 101212.

[46] H.Y. Zhang, V. Kodur, L. Cao, S.L. Qi, Fiber reinforced geopolymers for fire resistance applications, Procedia Eng., 71(2014) 153–158.

[47] I. Farina, M. Modano, G. Zuccaro, R. Goodall, F. Colangelo, Improving flexural strength and toughness of geopolymer mortars through additively manufactured metallic rebars, Compos. Part B Eng., 145(2018) 155–161.

[48] K. Korniejenko, E. Frączek, E. Pytlak, M. Adamski, Mechanical properties of geopolymer composites reinforced with natural fibers, Procedia Eng., 151(2016) 388–393.

[49] P. Duxson, J.L. Provis, G.C. Lukey, J.S.J. van Deventer, The role of inorganic polymer technology in the development of green concrete, Cem. Concr. Res., 37 (2007)1590–1597.

[50] J. Mishra, S. Das, R.S. Krishna, N. Bharadwaj, Utilization of ferrochrome ash as a source material for production of geopolymer concrete for a cleaner sustainable environment, Indian Concr. J., 94(2020) 40–49.

[51] J.S.J. van Deventer, J.L. Provis, P. Duxson, Technical and commercial progress in the adoption of geopolymer cement, Miner. Eng., 29(2012) 89–104.

[52] B. K. Singh, M. A. Hafeez, H. Kim, S. Hong, J. Kang, W. Um, Inorganic Waste Forms for Efficient Immobilisation of Radionuclides, ACS EST Engg., 1(2021) 1149–1170.

[53] Q. Li, Z. Sun, D. Tao, Y. Xu, P. Li, H. Cui, J. Zhai, Immobilisation of simulated radionuclide $133Cs^{+}$ by fly ash-based geopolymer, J. Hazard. Mater., 262(2013) 325-331.

[54] N. Deng, H. An, H. Cui, Y. Pan, B. Wang, L. Mao, J. Zhai, Effects of gamma-ray irradiation on leaching of simulated 133Cs+ radionuclides from geopolymer wasteforms, J. Nucl. Mater., 459(2015) 270-275.

[55] Z. Xu, Z. Jiang, D. Wu, X. Peng, Y. Xu, N. Li, Y. Qi, P. Li, Immobilisation of strontium-loaded zeolite A by metakaolin based-geopolymer, Ceram. Int., 43(2017) 4434-4439.

[56] S. Ma, H. Yang, S. Fu, P. He, X. Duan, Z. Yang, D. Jia, P. Colombo, Y. Zhou, Additive manufacturing of geopolymers with hierarchical porosity for highly efficient removal of $Cs^{+}$, J. Hazard. Mater., 443 (2023) 130161.

[57] W. Lin, H. Chen, C. Huang, Performance study of ion exchange resins solidification using metakaolin-based geopolymer binder, Prog. Nucl. Energy, 129(2020) 103508.

[58] J. T. Gourley, Geopolymer Cement; Environmental Considerations, Geopolymer Alliance, 2020.

[59] J. Davidovits, Environmentally Driven Geopolymer Cement Applications., Geopolymer 2002 Conference, Melbourne, Australia, 2002

# CHAPTER 2

# LITERATURE REVIEW

## 2.1 Geopolymer

### 2.1.1 Definition and concept

Geopolymer has been a subject of research and development for more than thirty years, and it has shown great potential as a substitute for traditional cement-based materials due to its environmentally friendly properties and wide range of applications [1]. Geopolymer is most commonly referred to as an inorganic aluminosilicate material that can react with an alkaline solution or an acidic phosphate component to form a binder through a polycondensation reaction [2, 3].

With the continuous advancement of research and development in the field of geopolymer technology, it has become evident that various types of aluminosilicate materials can be used as precursors for the synthesis of geopolymers [1]. These precursors can originate from a variety of sources, including but not limited to, natural minerals, industrial wastes, and byproducts [71]. Each precursor type possesses unique mineral compositions, morphologies, and chemical properties, which ultimately affect the resulting properties of the final geopolymer product [1, 2, 71]. For instance, metakaolin, fly ash, and slag are commonly used as precursor materials in geopolymer research. Metakaolin is a type of calcined kaolin clay that is rich in aluminium and silica and possesses a high pozzolanic activity [1, 10]. Fly ash is a byproduct of coal combustion and contains a significant amount of amorphous silica and alumina [1, 10]. Slag, on the other hand, is a byproduct of iron and steel production and contains a high concentration of calcium, silicon, and aluminium [72]. Other precursor materials, such as volcanic ash, rice husk ash, and natural clays, have also been investigated

for their potential use in geopolymer synthesis [1]. These materials offer unique mineral compositions and properties that may result in desirable geopolymer characteristics, such as improved mechanical strength and durability.

The formation of geopolymer generally involves several stages, including dissolution, nucleation, oligomerization, and polymerization [2, 3]. Take the process of alkali-activated geopolymerization as instance, the aluminate and silicate are dissolved from the raw material under alkali conditions. The dissolved Al and Si tetrahedrons undergo gelation, reorganization, and polymerization to form the hardened geopolymer paste [1]. The incorporation of alkali cations, such as $Na^+$ and $K^+$, is necessary to achieve charge balance due to the negative charges generated from Al tetrahedrons. Additionally, geopolymer is an amorphous substance with a zeolite-like structure, allowing for the exchange of alkali metals ($Na^+$ and $K^+$) with other cations, such as $Cs^+$, $Cd^{2+}$, and $Pb^{2+}$ [4].

Geopolymer can be used in a wide range of applications, including ceramics, casting, cement, concrete, fireproof materials, refractory products, decorative stones, building materials, adhesives, radiation, and the curing of toxic waste [9]. It offers several advantages over traditional cement-based materials, such as a lower carbon footprint, higher durability, better fire resistance, and resistance to acid and sulfate attacks [1].

### 2.1.2 Alkaline based geopolymer materials

In general, geopolymer refers to the alkaline-based variety, which is formed through depolymerisation, polycondensation, and gel networking of aluminosilicate industrial waste or activated aluminosilicate precursor mineral in a strong alkaline solution (such as

sodium/potassium hydroxide or silicate) [2]. The continuous occurrence of the depolymerization-polycondensation reaction promotes the continuous strengthening of geopolymer materials, gradually showcasing excellent properties such as high-temperature resistance and acid and alkali corrosion resistance [6, 7].

**A.**

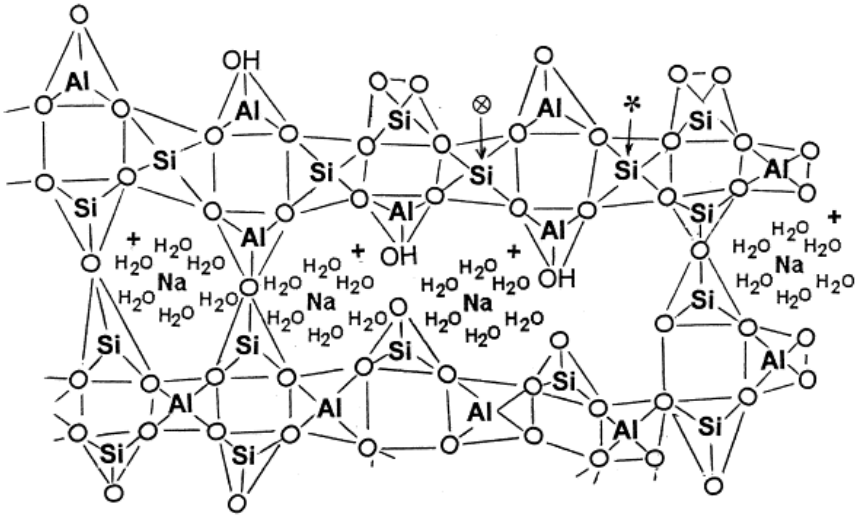


**B.**

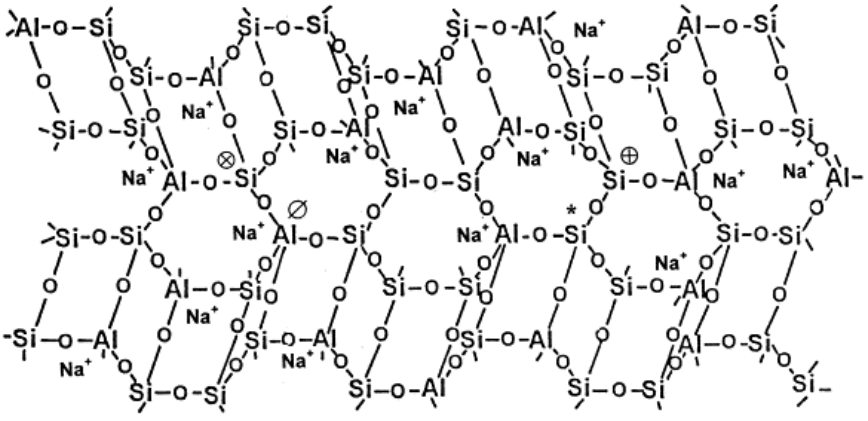

**Figure 2-1.** (A) Semi-schematic structure for Na–geopolymer. (B) Three-dimensional framework structure based on a suggested model for K–geopolymer. ⊗, $SiQ_4$(3Al) site; *, $SiQ_4$(2Al) site; ⊕, $SiQ_4$(1Al) site; ∅, $AlQ_4$(4Si) site [5].

Compared to cement materials, alkaline based geopolymers have a much higher degree of polymerization [1]. Cement materials contain a large amount of amorphous materials and hydrated crystals, making it difficult to withstand high temperatures [8]. In contrast, the three-dimensional network structure of geopolymer (shown in **Figure 2-1**) can maintain its structural integrity even at high temperatures, highlighting superior heat resistance. Davidovits' theory divides the formation process of alkaline based geopolymer into four stages [9]:

(1) Dissolution of aluminosilicate mineral powder in alkaline solution.

(2) Diffusion of silicon tetrahedron and aluminium tetrahedron from the surface of solid particles to the liquid phase.

(3) Polymerization of the alkali silicate solution with the aluminosilicate to form a gel phase.

(4) Rearrangement of the gel phase particles through dissolution, diffusion, and dehydration hardening to form an alkaline based geopolymer.

The procedure of alkali-activated geopolymerisation is illustrated in **Figure 2-2** [10]. Aluminosilicate precursors dissolve and form a gel, and the silicon tetrahedron and aluminium tetrahedron polymerize to form an amorphous or semi-crystalline three-dimensional spatial structure. During the polymerization process, aluminium converts from

the initial IV-coordinate, V-coordinate, and VI-coordinate states to IV-coordinate aluminium, which reacts with silicon oxide to form a network structure. The rest forms structural water or is adsorbed in the nanopores inside the material. After the gel solidifies, some of the water evaporates.

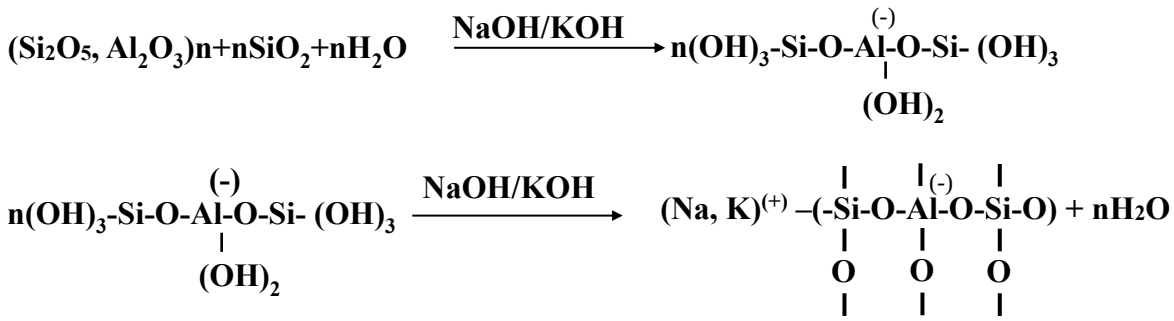


**Figure 2-2.** Reaction process of forming alkaline based geopolymer [10].

### 2.1.3 Acid based geopolymer materials

Acid-based geopolymers are becoming an attractive alternative to the popular alkaline-based geopolymers. They are either activated by phosphate-based acids or humic acids [10]. However, the use of humic acids in this area of research is limited due to the complexity of their composition. Therefore, acidic activation has been mainly limited to phosphate-based activators [10]. According to literature, the most commonly used phosphoric acid activator is pure commercial phosphoric acid $H_3PO_4$ 85% after its dilution with distilled water [11, 12, 13].

Unlike alkali-activated geopolymers, acid-activated geopolymers are affected by their acidity and P concentration due to the introduction of P in the reaction process, which can be summarized as follows [13]:

(1) In an acidic environment, the Al in metakaolin dissolves, resulting the process of dealumination.
    a) Under the relatively low P/Al ratio condition (0.52), the dissolved Al ions first react with $PO_4^{3-}$ to form the Al-O-P structure, where the [$PO_4$] units occupy the position of [$AlO_4$] in MK and are linked together with the silicate units through bridging oxygen to form the Si-O-P structure. In addition, the silicate tetrahedra in MK after dealuminisation may be linked together by condensation reactions to form the Si-O-Si structure.
    b) Under relatively high P/Al ratio conditions (0.64-0.84), the sub-stable intermediate P-O-P structure may be formed. With the depletion of $PO_4^{3-}$, the P-O-P structure is converted to the P-O-Al structure. In addition, the $Al_{VI}$ structure in MK disappeared completely after the reaction.
(2) The dissolved Al is mainly attached to the P structural unit, forming tetrahedral and octahedral structures of $Al_{IV}$-OP and $Al_{VI}$-OP. With the increase of P/Al molar ratio, the $Al_{IV}$-OP structure transforms into $Al_{VI}$-OP structure, indicating that Al prefers to be present in the $Al_{VI}$ structure.
(3) The P atom exists as a tetrahedral structure of $P(OAl)_x(H_2O)_{4-x}$, mainly located at defects in the matrix network or connected to Si and Al structural units, forming P-O-Al, Si-O-P-O-Al and Si-O-Al-O-P structural units.

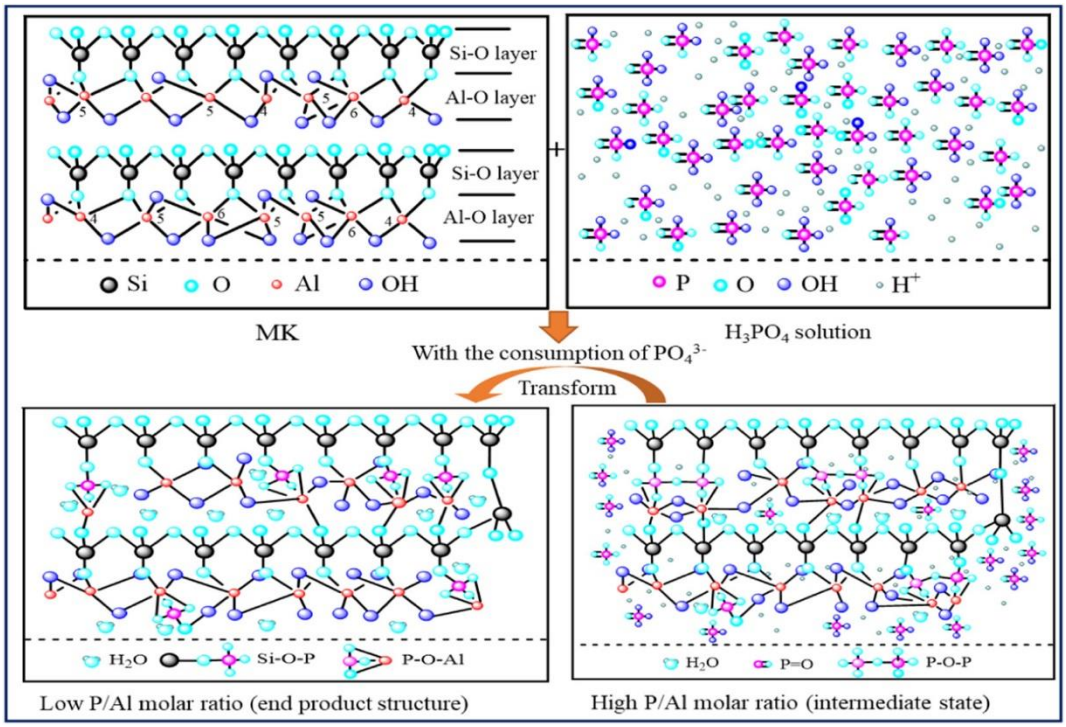


**Figure 2-3.** Geopolymerization mechanism of the Phosphoric acid activated geopolymers [13].

Phosphoric acid-based geopolymers exhibit impressive mechanical properties, with observed compressive strength values ranging from 10 MPa to 149 MPa [14, 15]. The wide variation in compressive strength values can be attributed to several factors such as the use of different aluminosilicate precursors [16], different Al/P molar ratios [17], different acidic concentrations [12, 13], different curing temperatures [18], and different aluminosilicate particle sizes [19].

Compared to alkaline-based geopolymers, phosphoric acid-based geopolymers demonstrate superior mechanical performance, dielectric performance, and thermal stability [20, 22]. A comparative study showed that the mechanical resistance of a metakaolin-based geopolymer

material obtained through phosphoric acid-activation can reach 93.8 MPa, while the same material obtained by alkali-activation does not exceed 63.8 MPa under the same synthesis conditions [21]. The difference in mechanical performance can be explained by suggesting that the compressive strength increases with the absence of alkaline ions and the increase in the number of bridging oxygens, which is more marked in the acid-based route [14].

Alkaline-based activators, such as sodium hydroxide or silicate solutions, have been questioned for their production and environmental impact. These activators require high temperatures above 1000°C for production, which results in a significant amount of energy consumption [23]. In contrast, phosphoric acid-based activators can be produced at a lower temperature below 300°C, making them more cost-effective. The manufacturing of alkaline-based activators also results in significant $CO_2$ emissions [23], while phosphoric acid-based activators have modest $CO_2$ emissions controlled by the use of sulfuric acid in their production. Additionally, aluminium phosphate-based activators do not emit any harmful gases. Hence, phosphoric acid-based activators are considered to be environmentally friendly compared to alkaline-based activators [24, 25]. Phosphoric acid-based activators are widely available globally, especially in countries with abundant deposits of operating phosphate rocks [26], making them a feasible choice for activators.

## 2.2 The chemistry of radionuclides

### 2.2.1 Cesium, strontium, and their radioisotopes

Cesium (Cs) and strontium (Sr) are two radioactive isotopes that are rarely found in nature and are typically caused by human activities [27, 28]. They are the radioactive isotopes of

the elements cesium and strontium, respectively, with Cs-137 having a long half-life of 30.17 years and Sr-90 having a half-life of 28.8 years [29, 30]. They are widely present in various human activities such as nuclear accidents, nuclear tests, medical radiation use, radioactive waste, industrial pollution, and agricultural pollution, causing serious impacts on humans and the environment [31]. The radioactive properties and toxicity of Cs and Sr pose a threat to both humans and the environment [32]. Cs-137 produces gamma rays and beta particles during radioactive decay, which can damage and mutate human cells, leading to diseases such as cancer [33]. Similarly, Sr-90 produces beta particles and can accumulate and harm human organs when inhaled or ingested [34].

One of the main sources of Cs and Sr contamination is nuclear accidents, such as the Chernobyl disaster in 1986 and the Fukushima disaster in 2011 [35, 36]. These accidents resulted in the release of large amounts of Cs and Sr into the environment, contaminating the air, water, and soil. As a result, many people were exposed to high levels of radiation, leading to various health problems.

Apart from nuclear accidents, Cs and Sr are also present in nuclear waste and the use of nuclear energy. Researchers have discovered the content of Cs and Sr on the Earth's surface and atmosphere is closely related to human activities [37]. The increase in human activities has significantly increased the content of Cs and Sr on the Earth's surface and atmosphere. In addition, researchers have also found some mechanisms for biological accumulation of these isotopes, such as certain marine organisms that can accumulate Sr-90, which has an important impact on ecosystem health [38].

### 2.2.2 Cobalt and its radioisotopes

Cobalt (Co) is a naturally occurring element widely used in various industrial and medical applications. However, anthropogenic activities have significantly increased the amount of Co in the environment, causing potential health and environmental risks [39]. Cobalt-60 is a radioactive isotope of Co with a half-life of 5.27 years, widely used in medical radiation therapy, industrial radiography, and food irradiation [40]. It produces gamma rays during radioactive decay, which can damage human cells and cause mutations, leading to cancer and other health problems [41].

Sources of radioactive cobalt isotopes include nuclear accidents, nuclear weapons testing, and nuclear power plant operations. The Chernobyl nuclear disaster in 1986 and the Fukushima nuclear disaster in 2011 released significant amounts of radioactive cobalt isotopes into the environment, leading to high levels of contamination in the air, water, and soil, with severe health and environmental impacts [35, 36]. Moreover, industrial processes, such as mining, refining, and manufacturing of batteries, alloys, and magnets, can also contribute to the release of radioactive cobalt isotopes into the environment. Workers involved in these processes are at risk of exposure to cobalt-60, leading to health problems, including radiation sickness and cancer [42].

It is crucial to take effective measures to mitigate the effects of cobalt contamination and ensure the safe handling and disposal of radioactive cobalt isotopes, especially to ensure the development of long-lasting and rational technologies in the disposal of fuel back-end of the nuclear power industry to protect human health and the environment.

### 2.2.3 Selenium and its radioisotopes

Selenium (Se) was discovered in 1817 by the Swedish chemist Jöns Jacob Berzelius [43]. It is a nonmetallic element that is commonly found in the Earth's crust and is widely distributed in the environment [43]. Selenium is an essential micronutrient for living organisms and is involved in several biological processes, including the functioning of the immune system, thyroid hormone metabolism, and antioxidant defense [44]. Selenium has six stable isotopes, including $^{74}$Se, $^{76}$Se, $^{77}$Se, $^{78}$Se, $^{80}$Se, and $^{82}$Se. However, some isotopes of selenium, such as $^{79}$Se and $^{79}$Se, are radioactive and have long half-lives, making them hazardous to human health and the environment [45, 46].

Radioactive selenium isotopes are mainly produced by nuclear fission in nuclear reactors and nuclear weapons testing. During nuclear fission, unstable nuclei of certain isotopes, including $^{79}$Se and $^{75}$Se, are produced and released into the environment as part of the nuclear waste [47, 48]. Furthermore, selenium can exist in different forms in solution, including selenate ($SeO_4^{2-}$) and selenite ($SeO_3^{2-}$), which are the most common forms in the environment [49]. Both selenate and selenite are dominant under oxidizing conditions and are not only more bioavailable and toxic than reduced forms, but also more soluble granting them greater mobility [54]. They can form stable complexes with various metal ions, such as copper, lead, and zinc, leading to the accumulation of selenium in aquatic systems [50]. **Figure 2-4** displays the stability of inorganic selenium species in an aqueous solution.

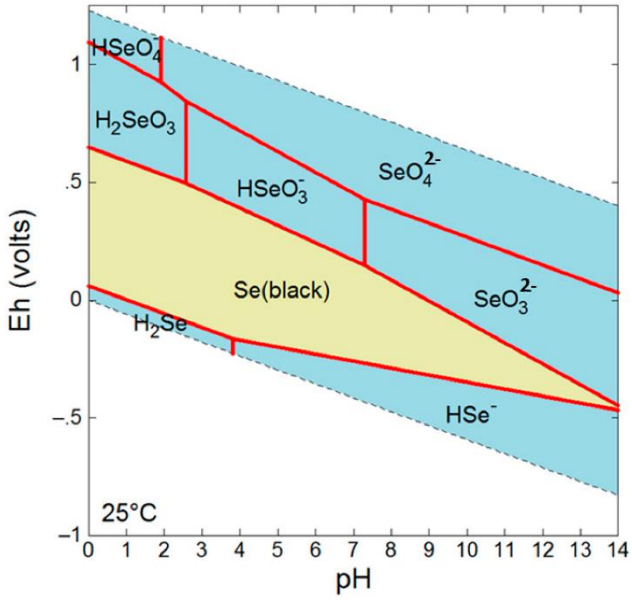


**Figure 2-4.** Eh-pH diagram for Se at 10 mM, 25 °C [55].

In addition, the $SeO_4^{2-}$ and $SeO_3^{2-}$ ions can also form salts with cations, such as ammonium, potassium, and sodium, to produce ammonium selenate ($(NH_4)_2SeO_4$), potassium selenate ($K_2SeO_4$), and sodium selenite ($Na_2SeO_3$) [51]. These compounds can also become contaminated with radioactive isotopes of selenium during nuclear fuel and waste disposal, further contributing to the release of radioactive selenium into the environment [52]. When these isotopes are released into the environment, they can be ingested by plants and animals and eventually enter the food chain, potentially exposing humans to radiation [52]. The toxicity of radioactive selenium isotopes is mainly due to their emission of high-energy radiation during decay, which can damage human cells and lead to various health problems, including cancer [53].

To minimize the release of radioactive selenium isotopes into the environment, strict regulations and safety measures should be in place to control and monitor the operation of nuclear power plants. The safe management and disposal of nuclear waste are also critical to preventing the release of radioactive isotopes into the environment.

### 2.2.4 Iodine and its radioisotopes

Iodine (I) is a common non-metallic element with a rich history and wide distribution in nature. It is primarily present in the form of iodides and iodates in the oceans, soil, and rocks. The discovery of iodine is attributed to the French chemist Bernard Courtois in 1811 [43]. Since then, iodine has been widely used in a variety of applications, including medicine, photography, and agriculture [56].

Iodine is a chemical element with only one stable isotope, $^{127}$I, but it also has 37 radioactive isotopes and isomers, ranging from atomic numbers 108 to 144 [57, 58]. Most of these radioactive isotopes have very short half-lives, ranging from minutes to a few hours [59]. Iodine is a chemical element that is characterized by only one stable isotope, namely, $^{127}$I. However, it also possesses 37 radioactive isotopes and isomers, spanning atomic numbers 108 to 144 [57, 58]. Most of these radioactive isotopes have short half-lives, lasting from a few minutes to a few hours [59]. Nonetheless, two particular radioactive isotopes, namely, $^{129}$I and $^{131}$I, are of significant concern due to their extended half-lives and high mobility in soil and aqueous systems [60, 61]. $^{131}$I has a half-life of approximately 8.02 days and is primarily generated from anthropogenic activities, with a yield of approximately 3% from $^{235}$U and $^{239}$Pu [62]. Notably, severe nuclear power plant accidents such as Chernobyl and

Fukushima released substantial quantities of $^{131}I$ [35, 36]. In contrast, $^{129}I$ has a relatively long half-life of $1.57 \times 10^7$ years and is an important fission product with a yield of 0.9% from $^{235}U$ and 1.9% from $^{239}Pu$ [62]. $^{129}I$ is the only naturally occurring radioactive isotope of iodine, produced by cosmic-ray interactions with xenon in the upper atmosphere and by spontaneous fission of $^{238}U$ in the geosphere [63]. The total naturally occurring $^{129}I$ in the surface environment is approximately 80 kg, with only $5 \times 10^{-4}$ kg found in the atmosphere [64].

The presence of both stable and radioactive isotopes of iodine in the environment can pose potential risks to human health [65]. Radioactive iodine isotopes, such as $^{129}I$ and $^{131}I$, can cause various health problems including cancer, radiation sickness, and thyroid gland dysfunction [66, 67]. $^{131}I$ is particularly dangerous due to its relatively short half-life and high mobility in the soil and water systems, making it easily transported over long distances and affecting a wide range of organisms [68]. In addition, the release of large amounts of radioactive iodine isotopes from nuclear accidents can lead to the contamination of food sources and water supplies, potentially leading to long-term health effects for humans and other organisms [69]. Even the stable isotope, $^{127}I$, can be toxic to the thyroid gland in excessive amounts and can affect its normal function [70]. Therefore, a deep understanding of the interaction of radioiodine nuclides with buffer materials in nuclear waste disposal is necessary for proper management and monitoring of radioiodine isotopes to minimize potential risks to the environment and human health.

## 2.3 Radionuclides treatment

### 2.3.1. Application of geopolymer in adsorption

Geopolymers are materials with a three-dimensional mesh structure that provides them with high porosity and a significant number of mesopores, which increases their specific surface area and enhances their adsorption capacity [1, 2, 4, 9, 10]. Alkaline based geopolymers have strong cationic adsorption performance and high contact sites benefit from the presence of negatively charged aluminium oxygen tetrahedra in the structure, making them advantageous in adsorption applications [2, 9, 10, 73]. One potential application of geopolymers is in heavy metal adsorption, as they have a strong cation exchange capacity and three-dimensional structure [74]. Adsorption experiments of $Cu^{2+}$ using fly ash and iron ore tailing to synthesize porous amorphous geopolymer showed a total porosity of 74.6%, and the uptake capacity reached the highest value of 113.41 mg/g at 40 °C [75]. The pH of the solution is an important factor affecting the adsorption capacity of the adsorbents, and pH regulation is often required to obtain the best adsorption effect [76]. Geopolymer adsorbent materials can also adsorb other cationic pollutants, such as $NH^{4+}$ [77]. Geopolymers can be modified to increase their adsorption rates for negatively charged species such as $SO_4^{2-}$ and anionic dyes [78, 79]. In research on the extraction of methylene blue from synthetic wastewater by fly ash-based geopolymer spheres, the removal efficiency of methylene blue uptake reached 79.7 mg/g and remained up to 83% after eight cycles of regeneration [79]. Geopolymers show promise in adsorption applications due to their unique properties, making them a potential solution for water pollution problems (**Figure 2-5**).

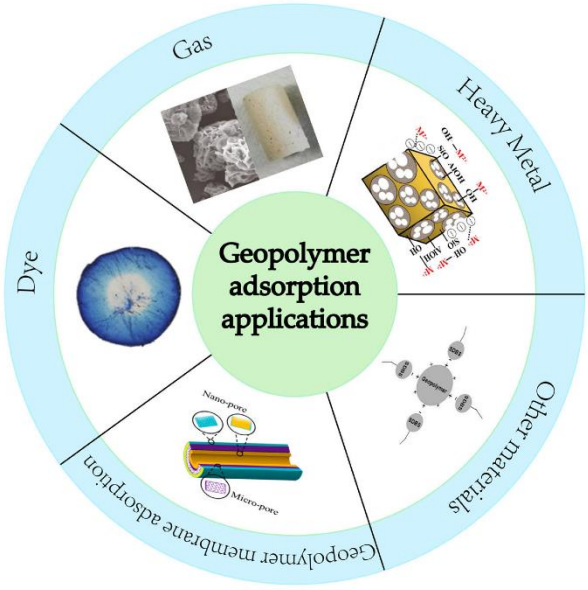


**Figure 2-5.** Application of geopolymer adsorption [73].

Geopolymers have been studied as a potential material for radioactive waste disposal facilities in industrialized countries [80, 81, 82]. Among the different types of geopolymers, metakaolin-based geopolymers have been shown to have a high capacity to adsorb heavy metal ions through ion exchange [83]. The adsorption behaviour of metakaolin-based geopolymers for heavy metals has been described using the Langmuir model, which indicates that there are various binding sites on the surface of metakaolin-based geopolymers that can immobilize different types of heavy metals [84].

$Cs^{+}$ and $Sr^{2+}$ are the most commonly investigated radionuclides in geopolymer wasteform studies, and have been extensively studied [85, 86]. Other radionuclide cations, such as Pb, Cu, Cd, Th, U, and Ca, found in radioactive wastewater, have also been successfully incorporated into geopolymers [87]. Despite this progress, there are limited studies on the

immobilisation mechanism of $Co^{2+}$, which is a high-content cationic radionuclide released in the FDNPS accident [88], along with $Cs^{+}$ and $Sr^{2+}$ in metakaolin-based geopolymers [83]. Metakaolin-based geopolymers has been identified as a potential material for adsorption of cations, but further investigation is needed to determine its effectiveness in immobilising $Co^{2+}$, $Cs^{+}$, and $Sr^{2+}$. Future research on this topic may help provide important insights into the development of safer and more effective radioactive waste disposal technologies.

### 2.3.2. Application of geopolymer in stabilization/solidification (S/S)

Solidification/stabilization (S/S) technology is a popular approach for converting hazardous waste into a stable, non-reactive, and impermeable material [89, 90, 91]. This technique involves mixing hazardous waste with a binding agent, such as cement, lime, or gypsum, to create a solid block that minimizes the environmental risks associated with hazardous waste [92, 93]. In recent years, the application of S/S technology for disposing of nuclear waste has gained significant attention. Low to intermediate-level radioactive waste (LLW and ILW) can be effectively stabilized and immobilized with S/S technology [94, 95]. This approach offers several benefits over other disposal methods, including waste volume reduction and density increase, which facilitate transportation and storage [96].

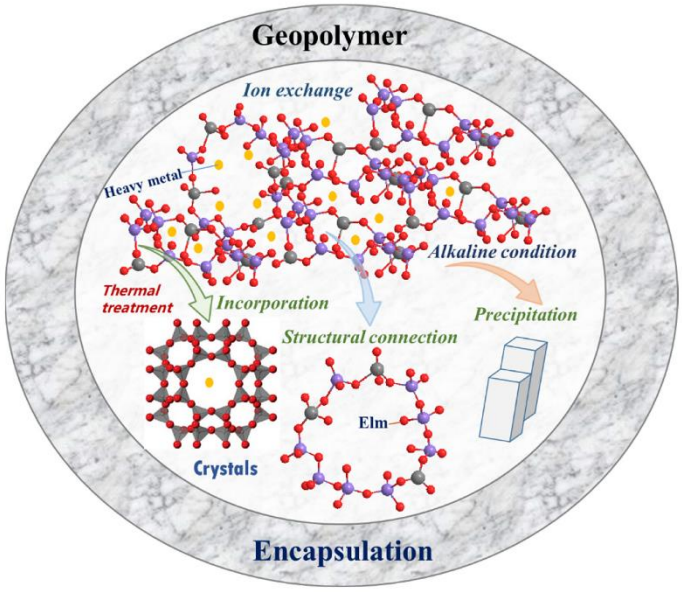


**Figure 2-6.** S/S mechanisms of heavy metals in geopolymer [97].

As **Figure 2-6** illustrates. Alkaline based geopolymers can stabilize and solidify certain species in waste modes by physical encapsulation, ion exchange, and co-precipitation processes, as well as through heat treatment and crystallization [98]. The geopolymer's physical encapsulation function can provide a strong mechanical structure to protect immobilized waste from solutions [99]. The negative charges generated by Al tetrahedrons allow for cation exchange with $Na^+$ or $K^+$ [100]. Thermal treatment can transform the amorphous structure of geopolymer into crystals, which can improve its S/S performance [101]. During geopolymerisation, some cations can be linked with Si directly by replacing Al [102]. The precipitation of cations is also an important role in geopolymer-based S/S [103].

Geopolymers have been extensively utilized for stabilizing and solidifying pollutants such as lead (Pb), zinc (Zn), and cadmium (Cd) [97]. Various raw materials, including fly ash, tailings,

drinking water, and lead-zinc smelting slags, have been used to synthesize geopolymers-based waste forms for the S/S [104, 105]. $Pb^{2+}$ can form covalent bonds in the Pb–O structure and can exchange with $Na^{+}$ or $K^{+}$ in the geopolymer's structure [106]. While geopolymers from diverse sources have been utilized for the adsorption of $Pb^{2+}$, zeolite-based adsorbents exhibit superior performance [107, 108, 109]. For Zn, the application of alkaline based geopolymers is effective for S/S, but Zn can dissolve in alkaline conditions [110]. The main reaction mechanisms for the geopolymer-based S/S of Zn involve physical encapsulation and electrostatic adsorption [111, 112]. However, research on the understanding of geopolymers for S/S of Cs and Sr is limited, which are the most hazardous radionuclides, possesses a long half-life (30 years and 28.8 years) and strong radioactivity [100].

In addition, studies on the curing ability of anions have also received attention, particularly chromium and selenium [97]. Chromium exists in both cationic and anionic forms, with Cr(VI) exhibiting higher toxicity than Cr(III) [113]. The S/S of Cr has been found to be restricted in geopolymer-based immobilisation [114]. Nonetheless, a more efficient strategy of reducing Cr(VI) to Cr(III) before solidification, followed by sorption and ion exchange in the geopolymer, has been suggested [115, 116, 117]. The studies on solidifying/stabilizing selenium have also been developed, which exists in several oxidation states, has been found to leach out from geopolymers in limited studies. Sodium silicate-activated geopolymers can reduce the leaching of Se [118], and electrostatic interaction is the primary association of $SeO_3^{2-}$ and $SeO_4^{2-}$ in geopolymers. However, based on previous research [100], it has been found that the negatively charged surface of alkaline-based geopolymers permanently limits the capacity for anion adsorption, including elements such as selenium or iodine. As a result,

the reliability and longevity of using alkaline-based geopolymers as a method of solidifying anionic nuclides such as selenium ($^{79}Se$) or iodine ($^{131}I$) is a cause for concern. Therefore, further investigation is required to determine the effectiveness of this approach for the long-term immobilisation of these hazardous materials.

### 2.3.3. Other immobilisation materials

#### 2.3.3.1 Ettringite

Ettringite is a hydrous calcium aluminate sulfate mineral that forms through the reaction of aluminate with sulfate [119]. According to previous literature [120, 121, 122], ettringite has a complex crystal structure that consists of columnar parts made up of $Al(OH)_6^{3-}$ octahedra and Ca-$O_8$ polyhedra, which are held together by $SO_4^{2-}$ ions and $H_2O$ molecules occupying the intercolumn space through electrostatic forces. Each Ca in the columnar parts is coordinated by four $H_2O$ molecules and four $OH^-$ groups, and the $Al(OH)_6^{3-}$ octahedra and Ca-$O_8$ polyhedra share $OH^-$ groups. The hydrogen bonding network in ettringite is also precisely arranged, contributing to its structural stability. These unique structural features of ettringite allow it to exhibit remarkable anion exchange properties, particularly for immobilising hazardous waste, such as selenium oxyanions, which are toxic pollutants. According to Solem-Tishmack et al. [123], Se oxyanions can be effectively adsorbed from aqueous solutions by ettringite derived from high-calcium coal combustion by-products. Another group of hydrous calcium aluminates commonly observed in cement hydration products, hydrocalumite, shows a lower Se oxyanion adsorption capacity, as reported by Zhang et al. [124]. Gou et al. [125, 126] discovered that ettringite can immobilize $SeO_4^{2-}$ by

forming $SeO_4^{2-}$-substituted ettringite, while $SeO_3^{2-}$ can be immobilized through ligand exchange with the Ca-$OH_2$ at the edges of its channels, leading to the formation of an inner sphere complex (**Figure 2-7**).

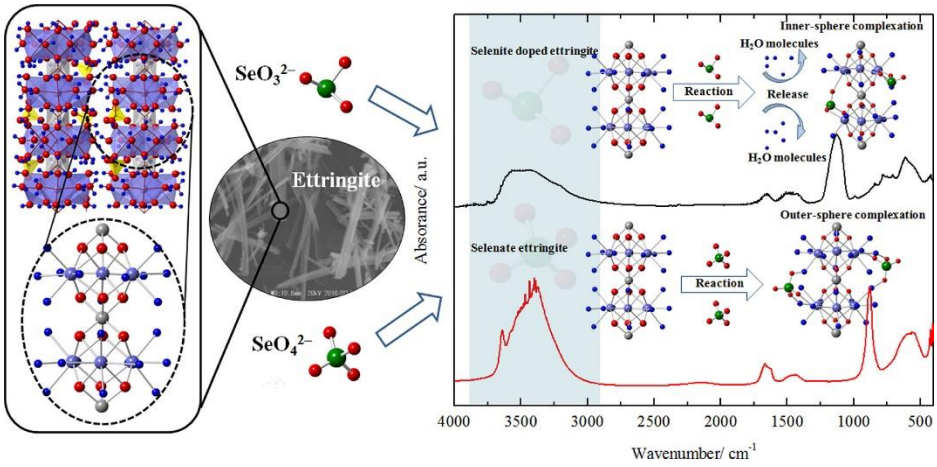


**Figure 2-7.** Mechanism of ettringite immobilising the oxyanions of Se [126].

Moreover, ettringite can form not only in Portland cement but also in alkali-activated reactions (geopolymerisation) when calcium and sulfur-rich additives are present, offering potential applications in the immobilisation of hazardous waste [127, 128, 129]. In addition, substitution of other anions or cations for $Ca^{2+}$, $Al^{3+}$, and $SO_4^{2-}$ in ettringite can result in compositional varieties, such as partial substitution of borate with sulfate and complete substitution of selenate or chromate with sulfate [130, 131, 132]. Ettringite is also found in natural alkaline environments associated with other minerals such as portlandite, gypsum, or afwillite [133]. The remarkable capacity of ettringite for anion exchange makes it a promising material for immobilising hazardous waste. Ettringite has shown promise in wastewater treatment due to its ability to immobilize selenium oxyanions through adsorption or ligand

exchange. Additionally, the formation of ettringite during alkali-activated reactions rich in aluminium offers a potential solution for immobilising hazardous waste. Hence, exploring the applications of ettringite and its integration with geopolymers in waste management could provide valuable insight into the potential of metakaolin-based geopolymers for anion immobilisation.

### 2.3.3.2 Layered double hydroxides (LDHs)

Layered double hydroxides (LDHs) are a group of minerals characterized by a layered structure derived from the hexagonal close-packed lattice structure of $Mg(OH)_2$, also known as brucite [134, 135]. The introduction of trivalent cations through partial substitution of divalent cations in the brucite-like structure leads to a positively charged layered arrangement [136]. The general formula for LDHs, which can vary depending on the specific elements involved, is expressed as $[M^{2+}_{1-x}M^{3+}_{x}(OH)_2]^{x+}[A^{m-}]_{x/m}\cdot nH_2O$ [137].

Layered double hydroxides (LDHs) and their thermally treated forms, known as calcined LDHs (CLDH), exhibit remarkable potential for removing anions from aqueous solutions. This ability is intricately linked to the chemical composition of the brucite-like layer, which encompasses the presence of different $M^{2+}$ elements (such as Cu, Zn, Ca, Mg), $M^{3+}$ elements (such as Fe, Al), the ratios between $M^{2+}$ and $M^{3+}$, and the initial anions occupying the interlayer space [138, 139, 140].

In the field of alkali-activated materials, two types of LDH that are commonly formed as reaction products are Mg-Al-LDHs (resembling hydrotalcite-like phases) and Ca-Al-LDHs (such as calcium aluminate monosulfate, referred to as AFm), which exhibit a hydrocalumite-

like structure (e.g., hemicarboaluminate, monocarboaluminate, or monosulfoaluminate) [141]. According to previous literature [2, 142, 143], the physicochemical properties of these LDHs are influenced by the composition of the precursor and the type of applied activator.

LDHs have been demonstrated significant potential in the immobilisation of anions, particularly in the solidification of major radionuclides like selenium (Se) and iodine (I). Extensive experimental and modeling evidence supports interlayer anion exchange as the dominant sorption mechanism for iodide ($I^-$) on AFm phases [144]. Furthermore, geopolymer-based materials, including layered double hydroxide/geopolymer (LDH/GEO) composites, exhibit promise in immobilising anionic species. Notably, geopolymer matrices retain their $Cs^+$ immobilisation ability while developing $SeO_4^{2-}$ immobilisation capabilities [145]. These findings highlight the suitability of LDHs and LDH/GEO composites for advanced anion immobilisation, thereby offering potential applications in environmental remediation and waste management.

## References

[1] P. Duxson, A. F. Jiménez, J. L Provis, G. C Lukey, A. Palomo, J. SJ. Deventer, Geopolymer technology: the current state of the art, J. Mater. Sci., 42(2007) 2917-2933.

[2] J. L. Provis, S. A. Bernal, Geopolymers and Related Alkali-Activated Materials, Annual Review of Materials Research, 44(2014) 299-327.

[3] H. Lin, H. Liu, Y. Li, X. Kong, Properties and reaction mechanism of phosphoric acid activated metakaolin geopolymer at varied curing temperatures, Cem. Concr. Res., 144(2021) 106425.

[4] S. A. Rasaki, B. Zhang, R. Guarecuco, T. Thomas, Y. Minghui, Geopolymer for use in heavy metals adsorption, and advanced oxidative processes: A critical review. J. Clean. Prod. 213(2019) 42–58.

[5] V. F.F Barbosa, K. J.D MacKenzie, C. Thaumaturgo, Synthesis and characterisation of materials based on inorganic polymers of alumina and silica: sodium polysialate polymers, Int. j. inorg. mater., 2(2000) 309-317.

[6] P.J. Ardhira, R. Ardra, Pooja Pallen Santhosh, Dhanya Sathyan, A review on structural performance of geopolymer beam and geopolymer for strengthening the beam, Materials Today: Proceedings, 64(2022) 74-78.

[7] L. Tian, D. He, J. Zhao, H. Wang, Durability of geopolymers and geopolymer concretes: A review, Reviews on advanced material science, 60(2021) 1-14.

[8] L. B. de Oliveira, A. R.G. de Azevedo, M. T. Marvila, E. C. Pereira, R. Fediuk, C. M. F. Vieira, Durability of geopolymers with industrial waste, Case Stud. Constr. Mater., 16(2022) e00839.

[9] J. Davidovits, Geopolymers: Inorganic polymeric new materials, J. Therm. Anal. 37 (1991) 1633–1656

[10] J. Davidovits, Geopolymer Chemistry and Applications, 2nd Ed., Geopolymer Institute, 2008

[11] D. Cao, D. Su, B. Lu, Y. Yang, Synthesis and structure characterization of geopolymeric material based on metakaolinite and phosphoric acid, J. Chin. Ceram. Soc., 33(2005) 1385-1389.

[12] H. K. Tchakouté, C. H. Rüscher, E. Kamseu, F. Andreola, C. Leonelli, Influence of the molar concentration of phosphoric acid solution on the properties of metakaolin-phosphate-based geopolymer cements, Appl. Clay Sci., 147(2017) 184-194.

[13] H. Lin, H. Liu, Y. Li, X. Kong, Properties and reaction mechanism of phosphoric acid activated metakaolin geopolymer at varied curing temperatures, Cem. Concr. Res., 144(2021) 106425.

[14] Y. He, L. Liu, L. He, X. Cui, Characterization of chemosynthetic $H_3PO_4$–$Al_2O_3$–$2SiO_2$ geopolymers, Ceram. Int., 42(2016) 10908-10912.

[15] H. Paiva, J. Yliniemi, M. Illikainen, F. Rocha, V.M. Ferreira, Mine tailings geopolymers as a waste management solution for a more sustainable habitat, Sustainability, 11(2019) 995.

[16] H. Xu, J.S. van Deventer, Geopolymerisation of multiple minerals, Miner. Eng., 15 (2002) 1131-1139.

[17] M. Zribi, B. Samet, S. Baklouti, Mechanical, microstructural and structural investigation of phosphate-based geopolymers with respect to P/Al molar ratio, J. Solid State Chem., 281(2020) 121025.

[18] D.S. Perera, J.V. Hanna, J. Davis, M. G. Blackford, B. A. Latella, Y. Sasaki, E. R. Vance, Relative strengths of phosphoric acid-reacted and alkali-reacted metakaolin materials, J. Mater. Sci., 43(2008) 6562-6566.

[19] S. Louati, S. Baklouti, B. Samet, Acid based geopolymerization kinetics: effect of clay particle size, Appl. Clay Sci., 132 (2016) 571-578.

[20] R.S. Krishna, J. Mishra, M. Zribi, F. Adeniyi, S. Saha, S. Baklouti, F. U. A. Shaikh, H.S. Gökçe, A review on developments of environmentally friendly geopolymer technology, Materialia, 20(2021) 101212.

[21] H. K. Tchakouté, C. H. Rüscher, Mechanical and microstructural properties of metakaolin-based geopolymer cements from sodium waterglass and phosphoric acid solution as hardeners: a comparative study, Appl. Clay Sci., 140(2017) 81-87.

[22] Y. S. Wang, J. G. Dai, Z. Ding, W. T. Xu, Phosphate-based geopolymer: formation mechanism and thermal stability, Mater. Lett., 190(2017) 09-212.

[23] M. Fawer, M. Concannon, W. Rieber, Life cycle inventories for the production of sodium silicates, Int. J. Life Cycle Assess., 4(1999) 207-212.

[24] S. I. Abu-Eishah, N. M. Abu-Jabal, Parametric study on the production of phosphoric acid by the dihydrate process, Chem. Eng. J., 81(2001) 231-250.

[25] Y. S. Wang, Y. Alrefaei, J. G. Dai, Silico-aluminophosphate and alkali-aluminosilicate geopolymers: a comparative review, Front. Mater., 6(2019) 106.

[26] B.V. Salas, M.S. Wiener, J.R.S. Martinez, M. Schorr, B. Valdez, Phosphoric acid industry: problems and solutions, Phosphoric Acid Industry - Problems and Solutions, IntechOpen (2017).

[27] S. K. Sahoo, N. Kavasi, A. Sorimachi, H. Arae, S. Tokonami, J. W. Mietelski, E. Łokas, S. Yoshida, Strontium-90 activity concentration in soil samples from the exclusion zone of the Fukushima daiichi nuclear power plant, Sci. Rep., 6(2016) 23925.

[28] S. Sharma, B. Singh, V. K. Manchanda, Phytoremediation: role of terrestrial plants and aquatic macrophytes in the remediation of radionuclides and heavy metal contaminated soil and water, Environ. Sci. Pollut. Res., 22(2015) 946–962.

[29] T. Lee, K. Lung, L. Ling, C. Chin, First detection of fallout Cs-135 and potential applications of 137Cs,135Cs ratios, Geochim. Cosmochim. Acta, 57(1993) 3493-3697.

[30] Y. Shikamori, K. Nakano, Feasibility study on the analysis of radioisotopes: Sr-90 and Cs-137, ICP-QQQ Applications in Geochemistry, Mineral Analysis, and Nuclear Science (2015) 66.

[31] N.I. Marmuleva, E.Ya. Barinov, V.L. Petukhov, Radionuclides accumulation in milk and its products, J. Phys. IV France, 107(2003) 827.

[32] A. Frydrych, M. Noga, J. Milan, E. K. Pietruszka, M. Krośniak, K. Jurowski, The Toxicological Analysis and Toxicological Risk Assessment of Chosen Elemental Impurities (Ag, Au, Co, Cr, Cs, Li, Mo, Se, and Sr) in Green Tea (Camellia sinensis (L.)) Infusions, Nutrients, 15(2023) 1460.

[33] A. A. Oglat, Gamma ray, beta and alpha particles as a sources and detection, J. Radiat. Res. Appl. Sci., 16(2023) 100503.

[34] B. Lee, J. Choi, K. Lee, H. Kang, H. Eom, K. Shin, H. Park, Separation and purification of Sr-90 nuclide from a waste mixture, J. Radioanal. Nucl. Chem., 331(2022) 275-281.

[35] M. Hatch, E. Ron, A. Bouville, L. Zablotska, G. Howe, The Chernobyl Disaster: Cancer following the Accident at the Chernobyl Nuclear Power Plant, Epidemiologic Reviews, 27(2005) 56–66.

[36] Y. Funabashi, K. Kitazawa, Fukushima in review: A complex disaster, a disastrous response. Bulletin of the Atomic Scientists, 68(2012) 9–21.

[37] S. S. Paatero, L. Thölix, R. Kivi, J. Paatero, Nuclear contamination sources in surface air of Finnish Lapland in 1965–2011 studied by means of 137Cs, 90Sr, and total beta activity, Environ. Sci. Pollut. Res., 26(2019) 21511–21523.

[38] L. Konovalenko, C. Bradshaw, E. Andersson, D. Lindqvist, U. Kautsky, Evaluation of factors influencing accumulation of stable Sr and Cs in lake and coastal fish, J. Environ. Radioact., 160(2016) 64-79.

[39] J. H. Kim, J. G. Herman, H. Paul, Cobalt and inorganic cobalt compounds, Vol. 69. World health organization, 2006.

[40] M. Ahmad, PRODUCTION OF COBALT-60 IN PARR-1/KANUPP (CANDU). Isotope Production Division, PINSTECH, Islamabad, Pakistan Atomic Energy Commission, 205(2013).

[41] L. P. Salter, J. H. Harley. "Trinitite": Cobalt-60, Cesium-137, and Europium-152, Science, 148.3672 (1965) 954-955.

[42] J. V. Dyk, J. J. Battista, P. R. Almond. A retrospective of Cobalt-60 radiation therapy:“The atom bomb that saves lives”, Med. Phys Int J 4 (2020).

[43] N.N. Greenwood, and A. Earnshaw, Chemistry of the Elements. Elsevier (2012).

[44] M. Kieliszek, S. Błażejak, Current Knowledge on the Importance of Selenium in Food for Living Organisms: A Review, Molecules, 21(2016) 609.

[45] G. Jörg, R. Bühnemann, S. Holla, N. Kivelc, K. Kossertd, S.V. Winckelb, and C. L. Gostomskia, Preparation of radiochemically pure 79Se and highly precise determination of its half-life. Appl. Radiat. Isotopes. 68(2010) 2339–2351.

[46] G. Audi, O. Bersillon, J. Blachot, and A.H. Wapstra, The NUBASE evaluation of nuclear and decay properties. Nuclear Physics A, 729(2003) 3-128.

[47] G. W. Leddicotte, The radiochemistry of selenium. No. NAS-NS-3030. Oak Ridge National Lab., 1961.

[48] S. Aguerre, C. Frechou, Development of a radiochemical separation for selenium with the aim of measuring its isotope $^{79}$Se in low and intermediate nuclear wastes by ICP-MS, Talanta, 69(2006) 565-571.

[49] P. Ježek, P. Škarpa, T. Lošák, J. Hlušek, M. Jůzl, P. Elzner, Selenium–an important antioxidant in crops biofortification, Antioxidant enzyme. IntechOpen Limited, London, UK (2012): 343-368.

[50] J. Torres, V. Pintos, S. Domínguez, C. Kremer, E. Kremer, Selenite and Selenate Speciation in Natural Waters: Interaction with Divalent Metal Ions, J. Solution Chem., 39(2010) 1–10.

[51] P. Gouda P. Arsenic, Selenium, Antimony Ultra-trace Analysis[M]. iUniverse, 2012.

[52] D. F. da Silva, P. E. Cipriano, R. R. de Souza, M. Siueia, V. Faquin, M. L. de S. Silva, L. R. G. Guilherme, Biofortification with selenium and implications in the absorption of macronutrients in Raphanus sativus L., J. Food Compost. Anal., 86(2020) 103382.

[53] T. Li, H. Xu, Selenium-containing nanomaterials for cancer treatment, Cell Reports Physical Science 1(2020).

[54] P. Cook, Y. Kim, K. Yuan, M. C. Marcano, U. Becker, Electrochemical, Spectroscopic, and Computational Investigations on Redox Reactions of Selenium Species on Galena Surfaces, Minerals, 9(2019) 437.

[55] C.M. Bethke, and S. Yeakel, The geochemist's workbench®, Release 10.0. Latest version available at The Geochemist's Workbench, (2015).

[56] J. B. Ristaino, W. Thomas, Agriculture, methyl bromide, and the ozone hole: can we fill the gaps? Plant Disease 81(1997) 964-977.

[57] V.R. Preedy, (Ed.). Selenium: Chemistry, Analysis, Function and Effects. Royal Society of Chemistry (2015).

[58] G. Audi, O. Bersillon, J. Blachot, and A.H. Wapstra, The NUBASE evaluation of nuclear and decay properties. Nuclear Physics A, 729(2003) 3-128.

[59] B. Clement, L. Cantrel, G. Ducros, F. Funke, L. Herranz, A. Rydl, G. Weber, and C. Wren, State of the art report on iodine chemistry (NEA-CSNI-R--2007-01). Nuclear Energy Agency of the OECD (NEA) (Feb 2007).

[60] G. Yang, H. Tazoe, M. Yamada, Can $^{129}$I track $^{135}$Cs, $^{236}$U, $^{239}$Pu, and $^{240}$Pu apart from $^{131}$I in soil samples from Fukushima Prefecture, Japan? Sci. Rep., 7(2017) 15369.

[61] I. Smičiklas, M. Šljivić-Ivanović, Radioactive contamination of the soil: assessments of pollutants mobility with implication to remediation strategies, Soil Contamination–Current Consequences and Further Solutions. Rijeka: InTech [Internet] (2016) 253-276.

[62] J. Lehto, X. Hou. Chemistry and analysis of radionuclides: laboratory techniques and methodology, John Wiley & Sons, (2011).

[63] Q.H. Hu, J.Q. Weng, and J.S. Wang, Sources of anthropogenic radionuclides in the environment: a review. Journal of environmental radioactivity, 101(2010) 426-437.

[64] J.E. Moran, S. Oktay, P.H. Santschi, and D.R. Schink, Atmospheric dispersal of $^{129}$Iodine from nuclear fuel reprocessing facilities, Environ. Sci. Technol., 33(1999) 2536-2542.

[65] Y. Luo, A. Kawashima, Y. Ishido, A. Yoshihara, K. Oda, N. Hiroi, T. Ito, N. Ishii, K. Suzuki, Iodine Excess as an Environmental Risk Factor for Autoimmune Thyroid Disease, Int. J. Mol. Sci., 15(2014) 12895-12912.

[66] J. Robbins, A. B. Schneider, Thyroid Cancer Following Exposure to Radioactive Iodine, Rev. Endocr. Metab. Disord 1(2000) 197–203.

[67] F.A. Alotaibi, Iodine in a Nutshell: What Do You Need to Know? Preprints.org, (2021) 2021080475.

[68] S. Koong, J. C. Reynolds, E. G. Movius, A. M. Keenan, K. B. Ain, M. C. Lakshmanan, J. Robbins, Lithium as a Potential Adjuvant to $^{131}$I Therapy of Metastatic, Well Differentiated Thyroid Carcinoma, J. Clin. Endocrinol. Metab., 84(1999) 912–916.

[69] S. Yamashita, S. Suzuki, Risk of thyroid cancer after the Fukushima nuclear power plant accident, Respir. Investig., 51(2013) 128-133.

[70] A. E. Mutlib, Application of Stable Isotope-Labeled Compounds in Metabolism and in Metabolism-Mediated Toxicity Studies, Chem. Res. Toxicol., 21(2008) 1672–1689.

[71] B. Singh, G. Ishwarya, M. Gupta, S.K. Bhattacharyya, Geopolymer concrete: A review of some recent developments, Constr. Build Mater., 85(2015) 78-90.

[72] H. Xu, W. Gong, L. Syltebo, K. Izzo, W. Lutze, I.L. Pegg, Effect of blast furnace slag grades on fly ash based geopolymer waste forms, Fuel, 133 (2014) 332–340.

[73] J. Xu, M. Li, D. Zhao, G. Zhong, Y. Sun, X. Hu, J. Sun, X. Li, W. Zhu, M. Li, Z. Zhang, Y. Zhang, L. Zhao, C. Zheng, X. Sun, Research and Application Progress of Geopolymers in Adsorption: A Review, Nanomaterials, 12(2022) 3002.

[74] T. Skorina, Ion exchange in amorphous alkali-activated aluminosilicates: Potassium based geopolymers, Appl. Clay Sci., 87(2014) 205–211.

[75] P. Duan, C. Yan, W. Zhou, D. Ren, Development of fly ash and iron ore tailing based porous geopolymer for removal of Cu (II) from wastewater, Ceram. Int., 42(2016) 13507–13518.

[76] I. Kara, D. Tunc, F. Sayin, S.T. Akar, Study on the performance of metakaolin based geopolymer for Mn (II) and Co (II) removal. Appl. Clay Sci., 161(2018) 184–193.

[77] T. Luukkonen, M. Sarkkinen, K. Kemppainen, J. Rämö, U. Lassi, Metakaolin geopolymer characterization and application for ammonium removal from model solutions and landfill leachate, Appl. Clay Sci., 119(2016) 266-276.

[78] H. Runtti, T. Luukkonen, M. Niskanen, S. Tuomikoski, T. Kangas, P. Tynjälä, E. T. Tolonen, M. Sarkkinen, K. Kemppainen, J. Rämö, U. Lassi, Sulphate removal over barium-modified blast-furnace-slag geopolymer, J. Hazard. Mater., 317(2016) 373-384.

[79] R. M. Novais, J. Carvalheiras, D. M. Tobaldi, M. P. Seabra, R. C. Pullar, J. A. Labrincha, Synthesis of porous biomass fly ash-based geopolymer spheres for efficient removal of methylene blue from wastewaters, J. Clean. Prod., 207(2019) 350-362.

[80] E.R. Vance, D.S. Perera, 18 - Geopolymers for nuclear waste immobilisation, In Woodhead Publishing Series in Civil and Structural Engineering, Geopolymers, (2009) 401-420.

[81] W. Xu, L. Gong, W. Syltebo, Lutze, I.L. Pegg, DuraLith geopolymer waste form for Hanford secondary waste: correlating setting behaviour to hydration heat evolution, J. Hazard. Mater., 133(2014) 332-340.

[82] T. Hanzlíček, M. Steinerova, P. Straka, Radioactive metal isotopes stabilized in a geopolymer matrix: determination of a leaching extract by a radiotracer method, J. Am. Ceram. Soc., 89 (11) (2006) 3541-3543.

[83] A.A. Siyal, M.R. Shamsuddin, M.I. Khan, N.E. Rabat, M. Zulfiqar, Z. Man, J. Siame, K.A. Azizli, A review on geopolymers as emerging materials for the adsorption of heavy metals and dyes, J. Environ. Manag., 224(2018) 327-339.

[84] F.J. López, S. Sugita, M. Tagaya, T. Kobayashi, Metakaolin-based geopolymers for targeted adsorbents to heavy metal ion separation, J. Mater. Sci. Chem. Eng., 02(2014), 16-27.

[85] C. Kuenzel, J.F. Cisneros, T.P. Neville, L.J. Vandeperre, S.J.R. Simons, J. Bensted, C.R. Cheeseman, Encapsulation of Cs/Sr contaminated clinoptilolite in geopolymers produced from metakaolin, J. Nucl. Mater., 466(2015) 94-99.

[86] N. Vandevenne, R.I. Iacobescu, Y. Pontikes, R. Carleer, Incorporating Cs and Sr into blast furnace slag inorganic polymers and their effect on matrix properties, J. Nucl. Mater., 503(2018) 1-12.

[87] B. Walkley, X. Ke, O.H. Hussein, S.A. Bernal, J.L. Provis, Incorporation of strontium and calcium in geopolymer gels, J. Hazard. Mater., 382(2020) 121015.

[88] Y. Zhu, J. Hu, J. Wang, Removal of Co2+ from radioactive wastewater by polyvinyl alcohol (PVA)/chitosan magnetic composite, Prog. Nucl. Energy, 71 (2014) 172-178.

[89] R. Pojasek, Stablilization, solidification of hazardous wastes, Environ. Sci. Technol., 12(1978) 382-386.

[90] J. R. Conner, S. L. Hoeffner, The History of Stabilization/Solidification Technology, Environ. Sci. Technol., 28(1998) 325-396.

[91] C. C. Wiles, A review of solidification/stabilization technology, J. Hazard. Mater., 14(1987) 5-21.

[92] J. Zhang, P. L Bishop, Stabilization/solidification (S/S) of mercury-containing wastes using reactivated carbon and Portland cement, J. Hazard. Mater., 92(2002) 199-212.

[93] S. A. A. Tajudin, M.A.M. Azmi, A.T.A. Nabila, Stabilization/Solidification Remediation Method for Contaminated Soil: A Review, IOP Conf. Ser.: Mater. Sci. Eng., 136(2016) 27-29.

[94] S.B. Eskander, S.M. Abdel Aziz, H. El-Didamony, M.I. Sayed, Immobilisation of low and intermediate level of organic radioactive wastes in cement matrices, J. Hazard. Mater., 190(2011) 969-979.

[95] S. Kearney, A. S. Yorkshire, D. A. Geddes, T. Hanein, S. Nelson, J. L. Provis, B. Walkley, Chapter 25 - Cement-based stabilization/solidification of radioactive waste, Low Carbon Stabilization and Solidification of Hazardous Wastes, 2022 407-431.

[96] M. I. Ojovan, H. J. Steinmetz, Approaches to Disposal of Nuclear Waste, Energies, 15(2022) 7804.

[97] Q. Tian, Y. Bai, Y. Pan, C. Chen, S. Yao, K. Sasaki, H. Zhang, Application of Geopolymer in Stabilization/Solidification of Hazardous Pollutants: A Review, Molecules, 27(2022) 4570.

[98] G. Jiang, X. Min, Y. Ke, Y. Liang, X. Yan, W. Xu, Z. Lin, Solidification/stabilization of highly toxic arsenic-alkali residue by MSWI fly ash-based cementitious material containing Friedel's salt: Efficiency and mechanism, J. Hazard. Mater., 425(2022) 127992.

[99] W. Long, J. Peng, Y. Gu, J. Li, B. Dong, F. Xing, Y. Fang, Recycled use of municipal solid waste incinerator fly ash and ferronickel slag for eco-friendly mortar through geopolymer technology, J. Clean. Prod., 307(2021) 127281.

[100] X. Niu, Y. Elakneswaran, C. R. Islam, J. L. Provis, T. Sato, Adsorption behaviour of simulant radionuclide cations and anions in metakaolin-based geopolymer, J. Hazard. Mater., 429(2022) 128373.

[101] L. M. Kljajević, S. S. Nenadović, M. T. Nenadović, N. K. Bundaleski, B. Ž. Todorović, V. B. Pavlović, Z. Lj. Rakočević, Structural and chemical properties of thermally treated geopolymer samples, Ceram. Int., 43(2017) 6700-6708.

[102] J. Zhang, Y. Gao, Z. Li, C. Wang, $Pb^{2+}$ and $Cr^{3+}$ immobilisation efficiency and mechanism in red-mud-based geopolymer grouts, Chemosphere, 321(2023) 137129.

[103] W. Long, T. Ye, F. Xing, K. H. Khayat, Decalcification effect on stabilization/solidification performance of Pb-containing geopolymers, Cem. Concr. Compos., 114(2020) 103803.

[104] Z. Ji, L. Su, Y. Pei, Synthesis and toxic metals (Cd, Pb, and Zn) immobilisation properties of drinking water treatment residuals and metakaolin-based geopolymers, Mater. Chem. Phys., 242(2020) 122535.

[105] Z. Ji, Y. Pei, Immobilisation efficiency and mechanism of metal cations ($Cd^{2+}$, $Pb^{2+}$ and $Zn^{2+}$) and anions ($AsO_4^{3-}$ and $Cr_2O_7^{2-}$) in wastes-based geopolymer, J. Hazard. Mater., 384(2020) 121290.

[106] S. J. O'Connor, K. J. D. MacKenzie, M. E. Smith, J. V. Hanna, Ion exchange in the charge-balancing sites of aluminosilicate inorganic polymers, J. Mater. Chem., 20(2010) 10234-10240.

[107] P. He, Y. Zhang, X. Zhang, H. Chen, Diverse zeolites derived from a circulating fluidized bed fly ash based geopolymer for the adsorption of lead ions from wastewater, J. Clean. Prod., 312(2021) 127769.

[108] E. Wei, K. Wang, Y. Muhammad, S. Chen, D. Dong, Y. Wei, T. Fujita, Preparation and conversion mechanism of different geopolymer-based zeolite microspheres and their adsorption properties for $Pb^{2+}$, Sep. Purif. Technol., 282(2022) 119971.

[109] Q. Su, Y. He, S. Yang, H. Wan, S. Chang, X. Cui, Synthesis of NaA-zeolite microspheres by conversion of geopolymer and their performance of Pb (II) removal, Appl. Clay. Sci., 200(2021) 105914.

[110] R.D. Armstrong, M.F. Bell, The active dissolution of zinc in alkaline solution, Journal of Electroanalytical Chemistry and Interfacial Electrochemistry, 55(1974) 201-211.

[111] Q. Wan, F. Rao, S. Song, Y. Zhang, Immobilisation forms of ZnO in the solidification/stabilization (S/S) of a zinc mine tailing through geopolymerization, J. Mater. Res. Technol., 8(2019) 5728-5735.

[112] L. Wang, D. A. Geddes, B. Walkley, J. L. Provis, V. Mechtcherine, D. C.W. Tsang, The role of zinc in metakaolin-based geopolymers, Cem. Concr. Res., 136(2020) 106194.

[113] M. Costa, Toxicity and carcinogenicity of Cr (VI) in animal models and humans. Crit. Rev. Toxicol., 27(1997) 431–442.

[114] A. Al-Mashqbeh, S. Abuali, B. El-Eswed, F. I. Khalili, Immobilisation of toxic inorganic anions ($Cr_2O_7^{2-}$, $MnO_4^-$ and $Fe(CN)_6^{3-}$) in metakaolin based geopolymers: A preliminary study, Ceram. Int., 44(2018) 5613-5620.

[115] X. Huang, F. Muhammad, L. Yu, B. Jiao, Y. Shiau, D. Li, Reduction/immobilisation of chromite ore processing residue using composite materials based geopolymer coupled with zero-valent iron, Ceram. Int., 44(2018) 3454-3463.

[116] J. Chen, Y. Wang, H. Wang, S. Zhou, H. Wu, X. Lei, Detoxification/immobilisation of hexavalent chromium using metakaolin-based geopolymer coupled with ferrous chloride, J. Environ. Chem. Eng., 4(2016) 2084-2089.

[117] J. Zhang, J. L. Provis, D. Feng, J. S.J. van Deventer, The role of sulfide in the immobilisation of Cr(VI) in fly ash geopolymers, Cem. Concr. Res., 38(2008) 681-688.

[118] Q. Tian, B. Guo, K. Sasaki, Immobilisation mechanism of Se oxyanions in geopolymer: Effects of alkaline activators and calcined hydrotalcite additive, J. Hazard. Mater., 387(2020) 121994.

[119] H.F.W. Taylor, Cement Chemistry, 2nd edition, Academic Press Limited, New York (1997).

[120] H.F.W. Taylor, Crystal structures of some double hydroxide minerals, Mineralogical Magazine, 39(1973) 377-389.

[121] A.E. Moore and H.F.W. Taylor, Crystal structure of ettringite. Acta Crystallogr, B26 (1970) 386–393.

[122] M.R. Hartman, S.K. Brady, R. Berliner, and Conradi M.S.; The evolution of structural changes in ettringite during thermal decomposition. J. Solid State Chem., 179(2006) 1259-1272.

[123] J.K. Solem-Tishmack, G.J. McCarthy, B. Docktor, K.E. Eylands, J.S. Thompson, D.J. Hassett, High-calcium coal combustion by-products: Engineering properties, ettringite formation, and potential application in solidification and stabilisation of selenium and boron, Cem Concr Res., 25 (1995) 658-670.

[124] M. Zhang and E. J. Reardon, Removal of B, Cr, Mo, and Se from Wastewater by Incorporation into Hydrocalumite and Ettringite, Environ. Sci. Technol., 37(2007) 2947-2952.

[125] B. Guo, K. Sasaki, T. Hirajima, Characterisation of the intermediate information of selenate-substituted ettringite, Cem. Concr. Res., 99(2017) 30-37.

[126] B. Guo, K. Sasaki, T. Hirajima, Selenite and selenate uptaken in ettringite: Immobilisation mechanisms, coordination chemistry, and insights from structure, Cem. Concr. Res., 100(2017) 166-175.

[127] S. Wang, K. L. Scrivener, Hydration products of alkali-activated slag cement, Cem. Concr. Res., 25(1995) 561-571.

[128] C. Li, H. Sun, L. Li, A review: The comparison between alkali-activated slag (Si+Ca) and metakaolin (Si+Al) cements, Cem. Concr. Res., 40(2010) 1341-1349.

[129] A. Palomo, M. Palacios, Alkali-activated cementitious materials: Alternative matrices for the immobilisation of hazardous wastes: Part II. Stabilisation of chromium and lead, Cem. Concr. Res., 33(2003) 289-295.

[130] P. Kumarathasan, G.J. McCarthy, D.J. Hassett, and F. Debra, Oxyanion substituted ettringites: synthesis and characterization; and their potential role in immobilisation of As, B, Cr, Se and V. MRS Proceedings. Cambridge University Press., 178(1990) 83-104.

[131] D.J. Hassett, G.J. McCarthy, P. Kumarathasan, and D. Pflughoeft-Hassett, Synthesis and characterization of selenate and sulfate-selenate ettringite structure phases, Mater. Res. Bull.25(1990) 1347–1354.

[132] R.B. Perkins, and C.D. Palmer, Solubility of Ca6 [Al (OH) 6] 2 (CrO4) 3· 26H2O, the chromate analog of ettringite; 5–75° C. Applied Geochemistry, 15(2000) 1203-1218.

[133] J.W. Anthony, R.A. Bideaux, K.W. Bladh, M.C. Nichols, Handbook of Mineralogy: Borates, Carbonates, Sulfates; Mineral Data Publishing. Tuscon, AZ, (2003).

[134] M. C. Gastuche, G. Brown, M. M. Mortland, Mixed magnesium-aluminiun hydroxides. I. Preparation and characterization of compounds formed in dialysed systems, Clay Minerals, 7(1967) 177-192.

[135] M. C. Gastuche, G. Brown, M. M. Mortland, Mixed magnesium-aluminium hydroxides. II. Structure and structural chemistry of synthetic hydroxycarbonates and related minerals and compounds. Clay Minerals, 7(1967) 193-201.

[136] Q. Wang, D. O'Hare, Recent Advances in the Synthesis and Application of Layered Double Hydroxide (LDH) Nanosheets, Chem. Rev., 112(2012) 4124–4155.

[137] X. Duan, D. G. Evans, eds. Layered double hydroxides, Springer Science & Business Media, 119(2006).

[138] S. Miyata, Anion-Exchange Properties of Hydrotalcite-Like Compounds, Clays Clay Miner., 31(1983) 305–311.

[139] K. Morimoto, S. Anraku, J. Hoshino, T. Yoneda, T. Sato, Surface complexation reactions of inorganic anions on hydrotalcite-like compounds, J. Colloid Interface Sci., 384(2012) 99-104.

[140] F. L. Theiss, S. J. Couperthwaite, G. A. Ayoko, R. L. Frost, A review of the removal of anions and oxyanions of the halogen elements from aqueous solution by layered double hydroxides, J. Colloid Interface Sci., 417(2014) 356-368.

[141] X. Ke, S. A. Bernal, J. L. Provis, Uptake of chloride and carbonate by Mg-Al and Ca-Al layered double hydroxides in simulated pore solutions of alkali-activated slag cement, Cem. Concr. Res., 100(2017) 1-13.

[142] M. Ben Haha, B. Lothenbach, G. Le Saout, F. Winnefeld, Influence of slag chemistry on the hydration of alkali-activated blast-furnace slag — Part I: Effect of MgO, Cem. Concr. Res., 41(2011) 955-963.

[143] S. A. Bernal, J. L. Provis, R. J. Myers, R. S. Nicolas, J. S. J. van Deventer. Role of carbonates in the chemical evolution of sodium carbonate-activated slag binders, Mater. Struct., 48(2015) 517–529.

[144] L. Nedyalkova, J. Tits, G. Renaudin, E. Wieland, U. Mäder, B. Lothenbach, Mechanisms and thermodynamic modelling of iodide sorption on AFm phases, J. Colloid Interface Sci., 608(2022) 683-691.

[145] Q. Tian, K. Sasaki, A novel composite of layered double hydroxide/geopolymer for co-immobilisation of $Cs^{+}$ and $SeO_4^{2-}$ from aqueous solution, Sci. Total Environ., 695(2019) 133799.

# CHAPTER 3

## ADSORPTION BEHAVIOUR OF SIMULANT RADIONUCLIDE CATIONS AND ANIONS IN METAKAOLIN-BASED GEOPOLYMER

## 3.1 Introduction

The contamination of cooling water with radionuclides and the radioactive waste generated from water is a serious concern in the decommissioning process of the Fukushima Daiichi Nuclear Power Station (FDNPS) [1, 2]. The Tokyo Electric Power Company (TEPCO) has been removing radionuclides from cooling water with several types of adsorbents and plans to safely store the generated radioactive waste for a long time. Selection of the most suitable host material, with high solidification and immobilisation capacity for radioactive waste, is necessary for safe disposal. Moreover, the sealing materials should have low aqueous solubility and should provide stable phases for radionuclides immobilisation [3, 4]. Cement-based materials have been considered to solidify and encapsulate radioactive waste for a long time owing to their low cost and high durability [5, 6, 7]. Although cement-based materials show a good immobilisation capacity for some radionuclides, their incompatibilities with several other radionuclides and high free water content, which may cause problematic hydrogen generation, limit their usage in some applications [8, 9, 10]. Moreover, high $CO_2$ emissions and high-energy consumption are unavoidable during the Portland cement manufacturing process [11]. Therefore, it is important to develop an environmentally friendly solidification material for safe disposal and environmental remediation of nuclear waste.

Geopolymer materials are a class of alkaline-activated materials that can be produced from a chemical process of depolymerisation, polycondensation, and gel networking of an aluminosilicate part commonly referred to as ‘precursor’ in strong alkaline solution or the activator [12, 13]. Recently, geopolymers have attracted attention as alternative materials for

traditional Portland cement in concrete [14]. Compared with cement-based materials, geopolymers can have superior chemical durability characteristics which are often attributed to their increased degree of silicate polymerisation [15, 16]. Since geopolymers have a three-dimensional framework structure of oxygen-linked silicon and aluminium, the negative charge associated with the tetrahedral Al sites is typically balanced by alkali cations, including $Na^+$ or $K^+$ from the activator. A geopolymer can also be regarded as a disordered pseudo-zeolite [15, 17]. There are active sites on the surface of geopolymers owing to the presence of metal oxide groups and thus, they have increased potential in adsorbing heavy metal ions [18, 19]. The types of precursors, water/solid ratio, Si/Al ratio, alkalinity of alkali activation solution, and the curing temperature affect the geopolymerisation and could influence the adsorption property [20, 21].

The use of geopolymers for the proposal of radioactive waste disposal facilities has been considered in industrialised countries [22, 23, 24]. Metakaolin-based geopolymers (MK-GPs) have been proven to have a high ability to incorporate heavy metal ions through ion exchange [19]. The Langmuir model has been used to describe the adsorption behaviour of MK-GP for heavy metals and shows that there are multiple types of binding sites on the surface of MK-GP that can immobilise different types of heavy metals [25]. $Cs^+$ and $Sr^{2+}$ are the most common radionuclides investigated in geopolymer wasteform studies and have been investigated for many years [26, 27, 28]. Furthermore, some other radionuclide cations, including Pb, Cu, Cd, Th, U, and Ca, existing in radioactive wastewater can be incorporated into geopolymers [29, 30]. Currently, MK-GP is considered a potential material to solidify waste from FDNPS. However, there are few studies on the immobilisation of $Cs^+$, $Sr^{2+}$, and

$Co^{2+}$, which is also a high-content cationic radionuclide from the FDNPS accident [31], in the MK-GP [19]. Most studies on the immobilisation capacity of geopolymers for $Cs^{+}$ and $Sr^{2+}$ have mainly focused on the confirmation of incorporation, and the associated mechanisms are limited [9, 16, 26, 28, 29, 32]. On the other hand, understanding the interaction of MK-GP with anionic radionuclides, including $I^{-}$, $IO_3^{-}$, $SeO_3^{2-}$, and $SeO_4^{2-}$ is urgent and important, but this has rarely been discussed in previous studies. In addition, there is limited geochemical modelling studies in the geopolymer system compared with cementitious materials [33, 34]. Moreover, to the best of authors knowledge, the thermodynamic data on ion-exchange reactions in metakaolin-based geopolymer is still missing. Therefore, it is of great significance to explore and evaluate the potential ability of MK-GP to incorporate both cationic and anionic radionuclides. In this context, the main purpose of this study was to analyse the immobilisation capacity of MK-GP for both cationic radionuclides ($Cs^{+}$, $Sr^{2+}$, and $Co^{2+}$) and anionic radionuclides ($I^{-}$, $IO_3^{-}$ , $SeO_3^{2-}$, and $SeO_4^{2-}$). The zeta potential, binding of radionuclides, and leaching of alkalis were used to evaluate the uptake mechanism. Finally, a thermodynamic model was used to predict the binding of $Cs^{+}$ and $Sr^{2+}$ in the geopolymer.

## 3.2 Materials and methods

### 3.2.1 Materials and geopolymer preparation

Metakaolin from IMERYS-Metastar (hereafter referred to as MS) and Sobueclay, Japan (hereafter SC) were used to prepare the geopolymer, and the average particle size of the metakaolin was 2194.9 nm and 577.4 nm representatively for Metastar and Sobueclay. The chemical composition of metakaolin determined by X-ray fluorescence (XRF) is listed in **Table 3-1**, and the ratios of $SiO_2$:$Al_2O_3$ of MS and SC were 1.04 and 1.01 respectively. A potassium silicate alkali solution was used as an activator for the synthesis of geopolymers. The solutions of the composition $SiO_2/K_2O$ = R (R = 1.0 and 2.1) and $H_2O/K_2O$ = 11 and 13 were prepared by mixing an aqueous potassium silicate solution (WAKO, originally containing 29.1 wt% $SiO_2$, 21.9 wt% $K_2O$, 49.0 wt% $H_2O$) into potassium hydroxide solutions of the required concentration until the solution become homogenous and clear. Potassium hydroxide solutions were prepared by dissolving KOH (WAKO 85 wt% KOH) in ultrapure wate. The prepared solutions were stored in a laboratory environment (20 °C and RH ≈ 60%) for 24 h to allow equilibration in the solution. The alkaline solutions used for the synthesis of the geopolymer samples are thus defined as $K_2O$: $SiO_2$: $H_2O$ (molar ratio) 1:1:11, 1:1:13, 1:2.1:11.7, and 1:2.1:13. Geopolymer samples were prepared by mechanically mixing stoichiometric amounts of metakaolin (Metastar/Sobueclay) with a sufficient quantity of alkaline silicate solution to give $Al_2O_3/K_2O$ = 1. The mixture was kneaded for 15 min to form a homogeneous slurry followed by an additional 15 min of vibration to remove entrained air before sealing into a mould [20]. The geopolymer slurry was sealed and cured at 40 °C for

28 days. Subsequently, the hardened geopolymer was demoulded and ground to powder with particle sizes less than 150 μm, and the powder particles were cured for another 3 days at 40 °C before the experiments.

**Table 3-1.** Chemical composition (wt%) of the MS-metakaolin and SC-metakaolin, as determined by X-ray fluorescence.

| Component | MS-Metakaolin | SC-Metakaolin |
|---|---|---|
| $SiO_2$ | 52.54 | 48.59 |
| $Al_2O_3$ | 44.81 | 43.11 |
| $Fe_2O_3$ | 0.38 | 0.54 |
| CaO | 0.04 | 0.21 |
| MgO | 4.03 | 3.66 |
| $Na_2O$ | 2.69 | 2.25 |
| $K_2O$ | 0.12 | 0.13 |
| $TiO_2$ | 0.79 | 1.27 |
| $P_2O_5$ | 0.48 | 1.08 |
| L.O.I.* | 0.49 | 1.74 |

*: L.O.I. is loss of ignition at 1100℃ for 12h.

## 3.2.2 Experimental procedure

The slump flow experiment specified in JASS15M-103 (which used a cylindrical Φ50 mm× H50 mm mould) was conducted at four different composition ratios (1:1:11, 1:1:13, 1:2.1:11.7, and 1:2.1:13) to select the most suitable composition for the alkaline activator,

while achieving a high workability of the geopolymer to meet the requirements for large-scale wasteform production. The slump flow value was measured at 0, 20, 60, and 120 min after mixing. The synthesised geopolymers were characterised by a Rigaku X-ray diffractometer with CuKα radiation, and the measurement conditions were a tube voltage of 40 kV, scanning range of 5°–70° 2θ, step size of 0.02° 2θ, and scan speed of 6.5°/min.

A geopolymer suspension with a solid to liquid ratio of 1 g/L was prepared for zeta potential measurements using a zeta potential and particle size analyser apparatus (ELSZ-1000ZS). The zeta potential of the geopolymer was determined in the presence of $CsNO_3$, $Sr(NO_3)_2$, $Co(NO_3)_2$ , KI, $KIO_3$, $K_2SeO_3$, and $K_2SeO_4$ solutions with ionic strengths of 10 and 100 mmol/L. In each case, $KNO_3$ solution was selected to adjust the ionic strength, whereas KOH was used to adjust the pH., To determine the equilibrium time for the adsorption of ions on geopolymer, the geopolymer was equilibrated with 2 and 4 mmol/L of $CsNO_3$, $Sr(NO_3)_2$ or $Co(NO_3)_2$ solutions (0.05 g geopolymer powder per 50 mL solution). The solution was filtered with the use of a syringe filter ($\varphi$ = 0.45 μm) after 1, 3, 5, 7, and 14 d of immersion time, and the concentrations of dissolved ions were measured using inductively coupled plasma-mass spectroscopy (ICP-MS, iCap Q ICP-MS, Thermo Scientific, USA, detection limit 0.01ppb-10ppb). Batch experiments were performed with $CsNO_3$, $Sr(NO_3)_2$, $Co(NO_3)_2$, KI, $KIO_3$, $K_2SeO_3$, and $K_2SeO_4$ solutions at 0.1, 1, 3, 5, and 10 mmol/L with a solid-to-liquid ratio of 1 g/L. After equilibration for 7 d, the liquid phase was filtered with a 0.45 μm syringe filter. The concentrations of the target ion and $K^+$ in the filtered solution were measured by ICP-MS. The amount of bound target ions and leached $K^+$ were calculated by eqs. 3.1 and 3.2:

$$A_b = (C_i - C_t)/R \quad (3.1)$$

$$A_l = \left(C_k - C_{pH}\right)/R \quad (3.2)$$

where $A_b$ is the binding amount of the target ion (mmol/g), $R$ is the solid to liquid ratio (g/L), $C_i$ is the initial concentration (mmol/L), $C_t$ is the concentration of the target ion (mmol/L), $A_l$ is the amount of leached $K^+$ (mmol/g), $C_k$ is the concentration of $K^+$ at time *t* (mmol/L), and $C_{pH}$ is the leached $K^+$ concentration in the blank solution in the absence of radionuclides at the target pH (mmol/L).

### 3.2.3 Modelling approach

The ion-exchange model available in the geochemical code PHREEQC was used for ion-exchange reactions between the geopolymer and radionuclide cations [35]. The activity coefficients were calculated based on the extended Debye–Huckel approach, whose parameters are available in the Phreeqc.dat database. The simulant radionuclides $Cs^+$, $Sr^{2+}$, and $Co^{2+}$ can be exchanged with the $K^+$ present in the geopolymer as:

$$X - K + Cs^+ \leftrightarrow X - Cs + K^+, K_{Cs} = \frac{[X-Cs][K^+]}{[X-K][Cs^+]} \quad (3.3)$$

$$2X - K + Sr^{2+} \leftrightarrow X_2 - Sr + 2K^+, K_{Sr} = \frac{[X_2-Sr][K^+]^2}{[X-K]^2[Sr^{2+}]} \quad (3.4)$$

$$2X - K + Co^{2+} \leftrightarrow X_2 - Co + 2K^+, K_{Co} = \frac{[X_2-Co][K^+]^2}{[X-K]^2[Co^{2+}]} \quad (3.5)$$

where $X$ is the exchange site, and $K_{Cs}$, $K_{Sr}$, and $K_{Co}$ are the exchange coefficients for $Cs^{+}$, $Sr^{2+}$, and $Co^{2+}$, respectively. The model can be implemented in PHREEQC using the keyword data block of EXCHANGE_MASTER_SPECIES, EXCHANGE_SPECIES, and EXCHANGE.

## 3.3 Results and discussion

### 3.3.1 Characteristics of geopolymer

The workability or flowability of the geopolymers was evaluated by slump flow experiments, as shown in **Figure 3-1**. The flow of the SC-geopolymer was higher than that of the MS-geopolymer. The difference likely to be related to particle size and/ or calcination condition of the metakaolin. Furthermore, an increase in the $SiO_2$ mole fraction in the alkali activator solution decreased the flow due to increased activator viscosity at higher silica content. Based on the slump flow testing, the geopolymer with a $K_2O$:$SiO_2$:$H_2O$ mole ratio of 1:1:13 had the highest flow and was selected for further analysis in this study.

X-ray diffraction (XRD) measurements were performed to confirm the synthesis of the geopolymer. **Figure 3-2** shows the XRD patterns of the metakaolins used for the synthesis and the geopolymer after the synthesis. Both MS and SC metakaolin have structures which are close to amorphous, as reported in previous studies [36, 37], but the patterns have confirmed the presence of kaolinite and quartz. Conversely, the XRD patterns of both geopolymers did not show any peaks of kaolinite, but a small amount of quartz remained in the geopolymer. Moreover, the geopolymers yielded a hump in the range of $2\theta$ = 27°–29°

which indicates amorphous products, and the results are consistent with those reported in many previous studies on metakaolin [38]. Prior to the evaluation of ionic interactions with the geopolymer, the surface electrostatic characteristics were evaluated using zeta potential measurements. It is worth to note that the prepared geopolymer suspension shows slightly basic pH in water and thus, the alkaline pH was selected for zeta potential experiment. **Figure 3-3** shows the results of the zeta potential of MS-and SC-based geopolymers in different pH solutions. The zeta potential of the geopolymer is negative and independent of pH, thus indicating the presence of a permanent charge on the surface of the geopolymer which is believed to be derived from the replacement of $SiO_4$ by $AlO_4$ in the tetrahedral framework structure [39], and the permanently charged surface can take up cations via electrostatic interactions. The decrease in ionic strength increases the absolute value of the zeta potential due to the formation of a thicker electrical double layer, which is consistent with the results obtained in other studies [40].

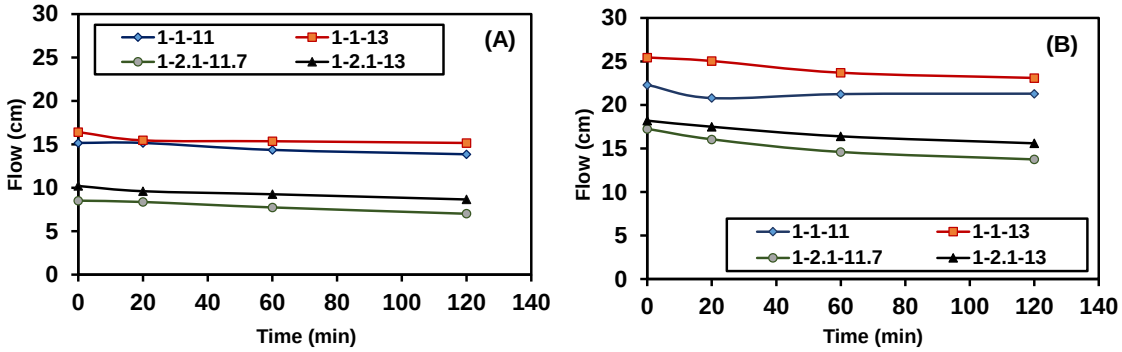


**Figure 3-1.** Slump flow diameters with time for (A) MK-based and (B) SC-based geopolymers (the ratios indicated in the figure legends are $K_2O$:$SiO_2$: $H_2O$).

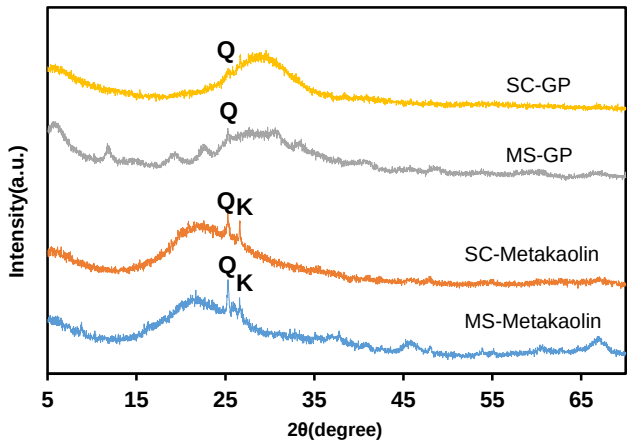


**Figure 3-2.** X-ray diffraction (XRD) patterns for MS and SC metakaolin and their geopolymers.

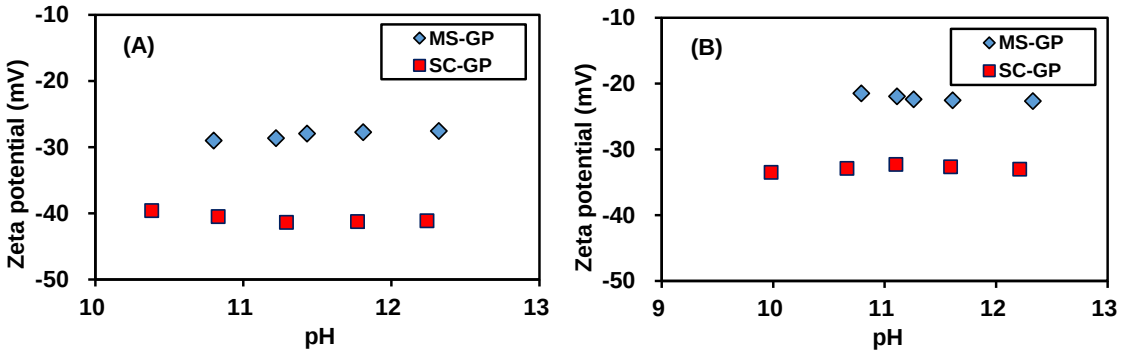


**Figure 3-3.** Zeta potential of geopolymer as a function of pH at the ionic strengths of (A) 10 mmol/L, (B) 100 mmol/L (MS-GP: Metastar metakaolin based geopolymer, SC-GP: Sobue clay metakaolin based geopolymer).

## 3.3.2 Experimental results on uptake of ions

The measured zeta potential of the geopolymers in the cation-containing solutions are shown in **Figure 3-4**. The effect of $Cs^+$ concentration on the zeta potential is insignificant compared

with that of $Sr^{2+}$ or $Co^{2+}$ solutions, consistent with the differences in the charge states of these respective ions. Moreover, the zeta potential of the geopolymer (for both types of metakaolin) in the $Cs^{+}$ solution was nearly equal to the value obtained for the sample without $Cs^{+}$ ions (**Figure 3-3)**, thus implying that partial replacement of $K^{+}$ by $Cs^{+}$ does not contribute to the surface charge variation on the geopolymer. By contrast, the zeta potential of the geopolymer in the $Sr^{2+}$ and $Co^{2+}$ solutions increases towards a positive value, which indicates that the variation in surface charge is caused by the divalent cations. This effect is prominent in the $Co^{2+}$ solution, which shows charge reversal in both geopolymers, even at low concentrations of $Co^{2+}$ ions (**Figure 3-4(E)** and **Figure 3-4(F)**). It should also be noted that a blue precipitate was observed in the geopolymer with $Co^{2+}$ solution, identified as cobalt blue ($CoAl_2O_4$). The effect of cobalt blue formation on the adsorption of $Co^{2+}$ ions on the geopolymer surface needs to be studied in the future, as there are possible competing pathways here, but the formation of cobalt blue does require some degree of extraction of Al from the geopolymer structure and so may have implications for the matrix stability.

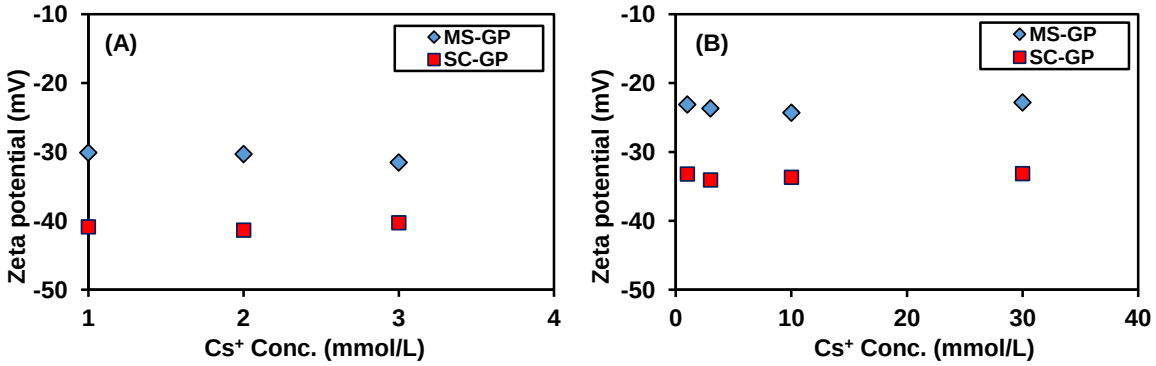

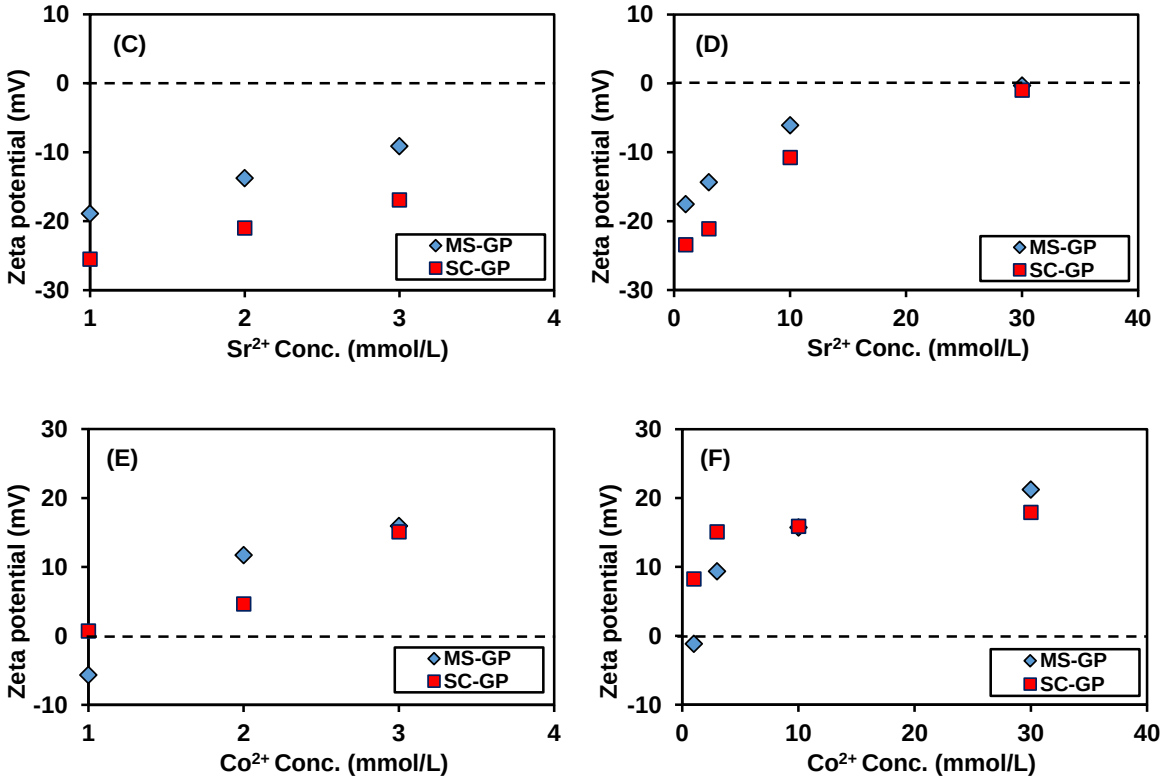


**Figure 3-4.** Zeta potential of geopolymer suspension in (A) $Cs^{+}$ solution with an ionic strength of 10 mmol/L, (B) $Cs^{+}$ solution with an ionic strength of 100 mmol/L, (C) $Sr^{2+}$ solution with an ionic strength of 10 mmol/L, (D) $Sr^{2+}$ solution with an ionic strength of 100 mmol/L, (E) $Co^{2+}$ solution with an ionic strength of 10 mmol/L, and (F) $Co^{2+}$ solution with an ionic strength of 100 mmol/L.

The measured zeta potentials in the presence of the anionic radionuclide simulant $I^{-}$, $IO_3^{-}$, $SeO_3^{2-}$, and $SeO_4^{2-}$ are independent of the anion concentration, and equal to the zeta potential in the blank solution of corresponding pH (**Figure 3-3**). These stable zeta potential results indicate that these ions do not appear to be specifically adsorbed on the surface of the geopolymers (**Figure 3-5**), consistent with the results of other researchers [41].

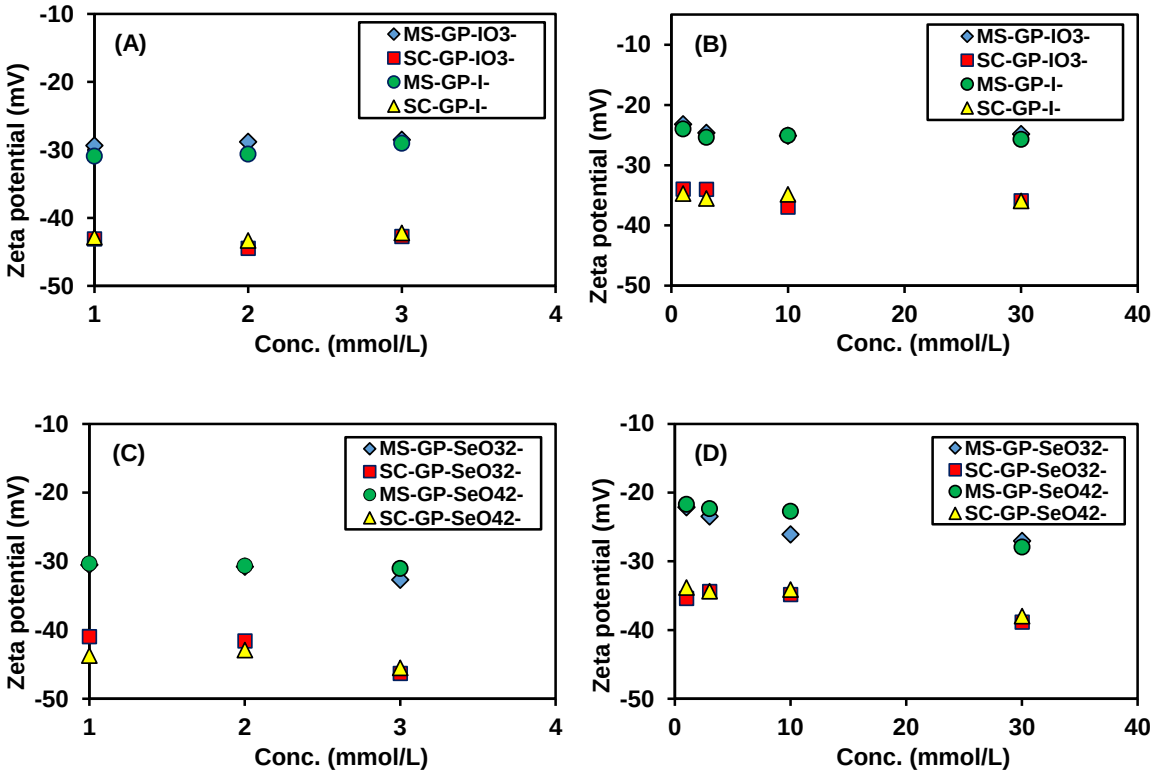


**Figure 3-5.** Zeta potential of geopolymer suspension in (A) $I^-$ or $IO_3^-$ solutions with an ionic strength of 10 mmol/L. (B) $I^-$ or $IO_3^-$ solutions with an ionic strength of 100 mmol/L. (C) $SeO_3^{2-}$ or $SeO_4^{2-}$ solutions with an ionic strength of 10 mmol/L. (D) $SeO_3^{2-}$ or $SeO_4^{2-}$ solution with an ionic strength of 100 mmol/L.

Before the evaluation of the binding of ions to the geopolymer, the time required to reach equilibrium was determined. The amount of bound $Cs^+$, $Sr^{2+}$, and $Co^{2+}$ on the SC-geopolymer as a function of time in solutions with concentrations of 2 and 4 mmol/L is shown in **Figure 3-6**. The results show that the bound amount reached 90% of the total binding in 1 d, and then slowly increased and became constant after 7 d of immersion. Similar results were obtained for each ion in the two solutions (concentrations: 2 or 4 mmol/L). Therefore, 7 d

were required to reach an equilibrium of bound ions on the geopolymer, and this is considered as the equilibration time for the binding experiment. The binding of $Cs^{+}$, $Sr^{2+}$, and $Co^{2+}$ after equilibrium for 7 d was determined, and the results are shown in **Figure 3-7 (A), (B) and (C)** as a function of concentration for both geopolymers. The total amount of bound cations on the geopolymer increased as a function of concentration, and a higher binding capacity was observed for divalent cations compared with monovalent ions. The maximum concentration of $Sr^{2+}$ (10.0 mmol/L) during the binding experiments was lower than it required for the saturation of $Sr(OH)_2$ (17.8 mmol/L) in the solution, and therefore it is believed that $Sr^{2+}$ was removed from solution only due to binding by the geopolymers. Moreover, the binding capacity of both types of geopolymers for $Sr^{2+}$ was higher than that for $Co^{2+}$. The type of metakaolin had an insignificant effect on the binding capacity. A similar experiment was conducted on anions, and the results for $I^{-}$, $IO_3^{-}$, $SeO_3^{2-}$, and $SeO_4^{2-}$ are shown in **Figure 3-7 (D), (E) (F)and (G)**. Regardless of the metakaolin type or the concentration of anions, the geopolymer does not take up any anion from the aqueous solution. This was in good agreement with the zeta potential results (**Figure 3-5**).

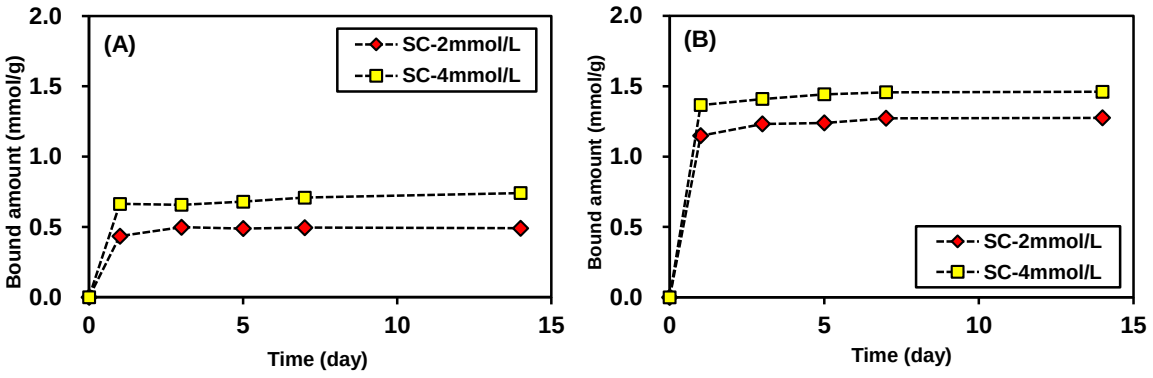

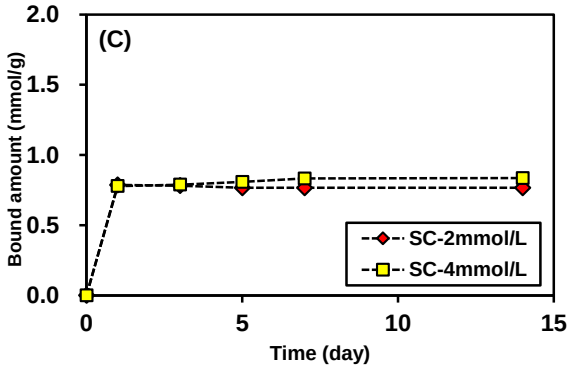


**Figure 3-6.** Binding of (A) $Cs^{+}$, (B) $Sr^{2+}$, and (C) $Co^{2+}$ on SC-geopolymer as a function of time.

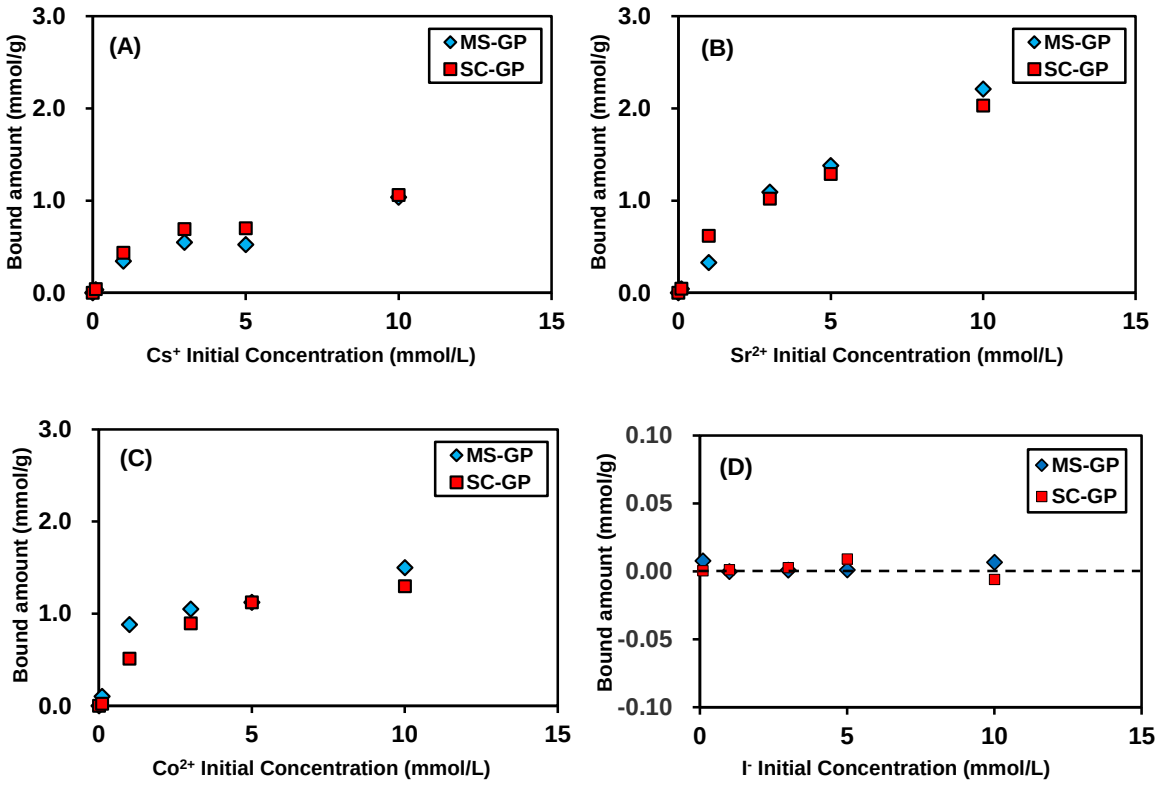

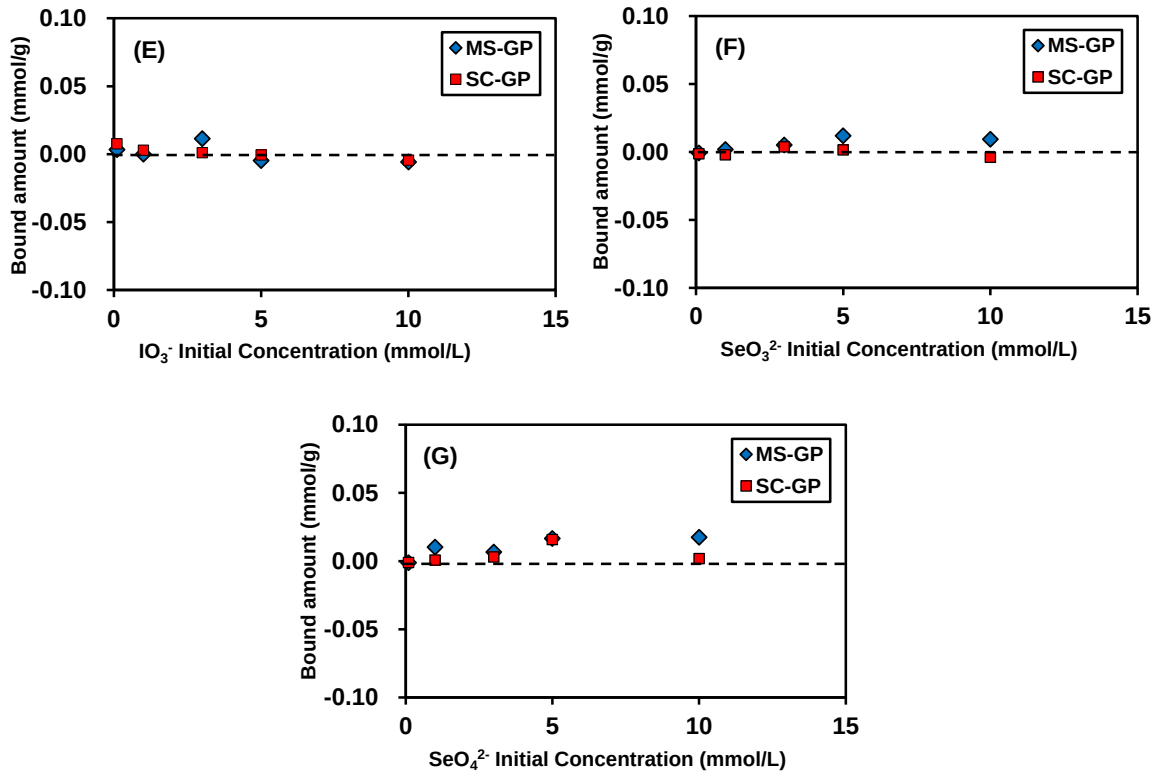


**Figure 3-7.** Binding of (A) $Cs^+$, (B) $Sr^{2+}$, (C) $Co^{2+}$, (D) $I^-$, (E) $IO_3^-$, (F) $SeO_3^{2-}$ and (G) $SeO_4^2$ on geopolymer as a function of concentration.

The geopolymer releases $K^+$ ions upon the uptake of cations from the aqueous environment, and it is important to understand the mechanisms by which this happens. To determine the $K^+$ ($A_l$) released in Eq. (2), $C_{pH}$ should be obtained from a batch of control experiments. $C_{pH}$ is the leached concentration of $K^+$ from the geopolymer in the blank solution without simulant radionuclides, and this reflects the washing-out of alkaline pore fluid from the geopolymers during the tests which is not connected to ion exchange processes. **Figure 3-8** shows that the leaching of $K^+$ from the geopolymer strongly depends on the solution's pH, where acidic and basic solutions enhance the leaching of $K^+$. According to the measured

initial pH of each cationic radionuclide solution (as marked in **Figure 3-8**), the values of the parameter $C_{pH}$ were determined to be 2.151, 0.84, and 1.498 mmol/L for $Co^{2+}$, $Cs^{+}$, and $Sr^{2+}$, respectively.

The amounts of leached $K^{+}$ and bound $Cs^{+}$, $Sr^{2+}$, and $Co^{2+}$ can be estimated from the coefficients for each ion and Eqs. (1) and (2), respectively. The relationship between the released $K^{+}$ and the bound cations is shown in **Figure 3-9**. As shown in **Figure 3-4**, the presence of $Cs^{+}$ in the solution did not affect the surface charge of the geopolymer. Furthermore, as shown in **Figure 3-9(A)**, the leaching amount of $K^{+}$ was almost equal to the binding amount of $Cs^{+}$ at each concentration. This indicates a one-to-one ion exchange process taking place between $Cs^{+}$ and $K^{+}$. Thus, the main mechanism for $Cs^{+}$ binding is ion exchange, which is consistent with the results reported in previous studies [42, 43, 44]. The same approach has been considered for $Sr^{2+}$ and $Co^{2+}$ (where one mole of divalent cation would replace two moles of $K^{+}$), and the results are shown in **Figure 3-9(B)** and **9(C)**. At low concentrations of $Sr^{2+}$, the uptake of $Sr^{2+}$ is governed by ion exchange although there is some discrepancy at 0.1 and 0.5 mmol/g of $Sr^{2+}$. However, a higher uptake of $Sr^{2+}$ than the release of stoichiometric $K^{+}$ was observed at high concentrations, which suggests that another mechanism, in addition to ion exchange, contributes to $Sr^{2+}$ binding in geopolymers. The uptake of $Co^{2+}$ and the release of $K^{+}$ was lower than that of $Sr^{2+}$ (**Figure 3-9(C)**), and the relationship between the released $K^{+}$ and bound $Co^{2+}$ was far from the y = 2x line. This implies that the binding mechanism for $Co^{2+}$ in the geopolymer is not dominated by ion exchange, as observed for $Cs^{+}$ and $Sr^{2+}$. It is worth to discuss the formation of $SrOH^{+}$ or

$CoOH^+$ ion pair, which can effectively act as a monovalent cation for one-to-one ion exchange [45, 46]. The thermodynamic speciation calculation was performed in PHREEQC under the similar condition as adopted for binding experiment, and it was found that the formation of $SrOH^+$ or $CoOH^+$ was negligible compared to $Sr^{2+}$ or $Co^{2+}$. Therefore, the deviation of leaching/binding ratio of $K^+$ to $Sr^{2+}$ and $Co^{2+}$ is attributed to charge-unbalanced ion exchange between $Sr^{2+}$ or $Co^{2+}$ and $K^+$ as well as the formation of cobalt blue in the case of $Co^{2+}$ solution. In this study, there was not a significant difference between the two types of metakaolin-based geopolymers in terms of cation binding and $K^+$ leaching.

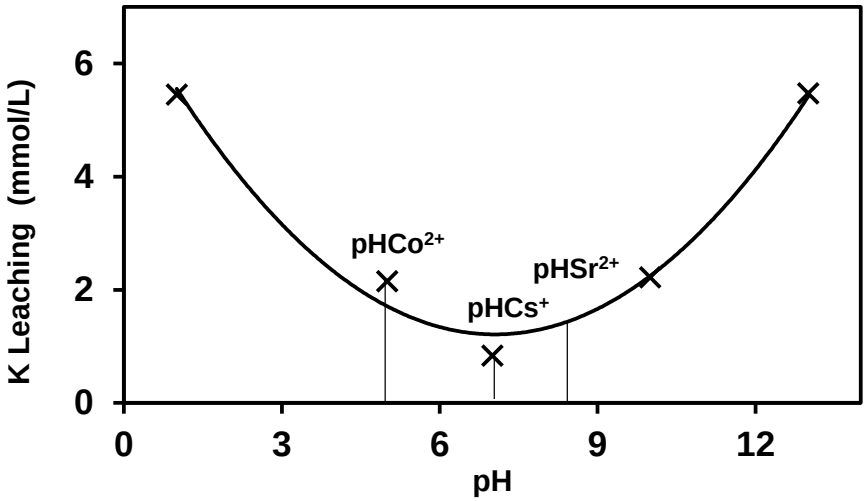


**Figure 3-8.** Leached concentration of $K^+$ from the geopolymer as a function of pH.

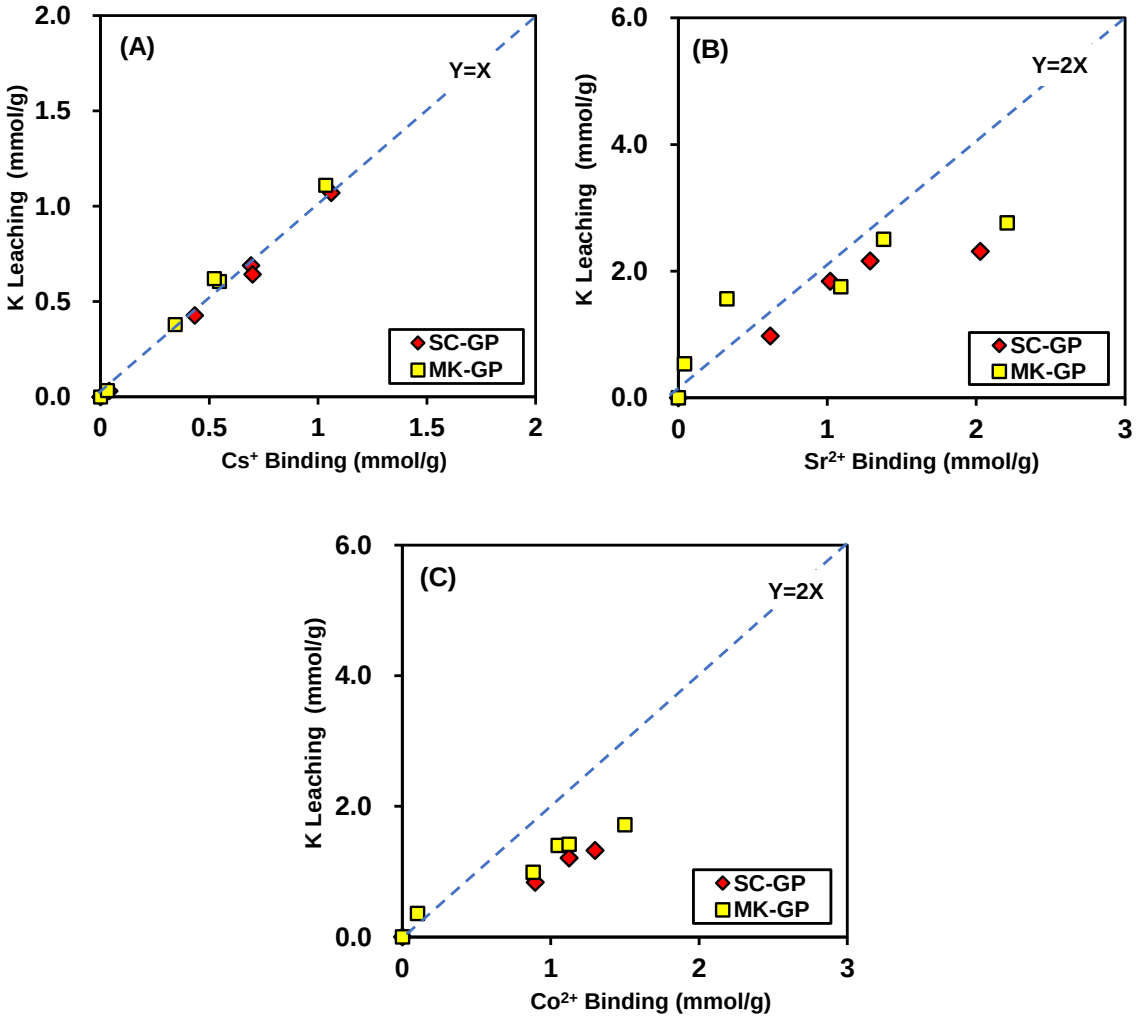


**Figure 3-9.** Relationship between released $K^+$ and bound cations for geopolymers exposed to (A) $Cs^+$, (B) $Sr^{2+}$, and (C) $Co^{2+}$.

### 3.3.3 Thermodynamic modelling and verification

The ion exchange model described in Section 3.2.3 was used to predict the binding of $Cs^+$ and $Sr^{2+}$. In the model, the equilibrium constant is the main adjustable parameter, and can be estimated by fitting the experimental results of the leaching amount of $K^+$. The fitting results

for $Cs^+$ and $Sr^{2+}$ are shown in **Figure 3-10(A) & (B)**. The type of metakaolin had no significant effect on leaching of $K^+$ (**Figure 3-9**), and thus the fitting was conducted to the two sets of data (both MK sources) all together. A high correlation between the experimental data and modelling results was obtained for both ions in the geopolymers. The estimated equilibrium constants (log_K) for the ion exchange reaction between $Cs^+$ and $K^+$, and $Sr^{2+}$ and $K^+$, were -1.275 and -2.025, respectively. **Figure 3-10(C) & (D)** shows the predicted amount of bound $Cs^+$ and $Sr^{2+}$ using the estimated log_K as a function of concentration. The model prediction shows good agreement with the experimental data for $Cs^+$, but it underestimates the experimental data at high concentrations of $Sr^{2+}$. It should be noted that the predictions are based on a pure ion exchange reaction which may not consider the complete incorporation mechanism. At low concentrations of $Sr^{2+}$, the binding can be considered as pure ion exchange: uptake of one mole of $Sr^{2+}$ releases two moles of $K^+$ (**Figure 3-9(B)**), and the proposed ion exchange model predicts the binding of $Sr^{2+}$ well. This is consistent with the results reported in previous studies [29]. At high concentrations (> 5 mmol/L), more $Sr^{2+}$ ions are incorporated compared with the predicted result due to one-to-one ion exchange and surface complexation (as shown in **Figure 3-4**), thus limiting the use of the proposed ion-exchange model. It should be noted that the concentration of $Sr^{2+}$ in the nuclear waste under discussion here (polluted water) is in the order of parts per million, and the proposed pure ion-exchange model would thus be applicable. Meanwhile, the ion exchange model performed for $Cs^+$ and $Sr^{2+}$ cannot be used for $Co^{2+}$ because its uptake is not only controlled by the ion exchange mechanism (**Figure 3-9(C)**) but also the formation of

cobalt blue and surface complexation. Therefore, it is necessary to consider other mechanisms to predict their incorporation more precisely in geopolymers.

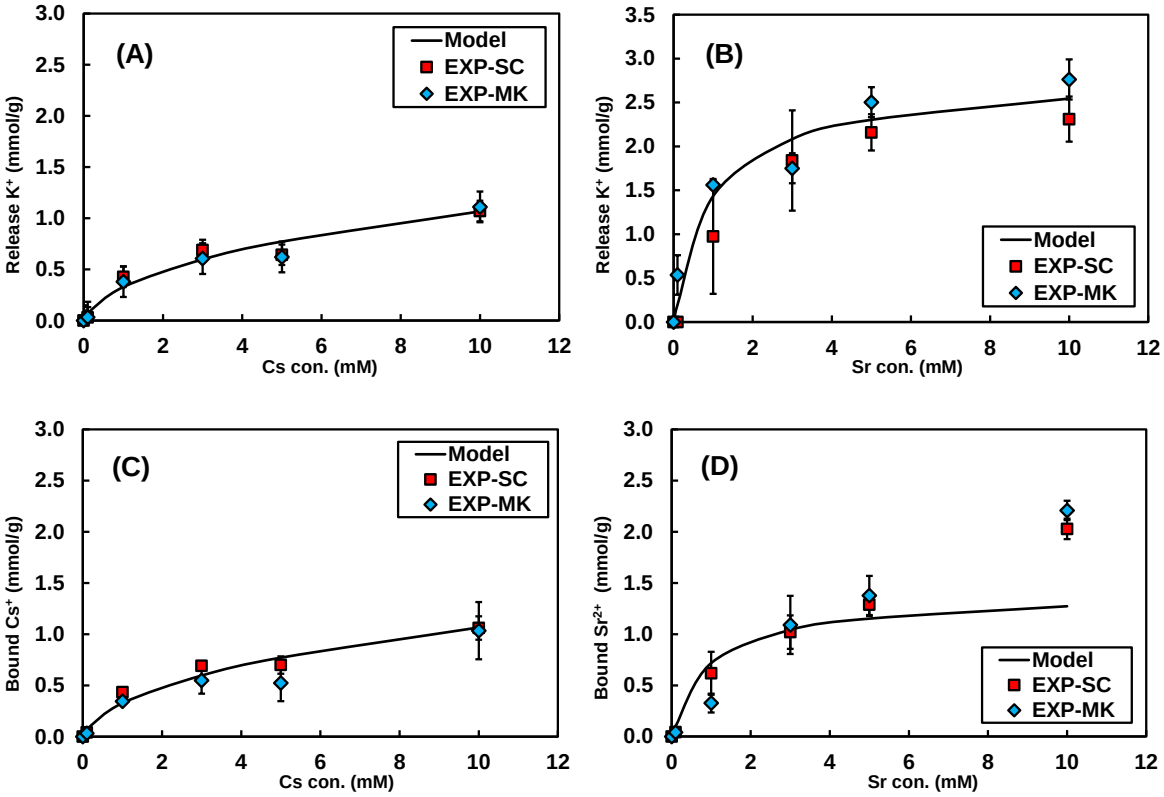


**Figure 3-10.** Fitting of experimental data with modelling results for (A) $Cs^+$ and (B) $Sr^{2+}$, and the comparison of the predicted and measured (C) $Cs^+$ and (D) $Sr^{2+}$ as a function of concentration.

## 3.3.4 Mechanism of cations binding on metakaolin-based geopolymer

The geopolymer has a three-dimensional cross-linked structure composed of $SiO_4$ and $AlO_4$-tetrahedra which share oxygen in an alternating manner. This creates a net negative charge in the framework structure, and the alkali activator ions balance the negative charge. The

constant zeta potential of the geopolymer after binding of $Cs^+$ ions (**Figure 3-4**) and a one-to-one exchange between $Cs^+$ and $K^+$ ions (**Figure 3-9(A)**) suggest that $Cs^+$ ions are incorporated by a pure ion-exchange mechanism, as illustrated schematically in **Figure 3-11(A)**. However, in the case of $Sr^{2+}$ and $Co^{2+}$, the ion exchange between $K^+$ and $Sr^{2+}$ or $Co^{2+}$ partially or fully compensated for the negative charge of the geopolymer, and eventually produced a positive charge (**Figure 3-4**). This suggests that one mole of $K^+$ may be replaced by up to one mole of $Sr^{2+}$ or $Co^{2+}$, which is significant in the $Co^{2+}$ solution as well as at high concentrations of $Sr^{2+}$ solution, wherein more $Sr^{2+}$ and $Co^{2+}$ ions are incorporated than the release of $K^+$ (**Figure 3-9**). Therefore, it is believed that both one-to-two and one-to-one ion exchanges between $K^+$ and $Sr^{2+}$ or $Co^{2+}$ occur. It has been reported that the $SrCO_3$ is the main form of $Sr^{2+}$ suppression in ion-exchanger encapsulated by geopolymer [47]. It is confirmed by thermodynamic modelling as well. However, in the present study, the carbonation of $Sr^{2+}$ in the geopolymer can be negligible and did not consider in the calculation. The binding mechanisms for $Sr^{2+}$ and $Co^{2+}$ are schematically shown in **Figure 3-11(B)** and **Figure 3-11(C),** respectively. The formation of cobalt blue also contributed to the removal of $Co^{2+}$ from the aqueous solution. As shown in **Figure 3-9(B)** and **9(C)**, the leached amount of $K^+$ from the geopolymer in the presence of $Co^{2+}$ was much lower than in the presence of $Sr^{2+}$, even at low concentrations, thus suggesting low binding of $Co^{2+}$ despite the formation of cobalt blue (**Figure 3-7**).

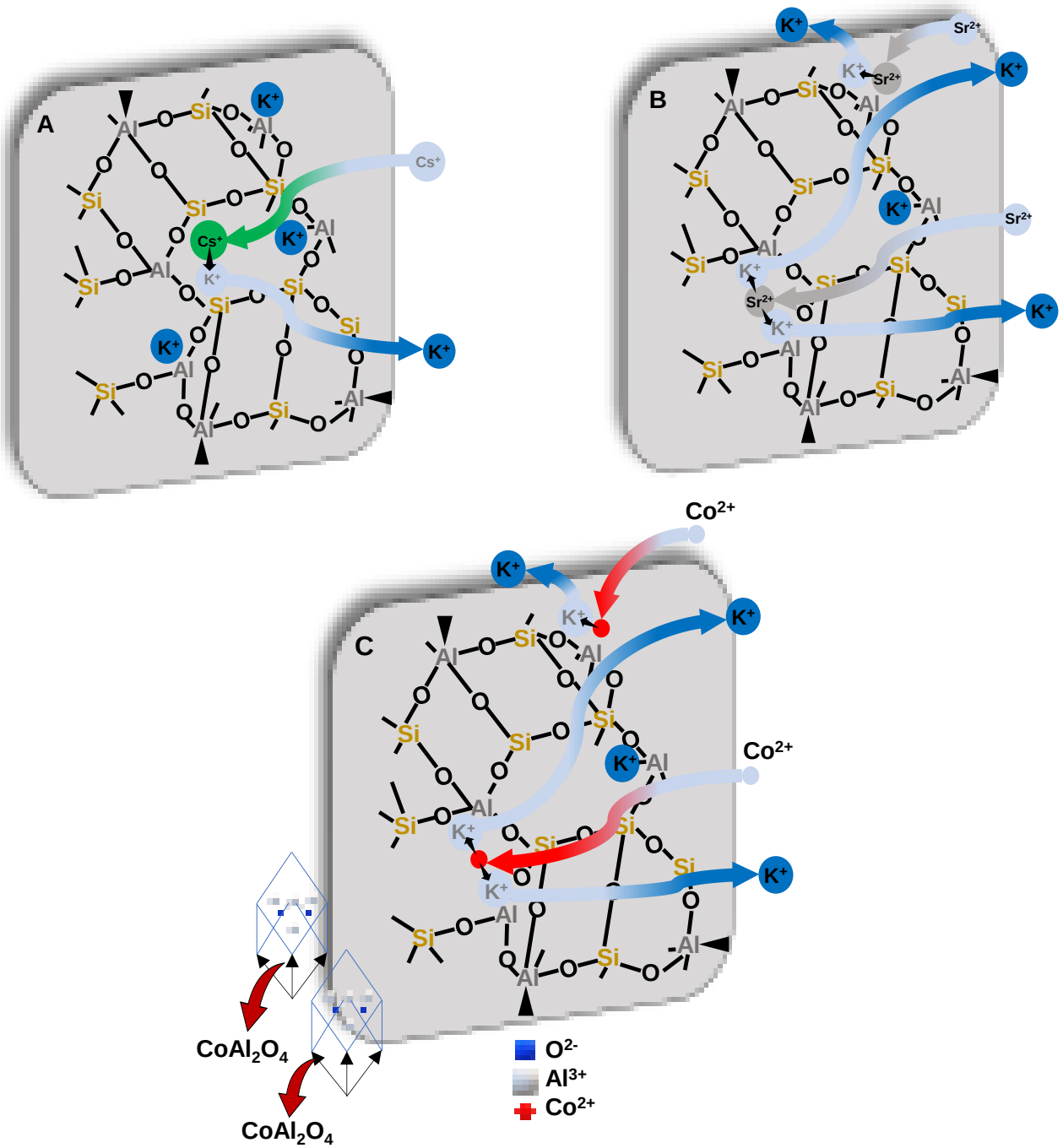


**Figure 3-11.** Proposed binding mechanism for (A) $Cs^{+}$, (B) $Sr^{2+}$, and (C) $Co^{2+}$ on geopolymer.

## 3.4 Conclusion

Metakaolin-based geopolymers with the composition of $K_2O:SiO_2:H_2O$ of 1:1:13 have a high capacity to uptake cationic radionuclides such as $Cs^+$, $Sr^{2+}$, and $Co^{2+}$; however, the geopolymer does not have the ability to directly uptake anions of $I^-$, $IO_3^-$, $SeO_3^{2-}$, and $SeO_4^{2-}$. Specific findings from this work include:

- The geopolymers framework held a permanent negative charge in an aqueous solution.
- Ion exchange is the main mechanism for the uptake of radionuclide cations, wherein a one-to-one exchange was observed between $Cs^+$ and $K^+$ whereas both one-to-two and one-to-one exchanges were possible in the cases of $Sr^{2+}$ and $Co^{2+}$. The formation of cobalt blue ($CoAl_2O_4$) also contributed to the incorporation of $Co^{2+}$.
- Thermodynamic modelling was conducted based on an ion exchange mechanism, which accurately predicts the binding behaviour of $Cs^+$ and $Sr^{2+}$ at low concentrations. However, the model requires modification such as inclusion of precipitation and non-charge balanced ion exchange mechanism for better prediction at high concentrations of $Sr^{2+}$ and $Co^{2+}$.

## References

[1] TEPCO, 2013. Basic Policy for the Contaminated Water Issue at the TEPCO's Fukushima Daiichi Nu-clear Power Station.

[2] TEPCO, n.d. Contaminated Water Treatment.

[3] INTERNATIONAL ATOMIC ENERGY AGENCY, Combined Methods for Liquid Radioactive Waste Treatment, IAEA-TECDOC-1336, IAEA, Vienna (2003).

[4] M.I. Ojovan, W.E. Lee, Glassy wasteforms for nuclear waste immobilisation, Metall. Mater. Trans., A, 2010 (2010) 837-851.

[5] M. García-Gutiérrez, T. Missana, M. Mingarro, J. Morejón, J.L. Cormenzana, Cesium diffusi-on in mortars from different cements used in radioactive waste repositories, Appl. Geochem., 98(2018) 10-16.

[6] J. Koťátková, J. Zatloukal, P. Reiterman, K. Kolář, Concrete and cement composites used for radioactive waste deposition, J. Environ. Radioact., 178–179 (2017) 147-155.

[7] G. Bar-Nes, A. Katz, Y. Peled, Y. Zeiri, The mechanism of cesium immobilisation in densified silica-fume blended cement pastes, Cem. Concr. Res., 38(2008) 667-674.

[8] K. Volchek, M.Y. Miah, W. Kuang, Z. DeMaleki, F.H. Tezel, Adsorption of cesium on cement mortar from aqueous solutions, J. Hazard. Mater., 194(2011) 331-337.

[9] M. Arbel Haddad, E. Ofer-Rozovsky, G. Bar-Nes, E.J.C. Borojovich, A. Nikolski, D. Mogiliansky, A. Katz, Formation of zeolites in metakaolin-based geopolymers and their potential application for Cs immobilisation, J. Nucl. Mater., 493(2017) 168-179.

[10] R.M. Cornell, Adsorption of cesium on minerals: a review, J. Radioanal. Nucl. Chem., 1993(1993) 483-500.

[11] W. Chen, J. Hong, C. Xu, Pollutants generated by cement production in China, their impacts, and the potential for environmental improvement, J. Clean. Prod., 103(2015) 61-69.

[12] P. Duxson, A. Fernández-Jiménez, J.L. Provis, G.C. Lukey, A. Palomo, J.S.J. Van Deventer, Geopolymer technology: the current state of the art, J. Mater. Sci., 42(2007) 2917-2933.

[13] J.L. Provis, S.A. Bernal, Geopolymers and related alkali-activated materials, Annu. Rev. Mater. Res., 44(1)(2014) 299-327.

[14] C. Shi, B. Qu, J.L. Provis, Recent progress in low-carbon binders, Cem. Concr. Res., 122(2019) 227-250.

[15] Y. Huang, M. Han, The influence of α-Al2O3 addition on microstructure, mechanical and forma-ldehyde adsorption properties of fly ash-based geopolymer products, J. Hazard. Mater., 193(2011) 90-94.

[16] Q. Li, Z. Sun, D. Tao, Y. Xu, P. Li, H. Cui, J. Zhai, Immobilisation of simulated radionuclid-e 133Cs+ by fly ash-based geopolymer, J. Hazard. Mater., 262(2013) 325-331.

[17] A. Palomo, A. Fernández-Jiménez, M. Criado, Geopolymers: same basic chemistry, different microstructures, Mater. Constr., 54(275)(2004) 77-91.

[18] Z. Ji, Y. Pei, Bibliographic and visualized analysis of geopolymer research and its application in heavy metal immobilisation: a review, J. Environ. Manag., 231(2019) 256-267.

[19] A.A. Siyal, M.R. Shamsuddin, M.I. Khan, N.E. Rabat, M. Zulfiqar, Z. Man, J. Siame, K.A. Azizli, A review on geopolymers as emerging materials for the adsorption of heavy metals and dyes, J. Environ. Manag., 224(2018) 327-339.

[20] P. Duxson, J.L. Provis, G.C. Lukey, S.W. Mallicoat, W.M. Kriven, J.S.J. Van Deventer, Understanding the relationship between geopolymer composition, microstructure and mechanical properties, Colloids Surf. A Physicochem. Eng. Asp., 269(2005) 47-58.

[21] E.H. Borai, R. Harjula, A. P. L. malinen, Efficient removal of cesium from low-level radioactive liquid waste using natural and impregnated zeolite minerals, J. Hazard. Mater., 172(2009) 416-422.

[22] E.R. Vance, D.S. Perera, 18 - Geopolymers for nuclear waste immobilisation, In Woodhead Publishing Series in Civil and Structural Engineering, Geopolymers, (2009) 401-420.

[23] W. Xu, L. Gong, W. Syltebo, Lutze, I.L. Pegg, DuraLith geopolymer waste form for Hanford secondary waste: correlating setting behaviour to hydration heat evolution, J. Hazard. Mater., 133(2014) 332-340.

[24] T. Hanzlíček, M. Steinerova, P. Straka, Radioactive metal isotopes stabilized in a geopolymer matrix: determination of a leaching extract by a radiotracer method, J. Am. Ceram. Soc., 89 (11) (2006) 3541-3543.

[25] F.J. López, S. Sugita, M. Tagaya, T. Kobayashi, Metakaolin-based geopolymers for targeted adsorbents to heavy metal ion separation, J. Mater. Sci. Chem. Eng., 02(2014), 16-27.

[26] C. Kuenzel, J.F. Cisneros, T.P. Neville, L.J. Vandeperre, S.J.R. Simons, J. Bensted, C.R. Cheeseman, Encapsulation of Cs/Sr contaminated clinoptilolite in geopolymers produced from metakaolin, J. Nucl. Mater., 466(2015) 94-99.

[27] Q. Tian, K. Sasaki, Application of fly ash-based geopolymer for removal of cesium, strontium and arsenate from aqueous solutions: kinetic, equilibrium and mechanism analysis, Water Sci. Technol., 79(2019) 2116-2125.

[28] N. Vandevenne, R.I. Iacobescu, Y. Pontikes, R. Carleer, Incorporating Cs and Sr into blast furnace slag inorganic polymers and their effect on matrix properties, J. Nucl. Mater., 503(2018) 1-12.

[29] B. Walkley, X. Ke, O.H. Hussein, S.A. Bernal, J.L. Provis, Incorporation of strontium and calcium in geopolymer gels, J. Hazard. Mater., 382(2020) 121015.

[30] B.I. El-Eswed, O.M. Aldagag, F.I. Khalili, Efficiency and mechanism of stabilization/solidification of Pb(II), Cd(II), Cu(II), Th(IV) and U(VI) in metakaolin based geopolymers, Appl. Clay Sci., 140(2017) 148-156.

[31] Y. Zhu, J. Hu, J. Wang, Removal of Co2+ from radioactive wastewater by polyvinyl alcohol (PVA)/chitosan magnetic composite, Prog. Nucl. Energy, 71 (2014) 172-178.

[32] A.M. El-Kamash, M.R. El-Naggar, M.I. El-Dessouky, Immobilisation of cesium and strontium radionuclides in zeolite-cement blends, J. Hazard. Mater., 136(2006) 310-316.

[33] L. Gomez-Zamorano, M. Balonis, B. Erdemli, N. Neithalath, G. Sant, C-(N)-S-H and N-A-S-H gels: Compositions and solubility data at 25°C and 50°C, J. Am. Ceram. Soc., 100(2017) 2700-2711.

[34] T. Williamson, L.E. Katz, J. Han, H.A. Dobbs, B.F. Chmelka, G. Sant, M.C.G. Juenger, Relationship between aqueous chemistry and composition, structure, and solubility of sodium aluminosilicate hydrates, J. Am. Ceram. Soc., 103(2020) 2160-2172.

[35] Parkhurst, B.D.L., Appelo, C.A.J., 1999. User's guide to PHREEQC (version 2) — a computer program for speciation, and inverse geochemical calculations. Exch. Organ. Behav. Teach. J. 326. D.

[36] C. Kuenzel, T.P. Neville, S. Donatello, L. Vandeperre, A.R. Boccaccini, C.R. Cheeseman, In-fluence of metakaolin characteristics on the mechanical properties of geopolymers, Appl. Clay Sci., 83–84(2013) 308-314.

[37] Thi-Chau-Duyen Le Yaru Yang, Thi-Mai-Dung Do Isamu Kudo, Hisayuki Suematsu Koichi Niihara, Gordon Thorogood, Pore-forming process in dehydration of metakaolin-based geopolymer, Int J. Ceram. Eng. Sci., 3(5)(2021) 211-216.

[38] A. Gualtieri, M. Bellotto, Modelling the structure of the metastable phases in the reaction sequence kaolinite-mullite by X-ray scattering experiments, Phys. Chem. Miner., 25(6) (1998) 442-452.

[39] D.W. Zhang, D. min Wang, Z. Liu, F. zhu Xie, Rheology, agglomerate structure, and particle shape of fresh geopolymer pastes with different NaOH activators content, Constr. Build. Mater., 187(2018) 674-680.

[40] M. Takeya, A. Ubaidah, M. Shimokawara, H. Okano, T. Nawa, Y. Elakneswaran, Crude oil/ brine/rock interface in low salinity waterflooding: experiments, triple-layer surface complexation model, and DLVO theory, J. Pet. Sci. Eng., 188(2020) 106913.

[41] A. Al-Mashqbeh, S. Abuali, B. El-Eswed, F.I. Khalili, Immobilisation of toxic inorganic anions ($Cr_2O_7^{2-}$, $MnO^{4-}$ and $Fe(CN)_6^{3-}$) in metakaolin based geopolymers: a preliminary study, Ceram. Int., 44(2018) 5613-5620.

[42] P. Sylvester, T. Milner, J. Jensen, Radioactive liquid waste treatment at Fukushima Daiichi, J. Chem. Technol. Biotechnol., 88(2013) 1592-1596.

[43] Q. Tian, K. Sasaki, A novel composite of layered double hydroxide/geopolymer for co-immobilisation of $Cs^+$ and $SeO_4^{2-}$ from aqueous solution, Sci. Total Environ., 695(2019) 133799.

[44] J.L. Bell, P.E. Driemeyer, W.M. Kriven, Formation of ceramics from metakaolin-based geopolymers: Part I - Cs-based geopolymer, J. Am. Ceram. Soc., 92(2009) 1-8.

[45] H. Arcis, G.H. Zimmerman, P.R. Tremaine, Ion-pair formation in aqueous strontium chloride and strontium hydroxide solutions under hydrothermal conditions by AC conductivity measurements, Phys. Chem. Chem. Phys., 1(2014) 7688-17704.

[46] A. Coates Rebecca, P.B. Armentrout, Binding energies of hydrated cobalt hydroxide ion complexes: a guided ion beam and theoretical investigation, J. Chem. Phys., 147(2017) 064305.

[47] X. Ke, A.B. Susan, T. Sato, J.L. Provis, Alkali aluminosilicate geopolymers as binders to encapsulate strontium-selective titanate ion-exchangers, Dalton Trans., 48(2019) 12116-12126.

# CHAPTER 4

## DEVELOPMENT OF METAKAOLIN-BASED GEOPOLYMER FOR SELENIUM OXYANIONS UPTAKE THROUGH IN-SITU ETTRINGITE FORMATION

## 4.1 Introduction

Selenium (Se) is a widely occurring oxyanion-forming element. While it is considered a vital trace mineral in biological systems, it can pose a significant environmental and health hazard when its concentration surpasses certain levels. The aggregation of Se in high concentrations can be attributed to anthropogenic activities, and its cytotoxicity and carcinogenicity in animals have been demonstrated [1]. Among the various sources of Se aggregation, the nuclear industry is a particularly noteworthy contributor, as it has the potential to generate substantial amounts of the anionic radionuclide $^{79}Se$. This isotope, $^{79}Se$, is linked to fission, reprocessing, and accidents within the nuclear industry [2]. It is considered to be a high-priority radionuclide due to its long half-life of nearly $3.27 \times 10^5$ years and the presence of highly mobile oxidised forms, selenite ($SeO_3^{2-}$) and selenate ($SeO_4^{2-}$), which are regarded as particularly challenging species due to their high mobility in aqueous environments and severe toxicity [3,4]. Numerous techniques have been developed to mitigate the presence of selenium in wastewater effectively. Uptake methods utilising easily accessible sorbents, such as activated carbon, zeolites, resins, and iron-based materials, have demonstrated remarkable efficacy in removing selenium. These techniques have been successfully employed in the treatment of wastewater following the Fukushima Daiichi nuclear power plant accident [5,6,7,8,9]. In addition, emerging technologies such as membrane filtration [10], electrochemical processes [11,12], cationic layered rare earth hydroxide (LRHs) [13], tailored cationic polymeric [14], and cationic metal organic frameworks [15,16] have great potential for the effective immobilisation of many radioactive anions, including selenium

oxyanions. However, it is crucial to acknowledge that these treatment approaches may lead to accumulating medium to high concentrations of selenium aggregates, posing a potential risk of secondary contamination [17]. Hence, it is imperative to promptly develop encapsulate materials with low water solubility to ensure the formation of stable phases. Such materials can effectively immobilise selenium oxyanions and securely isolate selenium-bearing contaminants for long-term disposals, such as geological disposal [9].

Geopolymer materials (GP) are a well-known class of alkaline-activated materials. The geopolymerisation process can be succinctly described as the depolymerisation, polycondensation, and gel network formation of an aluminosilicate precursor in the presence of a strongly alkaline solution or activator [18,19]. As an alternative to Portland cement that is under assessment for nuclear waste management, the use of geopolymer has garnered interest worldwide [20]. Compared to conventional cementitious materials, the three-dimensional framework structure derived from oxygen-linked aluminium and silicon and the higher degree of silicate polymerisation, yield geopolymer materials with superior chemical durability [21,22].

The use of metakaolin-based geopolymers as a potential matrix for managing radionuclide-containing waste generated from the nuclear industry has received significant attention in recent years [23,24]. The nuclear industry is known to produce large quantities of contaminated wastewater containing radionuclides from various sources such as operation, maintenance, and accidents [2,25]. Extensive research has been conducted to explore the capabilities of metakaolin-based geopolymers as a disordered pseudo-zeolite for the

immobilisation of radionuclides. In their spatial structure, the tetrahedral aluminum sites present possess a negative charge, which can be effectively neutralised by alkali cations derived from activator solutions [26]. These negative sites impart a permanent net negative framework charge to the metakaolin-based geopolymers, creating many sites capable of binding cations [27]. The uptake behaviour of metakaolin-based geopolymers for heavy metal ions has been confirmed and studied extensively [28,29]. These geopolymers have also demonstrated remarkable efficiency in immobilising $^{137}Cs$ and $^{90}Sr$, which are the most prevalent cationic radionuclides found in water contaminated by nuclear activities [30-33]. In our previous study [33], the mechanisms of $^{137}Cs$, $^{90}Sr$ and $^{60}Co$ uptake by metakaolin-based geopolymers were clarified, and a thermodynamic model based on ion exchange mechanisms was proposed. However, the permanently negatively charged surface of metakaolin-based geopolymers restricts the potential for uptake of anionic radionuclides such as selenium ($^{79}Se$) or iodine ($^{131}I$). Hence, modifying the composition of metakaolin-based geopolymers to endow them with both cations and anions uptake capacities while retaining their chemical stability remains a topic of great interest in the field.

Ettringite ($3CaO{\cdot}Al_2O_3{\cdot}3CaSO_4{\cdot}32H_2O$) can be found as a naturally occurring mineral and is also one of the hydration products of Portland cement. It predominantly forms during the initial stages of cement hydration through the reaction between aluminate and sulphate, which can either be naturally present in the cement paste or intentionally added to the system [34]. Ettringite possesses a column-like structure wherein the $Al(OH)_6^{3-}$ octahedral units are interconnected with three adjacent Ca atoms. Each Ca atom demonstrates square antiprismatic coordination, involving eight surrounding entities consisting of 4 $H_2O$ ($-OH_2$)

molecules and 4 $OH^-$ ions. Notably, the $OH^-$ ions are shared between the $Al(OH)_6^{3-}$ octahedra and the Ca-$O_8$ square antiprismatic polyhedra, facilitating their structural connectivity [35]. The column-like structure saturated with sulphate ions and water molecules, and these columns are held together by the electrostatic attraction of the occupying species [36]. The abundant exchangeable sulphate ($SO_4^{2-}$) species in the inter-channels of its column-like structure endow ettringite with a remarkable capacity for anion exchange [37,38]. For this reason, ettringite has been extensively studied for its ability to immobilise selenium oxyanions. Solem-Tishmack et al. [39] found that ettringite derived from high-calcium coal combustion by-products can effectively adsorb Se oxyanions from aqueous solutions. Zhang et al. [40] reported that ettringite demonstrates a higher adsorption capacity for Se oxyanions than does hydrocalumite, which represents another family of hydrous calcium aluminates that is often observed among cement hydration products. Gou et al. found that ettringite can immobilise $SeO_4^{2-}$ through the formation of $SeO_4^{2-}$ -substituted ettringite, while it can immobilise $SeO_3^{2-}$ through a ligand exchange with the Ca-$OH_2$ at the edges of its channels, forming an inner sphere complex [41,42]. Moreover, ettringite can form in environments that are alkaline and rich in calcium, aluminium, and sulphur. Thus, it is feasible to form ettringite during aluminium-rich, alkali-activated reactions (geopolymerisation) in the presence of calcium and sulphur-rich additives, such as slag [43,44], which hold the potential for immobilising hazardous waste [45].

Several studies have examined ettringite formation in geopolymers made from multi-aluminosilicate precursor sources [46,47]. Few researchers also explored the potential of geopolymers based on different precursors to adsorb or immobilise anions including $I^-$,

$AsO_4^{3-}$ and $Cr_2O_7^{2-}$ [48,49]. Tian et al. [50] developed the uptake capability for Se oxyanions using layered double hydroxides (LDHs) based on geopolymer gel. However, to our knowledge, the effectiveness of incorporating ettringite into metakaolin-based geopolymers for the immobilisation of selenium oxyanions has not been reported and studied in detail.

The present study addresses this gap by synthesising and evaluating a metakaolin-based geopolymer with in-situ ettringite. The capacity and feasibility of ettringite to uptake Se oxyanions were evaluated through aqueous co-precipitation experiments, and the uptake mechanism of the modified ettringite-in-situ geopolymers was explored through a binding experiment. A combination of X-ray diffraction (XRD), zeta potential, scanning electron microscopy (SEM), and Raman spectroscopy was used to evaluate the solid-phase characteristics, while inductively coupled plasma mass spectrometry (ICP-MS) and ion chromatography (IC) were used to analyse the aqueous phase. Finally, a thermodynamic model was developed to understand selenite uptake in both synthetic ettringite and modified geopolymer with in-situ ettringite. This comprehensive analysis provides valuable insights into the synthesis of ettringite-in-situ metakaolin-based geopolymers and their ability to uptake Se oxyanions.

## 4.2 Experimental

### 4.2.1 Materials

Metakaolin obtained from Sobueclay (Japan), tricalcium aluminate (Taiheiyo Consultancy, Japan. $3CaO{\cdot}Al_2O_3$, abbreviated as $C_3A$), gypsum (WAKO, 98 wt.%, $CaSO_4{\cdot}2H_2O$,

abbreviated as Gyp), and ground granulated blast furnace slag (Ceramento A, Taiheiyo Cement Sales Co., Ltd., Japan) were used for the synthesis of geopolymer with in-situ ettringite. The chemical composition of metakaolin and slag determined by X-ray fluorescence (XRF) is listed in **Table 4-1**. The calcium content (in the form of CaO) in slag is approximately 0.01032 mol/g, and the molar ratio of $SiO_2$:$Al_2O_3$ of metakaolin is 1.01. An aqueous potassium silicate solution (WAKO, originally containing 29.1 wt.% $SiO_2$, 21.9 wt.% $K_2O$, 49.0 wt.% $H_2O$), a potassium hydroxide (WAKO, 86 wt.% KOH), and ultrapure water (TRUSCO, Japan) were used for making a potassium silicate alkali solution, which was used as an activator for the synthesis of geopolymers. $Al_2(SO_4)_3 \cdot 16\text{-}18H_2O$ and $Ca(OH)_2$ were used to synthesise ettringite. In addition, $K_2SeO_3$, $K_2SeO_4$ and $Sr(NO_3)_2$ were selected as the simulated radionuclide sources, purchased from WAKO (Japan).

**Table 4-1**. Chemical composition (wt%) of the metakaolin and slag as determined by X-ray fluorescence.

| Component | Metakaolin | Slag |
|---|---|---|
| $SiO_2$ | 48.59 | 23.43 |
| $Al_2O_3$ | 43.11 | 10.85 |
| $Fe_2O_3$ | 0.54 | 0.50 |
| CaO | 0.21 | 51.70 |
| MgO | 3.66 | 4.11 |
| $Na_2O$ | 2.25 | 2.54 |
| $K_2O$ | 0.13 | 0.62 |

| | | |
|---|---|---|
| $TiO_2$ | 1.27 | 0.51 |
| $P_2O_5$ | 1.08 | 1.23 |
| SO3 | - | 4.00 |
| L.O.I.* | 1.74 | 2.40 |

*: L.O.I. is loss on ignition at 1100℃ for 12h [33,57].

### 4.2.2 Ettringite synthesis and co-precipitation

The process for the ettringite synthesis with and without Se oxyanions is shown in **Figure 4-1(a)**. Initially, 10 mmol/L $Al_2(SO_4)_3 \cdot 16\text{-}18H_2O$ and 60 mmol/L $Ca(OH)_2$ were mixed with water at a liquid/solid ratio of 10 to give a $Ca^{2+}$ / $SO_4^{2-}$ molar ratio of 2. The suspension was continuously magnetically stirred for 24 hours at room temperature, followed by vacuum filtration and then drying at 40 ℃ for one day. In addition, co-precipitation of ettringite in the presence of Se oxyanions was conducted. The raw materials for the ettringite formation of 10 mmol/L $Al_2(SO_4)_3 \cdot 16\text{-}18H_2O$ and 60 mmol/L $Ca(OH)_2$ were introduced into 100 mL $K_2SeO_3$ or $K_2SeO_4$ aqueous solution, where the concentration of Se oxyanions was from 0 to10 mmol/L. Experimental groups in the presence of geopolymers were also set up in co-precipitation experiments. The synthetic geopolymer was added at a ratio of 1 g per 100 mL solution (**Figure 4-1(b)**), and they were subsequently mixed using a magnetic stirrer for 24 hours at room temperature. Then, the solid and liquid phases were separated by vacuum filtration for further analysis. All co-precipitation reactions were carried out in nitrogen-filled PE bottles to avoid $CO_2$ contamination. **Table 4-2** summarises the components included in

each group. In addition, all solid samples were dried at 40 °C for 24h in a thermostat before being ground to a particle size of less than 150μm.

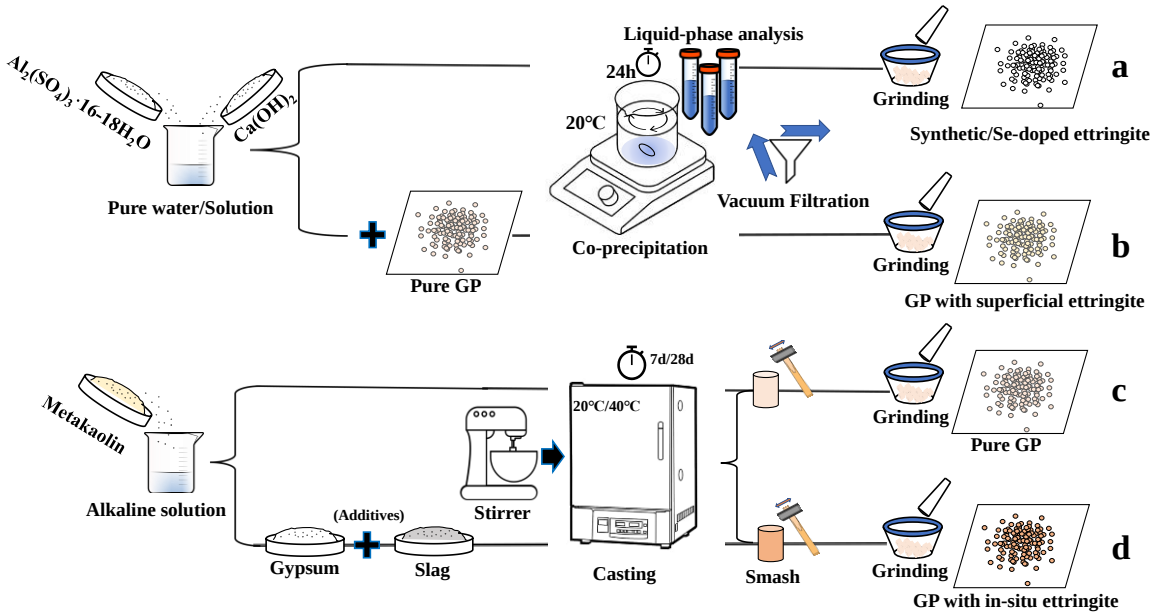


**Figure 4-1.** Schematic illustration of the procedure to conduct the co-precipitation experiment and to prepare the samples of **(a)** synthetic/Se-doped ettringite, **(b)** geopolymer with superficial ettringite, **(c)** pure geopolymers and **(d)** geopolymers with in-situ ettringite.

**Table 4-2.** Components contained in each group of co-precipitation experiment.

| Groups | $SeO_3^{2-}$ | $SeO_4^{2-}$ | Ettringite (raw material) | Geopolymer |
|---|---|---|---|---|
| 1. $SeO_4$-AFt-GP | | ✓ | ✓ | ✓ |
| 2. $SeO_4$-AFt | | ✓ | ✓ | |

| | | | |
|---|---|---|---|
| 3. $SeO_3$-AFt-GP | ✓ | ✓ | ✓ |
| 4. $SeO_3$-AFt | ✓ | ✓ | |

✓ indicates the presence of the component.

### 4.2.3 Ettringite in-situ geopolymer synthesis

The alkali-activated solution for synthesising the geopolymers samples was prepared from potassium silicate solution, potassium hydroxide and ultrapure water. **Figure 4-1(c)** and **Figure 4-1(d)** demonstrate the synthesis procedure of pure geopolymers and modified geopolymers with in-situ ettringite, respectively. Pure geopolymers were prepared by mechanically mixing stoichiometric amounts of metakaolin with a sufficient quantity of alkali-activated solution (**Figure 4-1(c)**), giving a final chemical composition of geopolymers (in ceramist nomenclature) of $1K_2O$: $1Al_2O_3$ :$1SiO_2$: $13H_2O$. The detailed synthesis procedure, the preparation of materials and the curing method were reported in our previous study [33]. Various additives such as $C_3A$, Gyp and blast furnace slag with different doses and curing conditions were tested to form the in-situ ettringite in geopolymer (**Table 4-3**). For simplicity, the samples were named according to the additives and the content added to the system. For instance, Gyp 10 wt% + 3Slag corresponds to the sample synthesised by externally adding 10 wt% gypsum and slag, the amount of slag added was determined as the molar amount of calcium in the slag was three times the molar amount of sulphate in added gypsum. After curing under specified conditions, the samples were characterised by XRD to identify ettringite formation. The only group for which in-situ ettringite could be detected

was Gyp 10 wt% + 3Slag, that had been kept at either 20 or 40 ℃ for 28 days.

**Table 4-3.** Compositions and conditions adopted for the formation of in-situ ettringite in geopolymer.

| Specimens with different additives | 20℃ 7 days | 20℃ 28 days | 40℃ 7 days | 40℃ 28 days |
|---|---|---|---|---|
| 1. Synthetic ettringite | | | | × |
| 2. Ettringite raw materials: $Al_2(SO_4)_3 \cdot 16\text{-}18H_2O$ and $Ca(OH)_2$ | | | | × |
| 3. $C_3A$ 5 wt% + Gyp 5wt% | | | × | × |
| 4. $C_3A$ 5wt% + Gyp 5wt% + 1Slag | | | × | × |
| 5. $C_3A$ 5wt% + Gyp 10wt% | | | × | × |
| 6. $C_3A$ 5wt% + Gyp 10wt% + 1Slag | | | × | × |
| 7. $C_3A$ 10wt% + Gyp 5wt% | | | × | × |
| 8. $C_3A$ 10wt% + Gyp 10wt% | | | × | × |
| 9. Gyp 5wt% | | | | × |
| 10. Gyp 5wt% + 1Slag | | | | × |
| 11. Gyp 5wt% + 3Slag | | × | × | × |
| 12. Gyp 5wt% + 5Slag | | × | | × |
| 13. Gyp 10wt% | | | | × |
| 14. Gyp 10wt% + 1Slag | | × | | × |
| 15. Gyp 10wt% + 3Slag | × | ✓ | × | ✓ |

×: No Ettringite was detected by XRD ; ✓: Ettringite was detected by XRD

### 4.2.4 Experimental procedure

A X-ray diffractometer (MultiFlex, Rigaku, Japan) was used to characterise the synthetic samples with CuKα radiation, scanning from 2θ=5-45° with a scan speed of 6.5° per min and a step size of 0.02°. The microstructure of the geopolymer with in-situ ettringite was examined by scanning electron microscopy (SEM: JSM-IT200, JEOL, Japan) with a 25kV acceleration voltage. A zeta potential & particle size analyser apparatus (ELSZ-1000ZS) was used to measure the zeta potential of the suspensions where the solid/liquid ratio of suspension was set to 1 g/L. In each case, $KNO_3$ was selected to adjust the ionic strength, whereas KOH was used to adjust the pH. The Raman spectra of the samples, including the structural variation of synthetic ettringite and geopolymer with in-situ ettringite after uptake of $SeO_3^{2-}$, were obtained using an XploRA PLUS Confocal Raman Microscope (HORIBA, Japan). The experimental parameters applied were a laser power of 532 nm, an x50 VIS objective lens, a 50-100% filter, a 100 μm slit, a 300 μm hole, an 1800 grating (450-850 nm), a measurement time of 40 seconds, and 6 accumulations. The water content change in ettringite samples after uptake of $SeO_3^{2-}$ was examined by a TG/DTA7220 (SEIKO, Japan), and the analysis was conducted by gradually increasing the temperature from 20 ℃ to 800 ℃ at a rate of 10 ℃/min, while maintaining a nitrogen flow rate of 200 mL/min. The suspensions of ettringite were equilibrated with 0.01, 0.1, 1, and 10 mmol/L of $K_2SeO_3$ and $K_2SeO_4$ solutions to measure the equilibrium time for the uptake of ions by ettringite (1g synthetic ettringite powder per 100 mL solution). After 7, 14, 21 and 35 days of immersion, the solution was filtered using a syringe filter (0.45 μm), and the concentrations of Se

oxyanions were assessed using inductively coupled plasma-mass spectrometry (ICP-MS, iCap Q ICP-MS, Thermo Scientific, USA, detection limit 0.01-10ppb), with the application of Yttrium internal standard method. A batch of binding experiments of synthetic ettringite and modified geopolymer with in-situ ettringite were performed with $K_2SeO_3$ solutions at 0.01, 0.05, 0.1, 0.5, 1, 5, and 10 mmol/L with an ettringite (in-situ ettringite) to solution ratio of 1g/100 mL. After equilibration, the liquid phase was filtered with a 0.45 μm syringe filter. The concentrations of Se oxyanions in the filtered solution were measured by ICP-MS, and the concentrations of $SO_4^{2-}$ were measured through ion chromatography (ICS-90, DIONEX, USA). In addition, the uptake capacity of geopolymer with in-situ ettringite for $Cs^+$ and $Sr^{2+}$ with in-situ ettringite was measured in the same way as given in our previous study [33]. It is important to note that a glove box filled with $N_2$ gas and a sealed wide-mouth flask were employed in the experiment. Therefore, the influence of oxygen was negligible. In addition, the redox state regions expressed by Eh-pH according to the boundary conditions set in terms of pH and initial concentration of $SeO_3^{2-}$ are shown in **Fig. S4-1**. The result illustrates that all the data points fall within the range dominated by $SeO_3^{2-}$. Hence, the oxidation of $SeO_3^{2-}$ to $SeO_4^{2-}$ in this study was found to be insignificant. Furthermore, it is known that $SeO_4^{2-}$ represents the highest oxidation state of selenium and is considerably more stable compared to $SeO_3^{2-}$, and it will rarely be actively reduced to $SeO_3^{2-}$ in the absence of a suitable reducing agent [51]. Given this understanding, it can be inferred that throughout this study, $SeO_3^{2-}$ and $SeO_4^{2-}$ retained their respective oxidation states without undergoing any notable redox reactions.

The amounts of bound Se oxyanions and leached $SO_4^{2-}$ were calculated by Eqs. 4.1 and 4.2:

$$A_B = \left(C_{Se\_i} - C_{Se}\right)\frac{V}{m}\ (mmol/g) \quad (4.1)$$

$$A_L = \left(C_S - C_{S\_b}\right)\frac{V}{m}\ (mmol/g) \quad (4.2)$$

The distribution ratio ($R_d$) was determined from Eq. 4.3:

$$R_d = A_B / C_{Se\_i}\ (L/g) \quad (4.3)$$

where $A_B$ is the bound amount of the Se (mmol/g), $A_L$ is the leached amount of $SO_4^{2-}$ (mmol/g), $C_{Se\_i}$ is the Se initial concentration (mmol/L), $C_{Se}$ is the equilibrium concentration of the Se (mmol/L), $C_S$ is the equilibrium concentration of $SO_4^{2-}$ (mmol/L), and $C_{S\_b}$ is the $SO_4^{2-}$ concentration when the synthetic ettringite or geopolymer with in-situ ettringite is immersed in pure water until reaching equilibrium (mmol/L). $V$ is the volume of the liquid phase (L), and $m$ is the mass (g) of the crystalline ettringite detected by XRD.

### 4.2.5 Modelling approach

The ion-exchange reaction between synthetic ettringite or in-situ ettringite and radionuclide anions of $SeO_3^{2-}$ was fitted and explained based on the ion-exchange module available in the geochemical code PHREEQC Version 3 [52]. The activity coefficients were calculated based on the extended Debye–Huckel equation, whose parameters are available in the database of WATEQ4F.dat [53]. The simulant radionuclide anion $SeO_3^{2-}$ can be exchanged with the $SO_4^{2-}$ present in the ettringite interlayers as:

$$Xg - SO_4 + {SeO_3}^{2-} \leftrightarrow Xg - SeO_3 + {SO_4}^{2-},\ Log_k = \frac{[Xg-SeO_3][{SO_4}^{2-}]}{[Xg-SO_4][{SeO_3}^{2-}]} \quad (4.4)$$

where $Xg$ are the exchange sites, simplifying the representation of ettringite interlayers. $Log_k$ is the exchange coefficients for $SeO_3^{2-}$. The module can be implemented in PHREEQC using the keyword data block of EXCHANGE_MASTER_SPECIES, EXCHANGE_SPECIES, and EXCHANGE. Also, the keyword data block of PHASES and EQUILIBRIUM_PHASES was used to introduce the ettringite phase into the reaction to simulate the pH changes and the $SO_4^{2-}$ environment in the solution. To obtain the best-fitting $Log_k$, a Python-coded loop was implemented to continuously adjust the parameter $Log_k$ in incremental steps. This iterative process involved comparing the quality of the fit controlled by $Log_k$ with the experimental data until the desired level of accuracy is achieved.

## 4.3 Results and discussion

### 4.3.1 Characterisation

X-ray diffraction (XRD) measurements were conducted to characterise the formation of in-situ ettringite in modified geopolymers. **Figure 4-2** shows the XRD patterns of pure geopolymer, synthetic ettringite, and geopolymer with in-situ ettringite cured at 20 ℃ and 40 ℃ for 28 days. A small amount of gypsum was found as an impurity in the synthetic ettringite, less than 2 % as determined using a corundum internal standard. The synthetic geopolymer XRD pattern exhibits a broad hump in the range of 2θ = 27°-29°, indicating disordered products. A faint signal of quartz was also detected in the XRD pattern of pure geopolymer, attributed to a very minor impurity in the metakaolin used. These findings are in line with earlier investigations on metakaolin-based geopolymers [33]. The characteristic

peaks of ettringite were detected in the XRD pattern of the geopolymer samples with in-situ ettringite; however, the presence of peaks of potassium sulphate was also identified, which could be a result of the precipitation of saturated sulphate with potassium ions in the pore solution of the geopolymer. It is believed that the presence of the sulphate ions would favour the formation of in-situ ettringite, although there may be some delay in this process [54]. The sample containing Gyp 10 wt% + 3Slag-40°C exhibited a significantly stronger ettringite peak, measuring 2.65% according to the internal standard method. Additionally, a calcite peak was observed in this sample, unlike in the Gyp 10% + 3Slag-20°C sample. These findings indicating that a relatively higher temperature favours crystallisation of these crystals and that the higher temperature used here is sufficiently low not to induce thermal destabilisation of the ettringite.

**Figure 4-3** shows the SEM images of pure geopolymers, synthetic ettringite and the Gyp 10 wt% + 3Slag-40°C samples. These images provide insights into the significant morphological changes prior and after in-situ ettringite formation in geopolymers. An amorphous geopolymer matrix is shown in **Figure 4-3 (a)**, the EDS analysis of which indicates that its main constituent elements are O, Al, Si in the structural and K balancing the negative charge sites. The characteristic needle-like hexagonal crystal structure of ettringite is clearly depicted in **Figure 4-3 (b)**. Notably, the EDS analysis reveals a slight elevation of approximately 3.5% in the S and Ca as compared to the anticipated theoretical values. This discrepancy can likely be attributed to the presence of $CaSO_4$ impurities, which may have influenced the detection results. Moving on to the modified geopolymers shown in **Figure 4-3 (c)**, the presence of in-situ ettringite embedded within the geopolymer matrix is evident.

The EDS analysis performed at specific points confirms the corresponding elemental composition of the substances. Although Ca was detected in the geopolymer matrix and Si in the in-situ ettringite, this occurrence might be attributed to their interaction during the detection process. Significantly, the in-situ ettringite within the geopolymer matrix is not observed in aggregated clusters, as typically observed in cementitious materials [55]. Instead, it appears as a distinct crystal structure, embedded within the geopolymer matrix. This phenomenon is likely a consequence of the electrostatic attraction between the positive charge on the surface of ettringite and the negative charge of the geopolymer matrix. This electrostatic interaction is further addressed in the subsequent sections of this paper, specifically in the discussion on zeta potential. It is therefore hypothesised that the in-situ ettringite present in the geopolymer matrix may have distinct properties compared to synthetic ettringite.

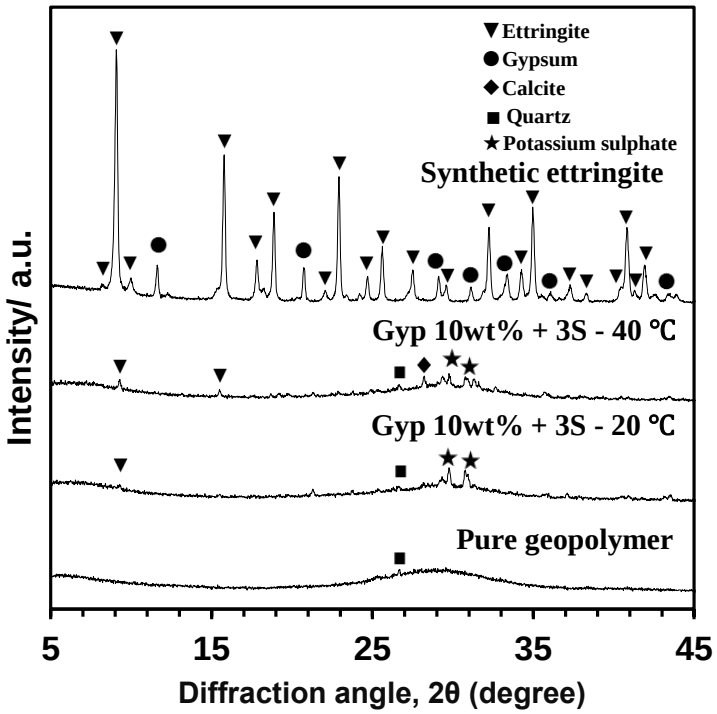


**Figure 4-2.** X-ray diffraction (XRD) patterns of synthetic ettringite, pure and modified geopolymers.

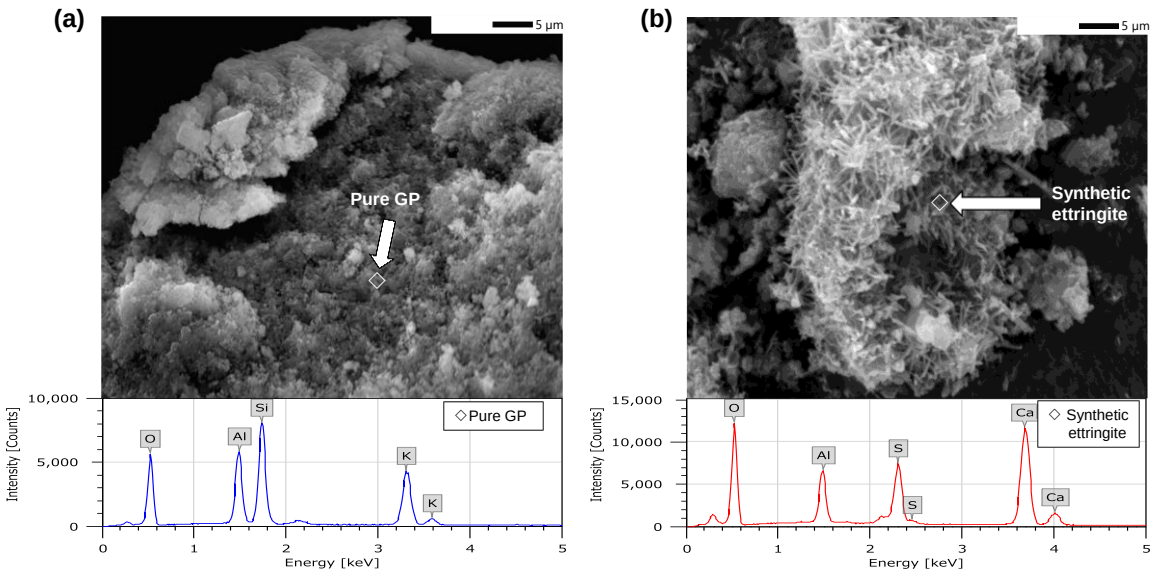

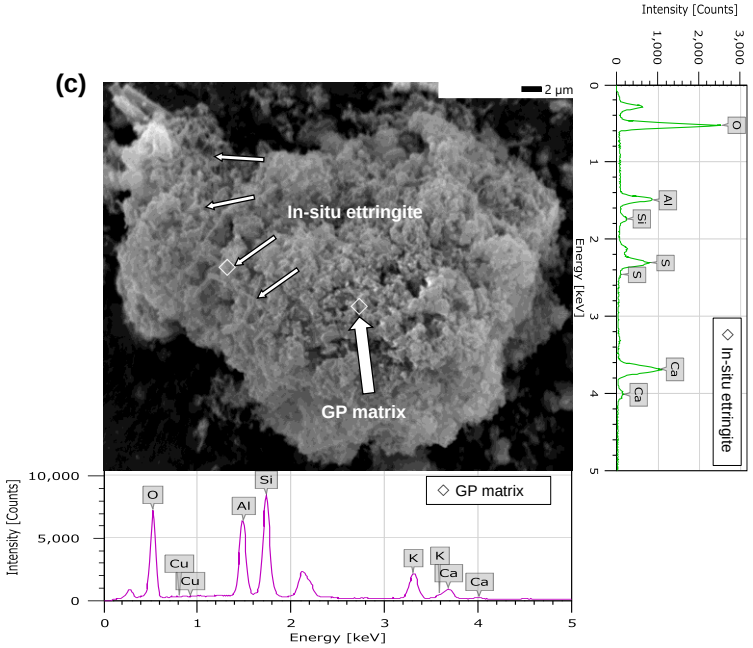


**Figure 4-3.** SEM micrographs of a (a) pure geopolymers (b) synthetic ettringite and (c) modified geopolymer and EDS analysis of the corresponding sites.

The zeta potential of each solid phase is demonstrated in **Figure 4-4**. Since those solid phases were in an alkali-activated environment, basic solutions were selected for zeta potential measurement at constant ionic strengths of 10 and 100 mmol/L. Synthetic ettringite shows a positive zeta potential that is independent of pH, indicating the presence of a permanent charge on its surface (**Figure 4-4 (a)**). The positive charges are considered to be derived from the unit cell of ettringite consisting of columnar $\{Ca_6[Al(OH)_6]_2 \cdot 24H_2O\}^{6+}$ [35]. Conversely, the zeta potential of pure geopolymer shows a consistent negative charge independent of pH (**Figure 4-4 (b)**). However, as the ionic strength decreased, a thicker electrical double layer formed, increasing the absolute magnitude of the zeta potential of the pure geopolymer. It is worth noting that the zeta potential of ettringite was independent of ionic strength, which

could be a significant characteristic difference in its behaviour compared to the zeta potential of geopolymer. Both the geopolymer with superficial ettringite from the co-precipitation process and the geopolymer with in-situ ettringite after modification demonstrated a reduced absolute value of zeta potential due to the positive surface of ettringite partially compensating the negatively charged geopolymer matrix (**Figure 4-4 (c) & (d)**). Moreover, due to the variation in the state of the space filled by ettringite, the zeta potential of the geopolymer with superficial ettringite exhibited a trend more like that of ettringite, while the surface of geopolymer with in-situ ettringite behaved similarly to pure geopolymer.

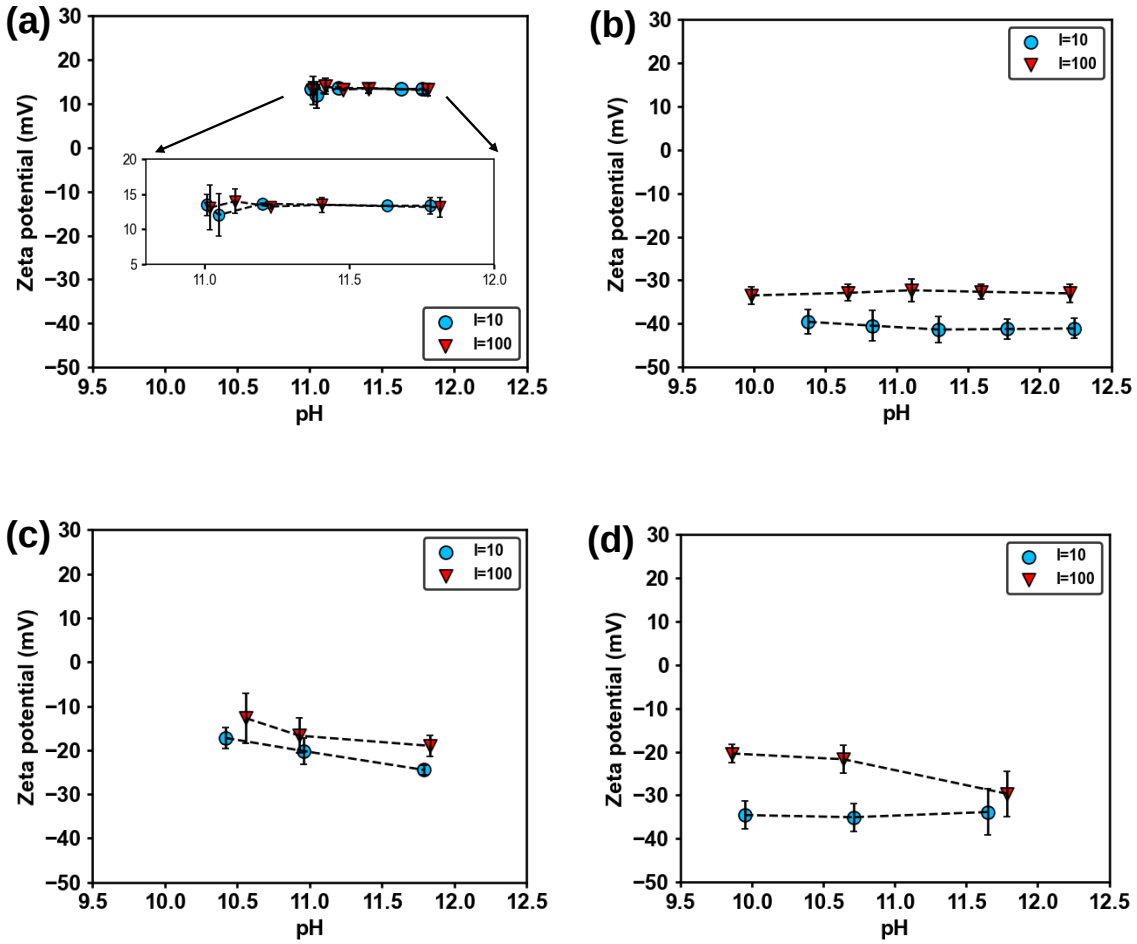

**Figure 4-4.** Zeta potential as a function of pH for (a) synthetic ettringite, (b) pure geopolymer, (c) geopolymer with superficial ettringite and (d) geopolymer with in-situ ettringite (legend entries indicate ionic strengths of 10 and 100 mmol/L).

The synthetic ettringite was characterised by Raman spectroscopy (**Figure 4-5a**). The peak at 989, 450, 1118 and 615 $cm^{-1}$ are (respectively) the $v_1$, $v_2$, $v_3$ and $v_4$ sulphate anion vibration modes and the peak at 549 $cm^{-1}$ is due to the bending vibration mode of $Al(OH)_6$ [56]. In addition, the Raman spectroscopic analysis of pure geopolymer and geopolymer with in-situ ettringite indicates the change of structure and components after modification (**Figure 4-5 (b)** and **Figure 4-5 (c)**). Previous studies have reported that the most sensitive and typical bands of geopolymer structure in Raman spectroscopy were in the range of 350-750 $cm^{-1}$ [57]. The peaks at 395(396), 509(507) and 635 $cm^{-1}$ are assigned to the vibration modes of the representative ring structures of aluminosilicate tetrahedra in geopolymers. The broadband at 372-421 $cm^{-1}$ (marked as light blue in **Figure 4-5**) is assigned to 8-membered rings (8R), the broadband in the region of 421-604 $cm^{-1}$ (marked as light green) represents double 6-membered rings (D6R), and the broadband at 604-712 $cm^{-1}$ (marked as light red) corresponds to 4-membered rings (4R). These are the main basic building units that constitute the three-dimensional network of the geopolymer, which is a disordered pseudo-zeolite [58]. It is important to note that the 8R, D6R, and 4R vibration modes of the modified geopolymer containing in-situ ettringite remained unaltered from the pure geopolymer (**Figure 4-5 (b)** and **Figure 4-5 (c)**); intensities and frequencies were nearly constant, indicating that the geopolymer matrix was not structurally altered by the addition of slag and gypsum to form in-situ ettringite. No evidently new chemical linkages were observed that would have

suggested a chemical connection between the geopolymer matrix and the ettringite. Additionally, the sample containing in-situ ettringite shows a minor calcium carbonate impurity due to adding calcium (as slag and gypsum) into the geopolymer (**Figure 4-5 (c)**).

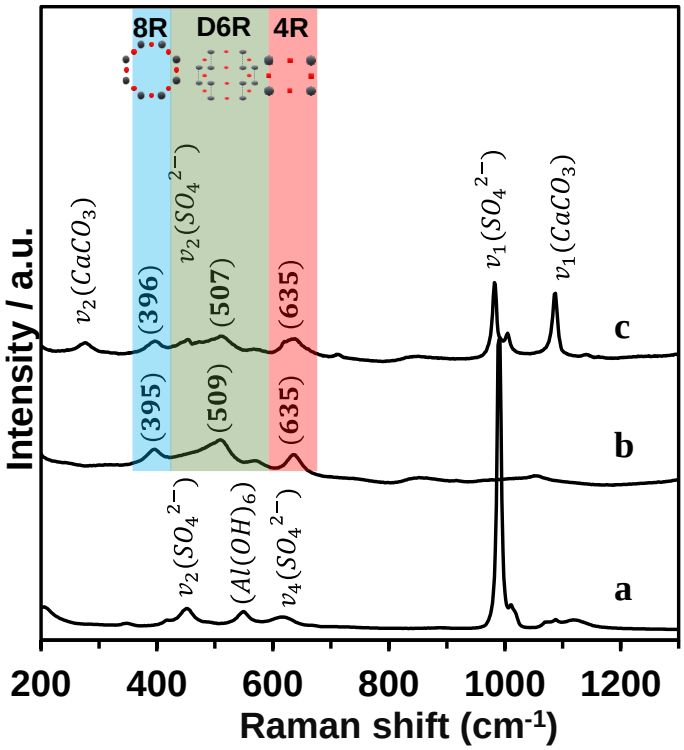


**Figure 4-5.** Raman spectra of (a) synthetic ettringite, (b) pure geopolymer, and (c) modified geopolymer with in-situ ettringite.

### 4.3.2 Co-precipitation analysis

The equilibrated Se oxyanions and sulphate concentration of co-precipitation groups 1-4 (as defined in **Table 4-2**) are shown in **Figure 4-6**. As the initial Se concentration increased, the removal of both $SeO_3^{2-}$ and $SeO_4^{2-}$ from the solution grew, and the difference between each group became more pronounced (**Figure 4-6 (a)**). According to a previous study [42, 59],

ettringite has been shown to immobilise $SeO_3^{2-}$ more effectively than $SeO_4^{2-}$, resulting in the formation of Se-doped ettringite and the results presented here are broadly consistent with that past study. The addition of geopolymer reduces the Se removal due to the charge repulsion caused by the negatively charged surface of the geopolymer (**Figure 4-4**). As the amount of immobilised Se increased (**Figure 4-6 (a)**), the concentration of sulphate ($SO_4^{2-}$) in the solution also rose correspondingly (**Figure 4-6 (b)**). This results from replacing sulphate as the free anion within the ettringite columnar structure by the Se oxyanions. Given that the original sulphate concentration was 30 mmol/L, the decrease in sulphate can be interpreted as an indication of the extent of ettringite formation. It is found that the presence of geopolymer hindered the formation of ettringite in a co-precipitation system to some extent.

Comparing the deviation in equilibrated concentrations of each species with the blank group (without Se) is crucial for understanding the uptake of ettringite during the co-precipitation process with Se oxyanions. The difference between the initial and equilibrated Se concentration for groups 1-4 at 10 mmol/L Se initial concentration (**Figure 4-6 (a)**), which could be regarded as the amount of Se taken up by the solid, were 1.81, 2.17, 6.94 and 9.36 mmol/L, respectively. Correspondingly, the differences in sulphate concentration between the blank and the equilibrated samples were 1.59, 2.16, 6.3 and 7.24 mmol/L, respectively (**Figure 4-6 (b)**), which could be regarded as the amount of $SO_4^{2-}$ displaced from ettringite. A very close relationship was thus found between the uptake amount of Se oxyanions and the displaced amount of $SO_4^{2-}$ in groups 1, 2, and 3, but there is a significant difference in group 4. It is believed that $SeO_4^{2-}$ and $SeO_3^{2-}$ uptake in groups 1-3 was primarily facilitated by the formation of Se-doped ettringite, in which Se oxyanions were immobilised as

interlayer anions through electrostatic forces. However, the immobilisation of Se in group 4 is not solely attributed to anion exchange with inter-column sulphate, suggesting another mechanism appears to play a role. A previous research study [42] suggested that ligand exchange with the -$OH_2$ groups at the channel edges to form complexes could be one of the dominant mechanisms for $SeO_3^{2-}$ uptake in ettringite, and it is possible that this is taking place in group 4. This mechanism will be discussed in more detail in the following section. The results of $R_d$ with an increasing initial concentration of Se are shown in **Figure 4-6 (c)**. The $R_d$ of ettringite for $SeO_3^{2-}$ is much higher than that of $SeO_4^{2-}$ and gradually decreases with an increasing initial concentration of Se. However, while the Rd for $SeO_4^{2-}$ exhibits a slight decrease with higher initial Se concentration, it is comparatively negligible when compared to the notable alterations observed in the $SeO_3^{2-}$ system. It can be observed that despite some negative effects of the presence of geopolymer on the immobilisation of Se oxyanions, ettringite still exhibits a significant ability to immobilise Se oxyanions.

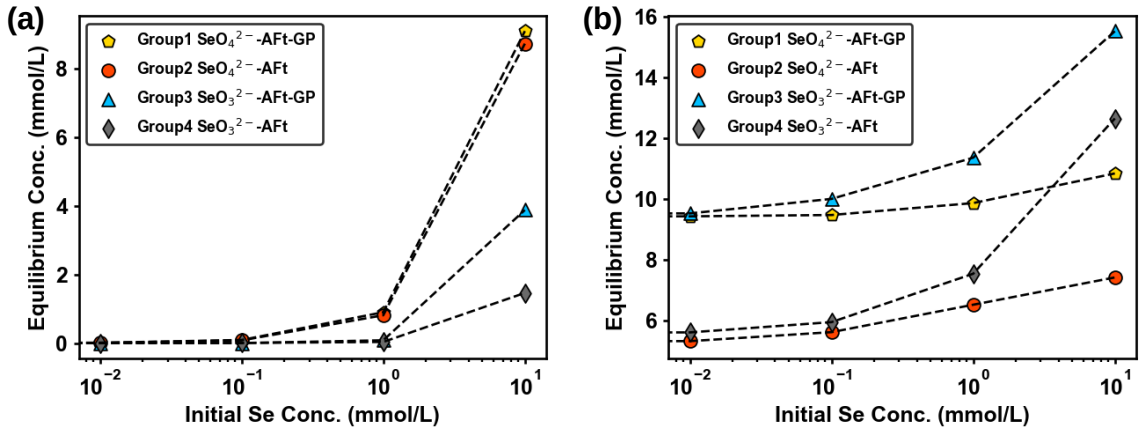

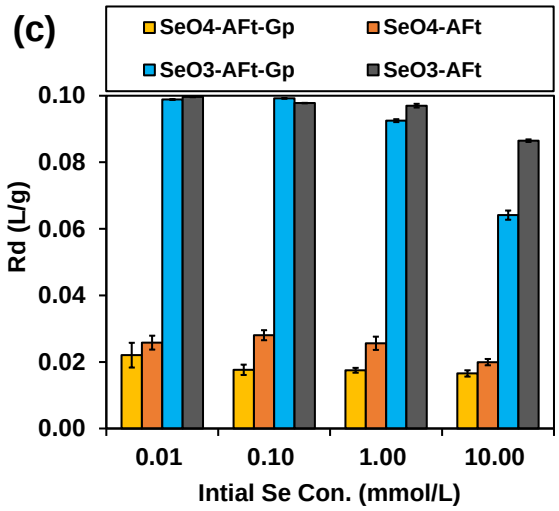


**Figure 4-6.** Concentration of (a) Se oxyanions, (b) $SO_4^{2-}$ at equilibrium, and (c) calculated distribution ratio ($R_d$) as a function of initial Se concentration (The pH range of systems with only ettringite was 10.5±0.1, and the pH range of systems with geopolymer was 11±0.1).

The XRD patterns of the solid phases resulting from the co-precipitation systems were analysed, and the interplanar distance at (100) crystal planes, $d_{100}$, was obtained by applying the Bragg formula to the 2θ angle of the (100)-plane peak. **Table 4-4** presents the $d_{100}$ values for synthetic ettringite, serving as a control, and the $d_{100}$ values of Se-doped ettringite equilibrated in a system containing an initial concentration of 10 mmol/L Se. The $d_{100}$ of ettringite in the control group had no significant difference in the presence or absence of geopolymer. After uptake of $SeO_4^{2-}$ and $SeO_3^{2-}$, the $d_{100}$ of ettringite increased and decreased, respectively. The state of the intercolumn free water has no impact on the size of a unit cell or crystal structure [60]; thus, the variation of the interplanar distance can be attributed to the uptake of Se oxyanions. The replacement of $SO_4^{2-}$ by the Se oxyanions appears to increase in the interplanar distance due to the larger size of $SeO_3^{2-}$ and $SeO_4^{2-}$, as the Se-O bond length

is longer than the S-O bond length [61]. However, the uptake of $SeO_3^{2-}$ did not increase $d_{100}$; the difference between the uptake behaviour of ettringite toward $SeO_3^{2-}$ and $SeO_4^{2-}$ can be attributed to the structural distinction between the two species [42, 62, 63].

It is noteworthy that the presence of geopolymer may significantly impact the change in $d_{100}$ of ettringite after the uptake of $SeO_3^{2-}$, while having a relatively small impact on the change in $d_{100}$ after the uptake of $SeO_4^{2-}$. This outcome suggests that geopolymer may impede the formation of complexes through ligand exchange, but the capacity of ettringite to immobilise Se oxyanions through interlayer electrical attraction is not significantly affected. In addition, it is important to note that the $d_{100}$ value of synthetic ettringite is influenced by various factors, such as the Ca/Al ratio, differences in crystallinity resulting from the growth environment of the crystals, and changes in orientation caused by cutting and grinding during sample preparation. Previous studies have reported $d_{100}$ values of ettringite ranging from 9.67 to 9.75 Å [35, 64-66]. Therefore, the $d_{100}$ value obtained for the synthetic ettringite in this study is considered to be within a reasonable range.

**Table 4-4.** The shift in the $d_{100}$-spacing of ettringite at a concentration of 10 mmol/L Se in each group, and the percentage change compared to synthetic ettringite.

| | $d_{100}$, ettringite control sample (Å) | $d_{100}$, ettringite equilibrated at 10 mmol/L Se (Å) | d100, change after uptake Se (10mmol/L) (%) |
|---|---|---|---|
| 1. $SeO_4$-AFt-GP | 9.733 ± 0.01 | 9.815 | + 0.842 |
| 2. $SeO_4$-AFt | | 9.812 | + 0.812 |

| | | |
|---|---|---|
| 3. $SeO_3$-AFt-GP | 9.697 | - 0.369 |
| 4. $SeO_3$-AFt | 9.676 | - 0.586 |

### 4.3.3 Uptake behaviour from solution

Prior to determining the Se oxyanion uptake from the solution onto the synthetic ettringite and the geopolymer with in-situ ettringite, the time required to attain equilibrium was determined. **Figure 4-7** presents the $R_d$ values of $SeO_3^{2-}$ and $SeO_4^{2-}$ on synthetic ettringite as a function of time in solutions with concentrations ranging from 0.1 to 10 mmol/L. The $R_d$ of $SeO_3^{2-}$ attained more than 95% of its highest value after 7 days and more than 99% of its highest value after 14 days. Similar trends were observed across all concentrations. As such, 14 days is considered as the equilibration time for the isothermal uptake experiment. On the other hand, little $SeO_4^{2-}$ could be immobilised even after 35 days of immersion, which indicates ettringite has a limited capacity to immobilise $SeO_4^{2-}$ from solution (as distinct from the co-precipitation route discussed in the previous section). Therefore, the primary emphasis of the isothermal uptake in this study is on $SeO_3^{2-}$ uptake by geopolymers with in-situ ettringite, and by synthetic ettringite.

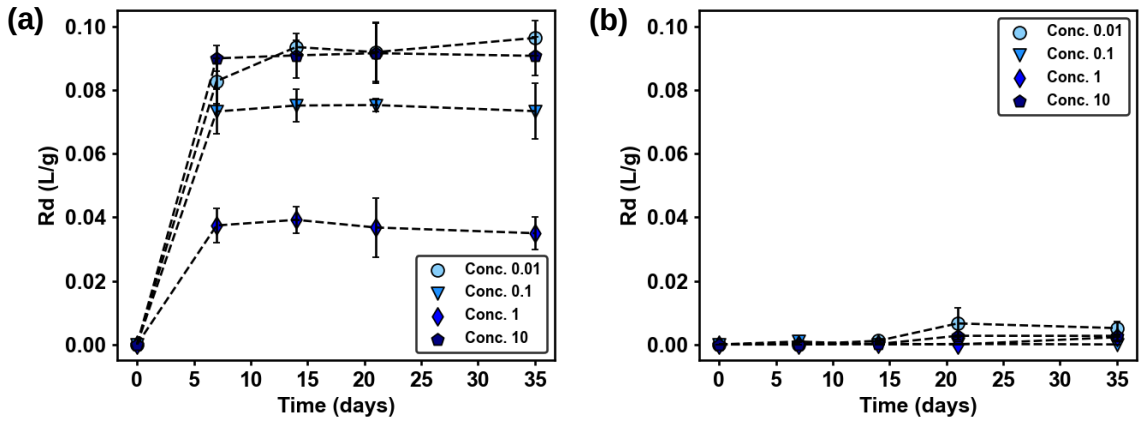


**Figure 4-7.** Relationship between distribution ratio ($R_d$) and immersion time for synthetic ettringite in (a) $SeO_3^{2-}$ and (b) $SeO_4^{2-}$ solutions of different concentrations (marked in the legends, in units of mmol/L, and the pH range of all concentration systems was 10.5±0.1).

The relationship between the quantity of leached $SO_4^{2-}$ ions from synthetic ettringite and from the modified geopolymer with in-situ ettringite, and the amount of bound $SeO_3^{2-}$ ions, is presented in **Figure 4-8**. The relationship between leached $SO_4^{2-}$ and bound $SeO_3^{2-}$ at initial $SeO_3^{2-}$ concentrations below 1 mmol/L displays a direct (1:1) linear correlation onto both synthetic ettringite and geopolymer with in-situ ettringite. However, at high $SeO_3^{2-}$ concentrations (5 and 10 mmol/L), both geopolymer with in-situ ettringite and synthetic ettringite exhibit correlations that deviate somewhat from the expected direct linear relationship. In particular, there is a slight deviation for geopolymer with in-situ ettringite and a significant deviation for synthetic ettringite. This suggests that the amount of bound $SeO_3^{2-}$ exceeded that of released $SO_4^{2-}$. Based on a previous study [67], the quantity of $SO_4^{2-}$ available for ion exchange in the ettringite is estimated to be 0.04 mmol $SO_4^{2-}$ per gram of ettringite, representing approximately 2-3% of the total sulphate present in the solid. The

results of the current study indicate that the experimental uptake of $SeO_3^{2-}$ and leaching of $SO_4^{2-}$ at an initial $SeO_3^{2-}$ concentration of 1 mmol/L (considered the maximum concentration for ion exchange) were approximately 0.037 mmol/g and 0.036 mmol/g, respectively. These findings are in good agreement with the estimated results and support the mechanism of ion exchange.

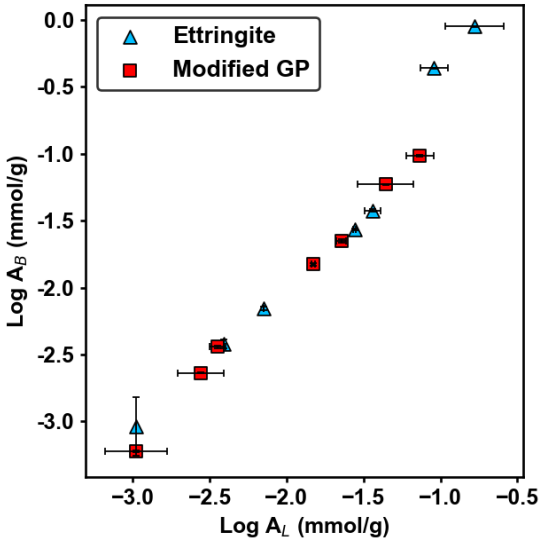


**Figure 4-8.** The relationship between bound $SeO_3^{2-}$ and released $SO_4^{2-}$ from synthetic ettringite (blue triangle) and geopolymer with in-situ ettringite (red squares), expressed in mmol of the oxyanions per g solids (The pH range of systems with ettringite was 10.5±0.1, and the pH range of systems with modified geopolymer was 11.5±0.2).

**Figure 4-9** displays the evaluation of $R_d$ and the leaching/binding ratio (L/B) as a function of increasing initial $SeO_3^{2-}$ concentration. The L/B ratio represents the molar ratio between the amount of leached $SO_4^{2-}$ and the amount of bound $SeO_3^{2-}$. The $R_d$ of geopolymer with in-situ ettringite continuously decreased with increasing $SeO_3^{2-}$ initial concentration, whereas

the L/B ratio remained close to 1 for concentrations below 1 mmol/L and showed a slight decline for concentrations greater than 1 mmol/L. Despite the fact that the L/B ratio significantly deviated from 1 at 0.01 mmol/L, possibly due to measurement uncertainty. As opposed to that, the $R_d$ of synthetic ettringite showed a "U"-shaped relationship with different initial $SeO_3^{2-}$ concentrations: in the concentration range from 0.01 to 1 mmol/L, the $R_d$ of synthetic ettringite decreased with increasing initial $SeO_3^{2-}$ concentration similar to the geopolymer with in-situ ettringite, while the $R_d$ sharply increased when the concentration was elevated to around 5 mmol/L, (approaching the same high $R_d$ as at 0.01 mmol/L), and it then remained constant up to 10 mmol/L initial concentration. The L/B ratio of $SeO_3^{2-}$ on synthetic ettringite fluctuated around 1 in the concentration range between 0.01 and 1 mmol/L $SeO_3^{2-}$, but rapidly decreased when the initial $SeO_3^{2-}$ concentration reached 5 mmol/L. These fluctuations suggest that the $SeO_3^{2-}$ uptake in ettringite, both synthetic form and in-situ form, is primarily controlled by anion exchange with $SO_4^{2-}$ from the interlayer at concentrations below 1 mmol/L. When the concentration of $SeO_3^{2-}$ exceeds 1 mmol/L, the uptake mechanism for $SeO_3^{2-}$ shifts to ligand exchange, which acts in conjunction with ion exchange. However, this mechanism is considerably impeded in the in-situ form of ettringite.

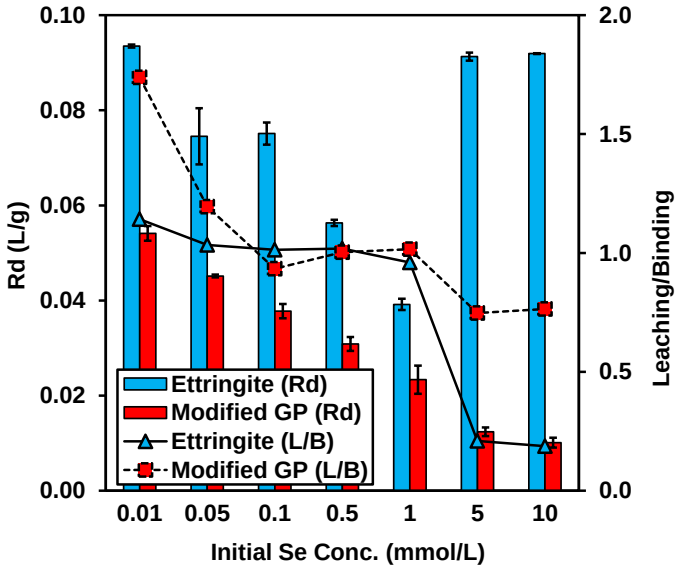


**Figure 4-9.** $R_d$ values and leaching/binding (L/B) ratios of $SeO_3^{2-}$ on synthetic ettringite, and on geopolymer with in-situ ettringite, as a function of initial $SeO_3^{2-}$ concentration (The pH range of systems with ettringite was 10.5±0.1, and the pH range of systems with modified geopolymer was 11.5±0.2).

The $Cs^+$ and $Sr^{2+}$ uptake capacities of pure geopolymer and geopolymer with in-situ ettringite were also analysed and compared, as depicted in **Figure 4-10**. It was observed that the capacity of pure geopolymer for both $Cs^+$ and $Sr^{2+}$ was consistently higher than that of the geopolymer with in-situ ettringite, with a more significant difference in capacity towards $Sr^{2+}$ as compared to $Cs^+$. While both pure geopolymer and geopolymer with in-situ ettringite exhibited an increase in cation uptake with increasing initial cationic concentration until a concentration of 5 mmol/L, the pure geopolymer continued to uptake more cations even when the initial concentration exceeded 5 mmol/L. However, the uptake capacity of geopolymer with in-situ ettringite appeared to reach saturation at around 5 mmol/L, unable to

continuously uptake more cations. This disparity can be attributed to the positive surface charge of the in-situ ettringite, which reduces the electrostatic attraction and leads to a partial loss of chemical sites available for cation exchange. However, it is important to note that the actual concentrations of cations like $Cs^{+}$ and $Sr^{2+}$ in pollutants are in the order of parts per million, thus even with the modification, geopolymer with in-situ ettringite still possesses a very useful uptake capacity for $Cs^{+}$ and $Sr^{2+}$.

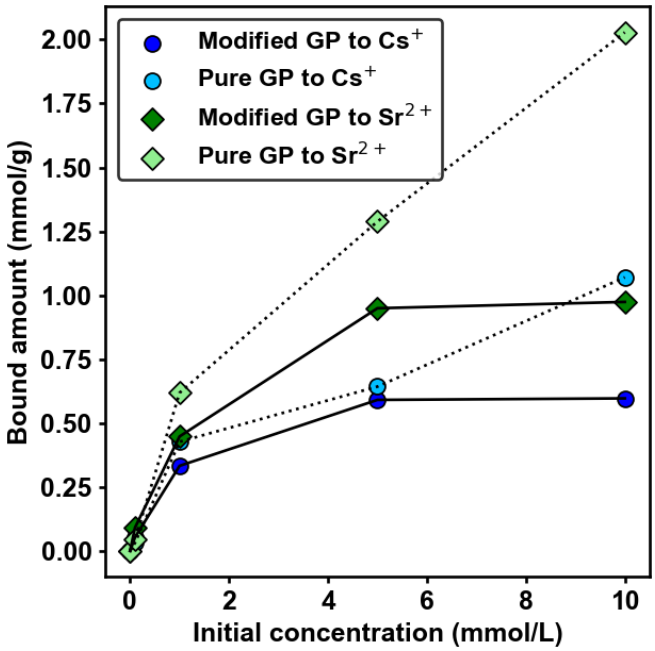


**Figure 4-10.** Uptake capacity of pure geopolymer (dotted lines) and geopolymer with in-situ ettringite (solid line) for $Cs^{+}$ and $Sr^{2+}$.

### 4.3.4 Structural change after uptake

The structural changes in synthetic ettringite, and geopolymer with in-situ ettringite, after $SeO_3^{2-}$ uptake can be characterised using Raman spectra, as shown in **Figure 4-11**. The

spectra in **Figure 4-11(a)** depicts the Raman spectra of synthetic ettringite before and after 14 days of immersion in solutions with varying $SeO_3^{2-}$ initial concentrations. As previously discussed (**Figure 4-5**), the peaks at 989, 450, 615, and 1118 $cm^{-1}$ correspond to the vibrations of $SO_4^{2-}$, while the peak at 549 $cm^{-1}$ is due to the bending vibration mode of $Al(OH)_6$. These peaks remained stable after 14 days of immersion and showed no significant changes with changes in the initial $SeO_3^{2-}$ concentration. The broad band between approximately 3000 $cm^{-1}$ to 3650 $cm^{-1}$ is caused by the overlapping bands of channel water, crystal water, and coordinated -$OH_2$ vibrations in the columnar unit of ettringite. Synthetic ettringite, and ettringite immersed in solutions with initial $SeO_3^{2-}$ concentrations ranging from 0 to 0.5 mmol/L exhibited identical spectra in the 3000 $cm^{-1}$ to 3650 $cm^{-1}$ range, but the intensity in this region decreased gradually with increasing initial $SeO_3^{2-}$ concentration, reaching a significant reduction when the initial $SeO_3^{2-}$ concentration reached 10 mmol/L. It is also worth mentioning that with increasing initial $SeO_3^{2-}$ concentration, new peaks attributed to $SeO_3^{2-}$ became gradually revealed at 829 $cm^{-1}$ and 773 $cm^{-1}$.

**Figure 4-11 (b)** shows the Raman spectra of the geopolymer with in-situ ettringite after 14 days of immersion. A comparison between the pure geopolymer and the geopolymer with in-situ ettringite demonstrates that the peaks associated with the typical geopolymer structure, situated between 371 $cm^{-1}$ and 712 $cm^{-1}$, remain unaltered. Conversely, vibrational peaks representing $SO_4^{2-}$ (989 $cm^{-1}$) and calcite (1085 $cm^{-1}$) were observed to emerge, as previously discussed (as depicted in **Figure 4-5**). When the geopolymer with in-situ ettringite was immersed in a solution, no significant alterations were observed as a function of the initial $SeO_3^{2-}$ concentration. However, there was a noticeable weakening in the intensity of the peak

associated with $SO_4^{2-}$ at 989 $cm^{-1}$, which may be attributed to the dissolution of potassium sulphate present in the geopolymer with in-situ ettringite. Nevertheless, it was still possible to observe peaks attributed to $SO_4^{2-}$ vibrations in the geopolymer with in-situ ettringite that are considered to be derived from the in-situ ettringite, and there was no significant change in these peaks. Unlike the synthetic ettringite, it had no significant change of the broadband between 3000 $cm^{-1}$ and 3650 $cm^{-1}$, especially the peak representing O-H (around 3620 $cm^{-1}$), as a function of the initial concentration of $SeO_3^{2-}$.

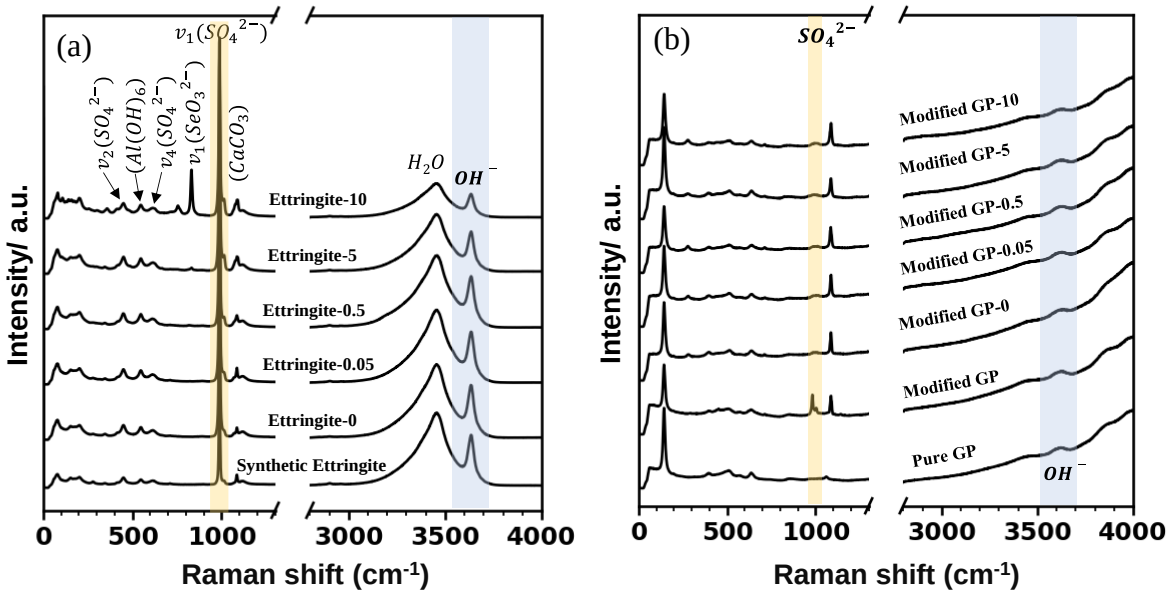


**Figure 4-11.** Raman spectra of (a) synthetic ettringite, and (b) geopolymer with in-situ ettringite, after 14 days of $SeO_3^{2-}$ uptake at various initial concentrations (as marked in the dataset labels; values in mmol/L). The vibration of each main functional group is marked in the figure by text annotations, and the vibrations of $OH^-$ and $SO_4^{2-}$ are marked in the ribbons of light blue and light yellow, respectively.

In order to gain a deeper understanding of the alteration of -$OH_2$ groups in the synthetic ettringite structure following the incorporation of $SeO_3^{2-}$, thermo gravimetric analysis (TG) was carried out. **Figure 4-12** presents the TG profiles of synthetic ettringite after being immersed in various $SeO_3^{2-}$ solutions. The most substantial weight loss of the synthetic ettringite was observed between 90 and 108 ℃ and increased progressively with increasing temperature. The maximum weight loss was reached when the temperature rose to approximately 800 ℃, which can be attributed to the quantity of water present in the ettringite structure [68]. As the initial $SeO_3^{2-}$ concentration increased, the water content in the ettringite structure after the uptake of $SeO_3^{2-}$ decreased, with a notably significant reduction observed at an initial $SeO_3^{2-}$ concentration of 10 mmol/L. The results are consistent with those obtained from the previous liquid phase analysis (represented in **Figure 4-8** and **Figure 4-9**) and provide evidence from the solid phase structure that the uptake of $SeO_3^{2-}$ into ettringite through anion exchange at low $SeO_3^{2-}$ concentrations does not alter the vibrational bond in the range of 3000 $cm^{-1}$ to 3650 $cm^{-1}$. However, ligand exchange in the intercolumn edge site can reduce the amount of -$OH_2$ groups coordinated with Ca, which decreases the water content in synthetic ettringite and weakens the vibrational bond in the range of 3000 $cm^{-1}$ to 3650 $cm^{-1}$.

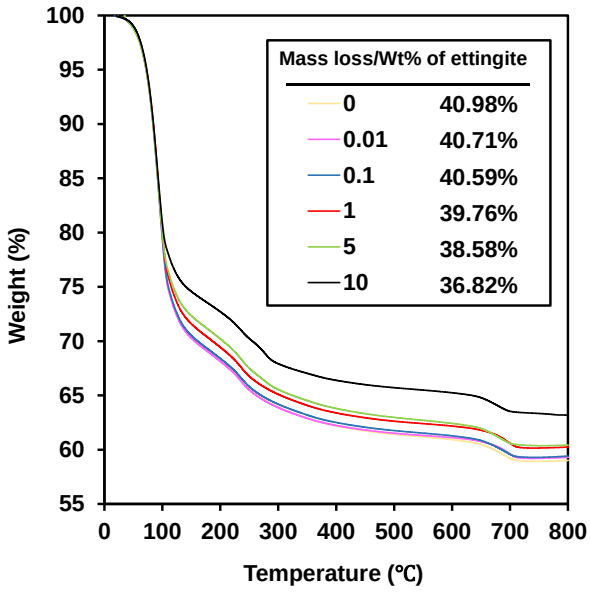


**Figure 4-12.** TG curves of synthetic ettringite after immersion in various concentrations of $SeO_3^{2-}$ solutions (as marked in the legend, in mmol/L) for 14 days.

### 4.3.5 Thermodynamic modelling and verification

The ion exchange model was used to predict $SeO_3^{2-}$ uptake at concentrations below 1 mmol/L, where uptake is primarily controlled via the ion exchange mechanism. The best fit of log_*K* was obtained through python-code fitting results with experimental data for $SO_4^{2-}$ leaching (**Figure 4-13 (a)** and **Figure 4-13 (c)**). A high correlation between experimental data and modelling results was observed for both cases. The estimated log_*K* for ion exchange reaction in the synthetic ettringite and modified geopolymers are 1.049 and 0.222, respectively. The estimated log_*K* indicates that the ion exchange capacity of in-situ ettringite present in modified geopolymers is somewhat weakened by the geopolymer matrix, supporting the results shown in the previous sections. **Figure 4-13 (b)** and **Figure 4-13 (d)**

depict the predicted amount of bound $SeO_3^{2-}$ corresponding to estimated log_$K$ as a function of concentration. The model prediction displays a good agreement with the experimental data, which describes and demonstrates the ion exchange mechanism at this concentration range. It is worth noting that radionuclide ionic concentration in nuclear waste is in parts per million order; thus, the proposed ion exchange model would be applicable.

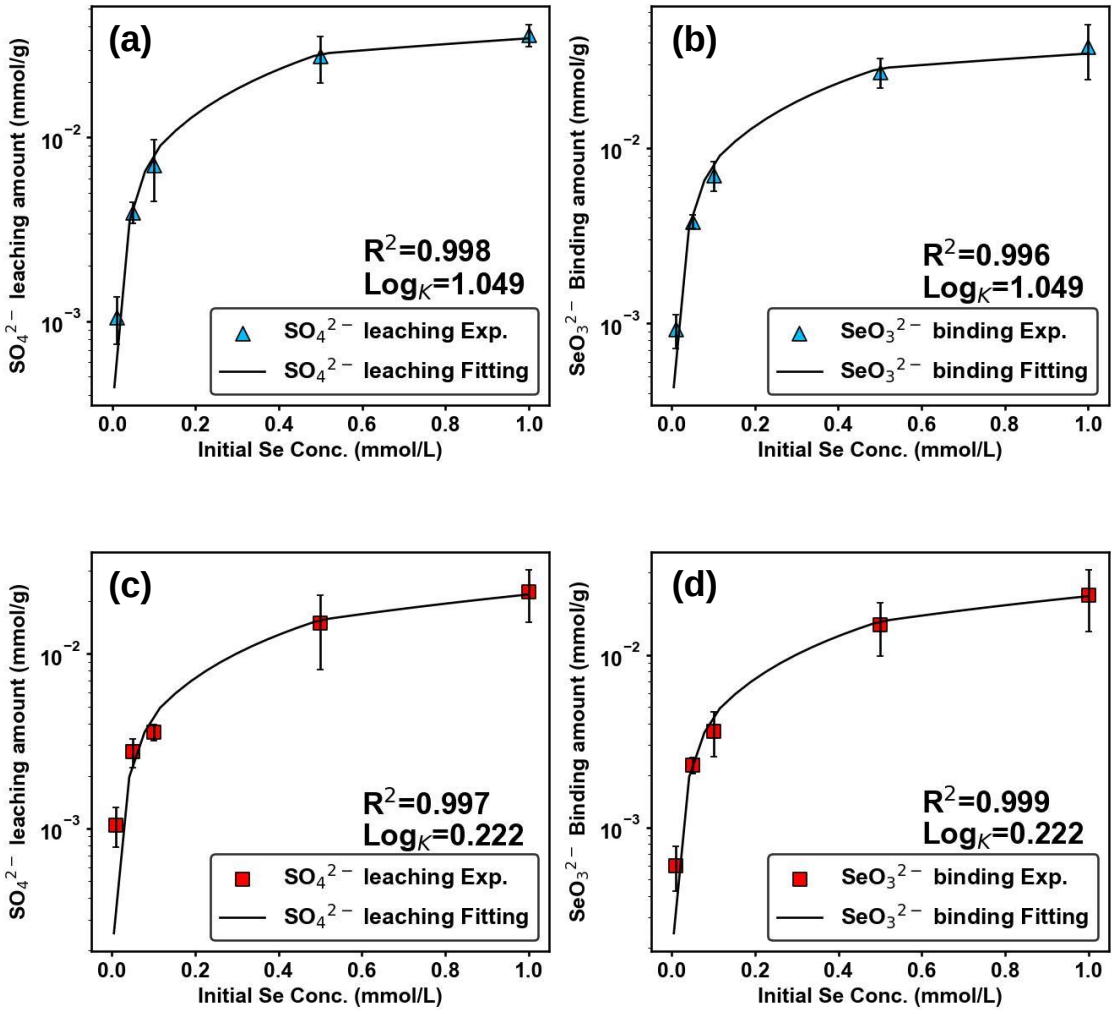

**Figure 4-13.** Fitting of experimental data with modelling results for (a) synthetic ettringite and (c) modified geopolymers, and the comparison of the predicted and measured (c) synthetic ettringite and (d) modified geopolymers as a function of concentration.

### 4.3.6 Mechanism of $SeO_3^{2-}$ uptake in geopolymer with in-situ ettringite

The uptake mechanism of the geopolymer with in-situ ettringite for $SeO_3^{2-}$ is schematically demonstrated in **Figure 4-14**. As discussed above, the mechanism for uptake of $SeO_3^{2-}$ by ettringite strongly depends on the concentration of $SeO_3^{2-}$ in the solution. At low concentrations (< 1 mmol/L), the uptake of $SeO_3^{2-}$ is primarily dominated by ion exchange with inter-channels $SO_4^{2-}$. However, as the initial $SeO_3^{2-}$ concentration increases, ettringite immobilises $SeO_3^{2-}$ through a ligand exchange with -$OH_2$ coordinated with Ca located on the channel edges. According to the bond valence theory [42], the preferred structure of complexes formed is shown in **Figure 4-14**. The reason for such a mechanistic shift may be attributed to the variation in the chemical potential generated by the concentrations of $SeO_3^{2-}$ in solution [69]. When the concentration of a $SeO_3^{2-}$ in a reaction system increases, the corresponding increase in its chemical potential can facilitate its exchange with coordinated hydroxyl through a ligand exchange mechanism [70]; this property of chemical potential is a critical factor that determines the selectivity and controllability of chemical reactions involving ligand and ion exchange mechanisms. However, when ettringite is present in its in-situ form in the geopolymer matrix, the positively charged embedded ettringite could be attracted by the negatively charged geopolymer matrix by electrostatic forces. Due to the polarity of the linked oxygen atoms, the proton in the channel edge functional group (Ca-

$OH_2$) in the ettringite structure may form hydrogen bonds with Al in the negatively charged tetrahedral $AlO_4$ on the geopolymer surface, thus rendering these -$OH_2$ ligands somewhat more stable. At the same time, the geopolymer matrix also covers most of the ettringite surface, physically obscuring to some degree the sites on the ettringite surface where ligand exchange with $SeO_3^{2-}$ can occur. Thus, the uptake capacity of in-situ ettringite in modified geopolymer to $SeO_3^{2-}$ through ligand exchange is sterically shielded by geopolymer matrix to some extent; as a result, ion exchange with inter-channels $SO_4^{2-}$ becomes the controlling uptake mechanism of geopolymer with in-situ ettringite for $SeO_3^{2-}$. The ion exchange capacities of ettringite and geopolymer, for anions and cations, respectively, are influenced by each other due to the compensation of mutually opposite charges. Nonetheless, it is noteworthy that the geopolymer incorporating in-situ ettringite continues to exhibit a reasonable capacity for immobilising both cationic and anionic radionuclides. These radionuclides are typically encountered in waste streams at concentrations ranging from parts per million.

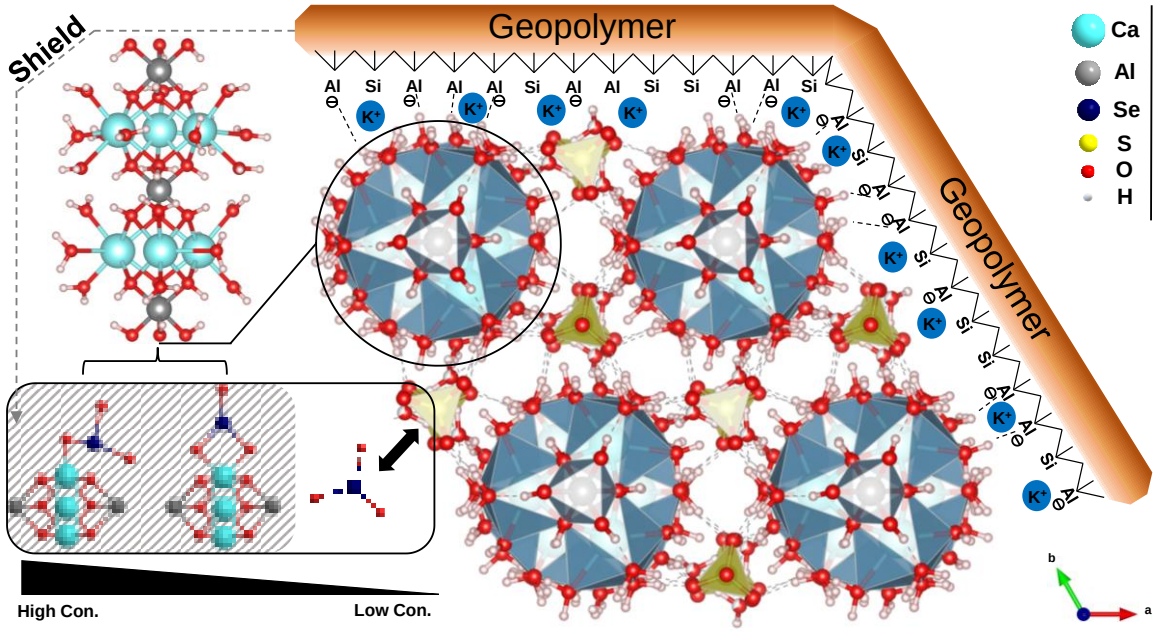


**Figure 4-14.** A proposed mechanism for $SeO_3^{2-}$ uptake in geopolymer with in-situ ettringite.

## 4.4 Conclusion

Modified geopolymers with in-situ ettringite were successfully synthesised with the addition of gypsum and ground granulated blast furnace slag (Gyp 10wt% + 3Slag). Ettringite was observed to have a high uptake potential for Se oxyanions, and so its in situ synthesis endows geopolymer with a greatly enhanced uptake capacity for Se oxyanions. Specific findings of this study include:

- Either in the in-situ form or by co-precipitation, the generated ettringite can act in combination with the permanently negatively charged geopolymer due to its positively charged surface, and this interaction compensates for the partial negative charge.

- The basic structure and cation uptake capacity of the geopolymer are retained after the modification by ettringite synthesis.
- Synthetic ettringite can immobilise both $SeO_3^{2-}$ and $SeO_4^{2-}$ through co-precipitation but can only uptake $SeO_3^{2-}$ through the binding process. The immobilisation of $SeO_3^{2-}$ during the binding process is primarily achieved through ion exchange with $SO_4^{2-}$ at low concentrations (<1 mmol/L), with a maximum ion exchange capacity of around 0.037 mmol/g observed at approximately 1 mmol/L. However, at higher concentrations (>1 mmol/L), the dominant mechanism shifts to ligand exchange with Ca-$OH_2$. A maximum $R_d$ value of approximately 0.092 was obtained in the concentrations of 0.01, 5, and 10 mmol/L.
- The uptake mechanism of ligand exchange to $SeO_3^{2-}$ is partially shielded by the electrostatic interaction and hydrogen bonding with the geopolymer matrix. However, the modified geopolymer retains the capacity to adsorb cationic radionuclides ($Cs^+$ and $Sr^{2+}$) and has developed significant uptake capacity for $SeO_3^{2-}$ by ion exchange as the controlling mechanism. The maximum immobilisation capacities for $Cs^+$, $Sr^{2+}$ and $SeO_3^{2-}$ were approximately 0.597, 0.974 and 0.096 mmol/g, respectively.
- Thermodynamic modelling was conducted based on an ion exchange mechanism, which predicts the uptake behaviour of both synthetic ettringite and modified geopolymers for $SeO_3^{2-}$ at low concentrations (< 1 mmol/L).

## References

[1] J.E.Spallholz, On the nature of selenium toxicity and carcinostatic activity, Free Radic. Biol. Med., 17(1994) 45-64.

[2] TEPCO, Basic Policy for the Contaminated Water Issue at the TEPCO's Fukushima Daiichi Nuclear Power Station, (2013).

[3] G. Jörg, R. Bühnemann, S. Hollas, N. Kivel, K. Kossert, S. V. Winckel, C. L. v. Gostomski, Preparation of radiochemically pure 79Se and highly precise determination of its half-life, Appl. Radiat. Isot., 68(2010) 2339-2351.

[4] H. Sekimoto, H. Nakamura, N. Takagi, Toxicity of radioactive wastes discharged from nuclear energy centre in the future equilibrium state, Ann. Nucl. Energy, 23(1996) 663-668.

[5] S. O. Okonji, L. Yu, J. A. Dominic, D. Pernitsky, G. Achari, Adsorption by Granular Activated Carbon and Nano Zerovalent Iron from Wastewater: A Study on Removal of Selenomethionine and Selenocysteine, Water, 13(2021) 23.

[6] X. Zhang, X. Li, Z. Jin, S. H. Tumrani, X. Ji, Selenium in wastewater can be adsorbed by modified natural zeolite and reused in vegetable growth, Sci. Prog., 104(2021) 1-20.

[7] T. Nishimura, H. Hashimoto, M. Nakayama, Removal of Selenium(VI) from Aqueous Solution with Polyamine‐type Weakly Basic Ion Exchange Resin, Sep. Purif. Technol., 42(2007) 3155-3167.

[8] S. O. Okonji, J. A. Dominic, D. Pernitsky, G. Achari, Removal and recovery of selenium species from wastewater: Adsorption kinetics and co-precipitation mechanisms, J. Water Process. Eng., 38(2020) 101666.

[9] TEPCO, n.d. Contaminated Water Treatment. (2023).

[10] M. H. Zeeshan, R. U. Khan, M. Shafiq, A. Sabir, Polyamide intercalated nanofiltration membrane modified with biofunctionalised core shell composite for efficient removal of Arsenic and Selenium from wastewater, J. Water Process. Eng., 34(2020) 101175.

[11] H. K. Hansen, S. F. Peña, C. Gutiérrez, A. Lazo, P. Lazo, L. M. Ottosen, Selenium removal from petroleum refinery wastewater using an electrocoagulation technique, J. Hazard. Mater., 364(2019) 78-81.

[12] E. Lichtfouse, N. M. Crini, C. Bradu, Y. A. Boussouga, M. Aliaskari, A. I. Schäfer, S. Das, L. D. Wilson, M. Ike, D. Inoue, M. Kuroda, S. Déon, P. Fievet, G. Crini, Technologies to Remove Selenium from Water and Wastewater, Emerg. Contam. Vol. 2., 2(2021) 207-304.

[13] L. Zhu, L. Zhang, J. Li, D. Zhang, L. Chen, D.. Sheng, S. Yang, C. Xiao, J. Wang, Z. Chai, T. E. Albrecht-Schmitt, S. Wang, Selenium Sequestration in a Cationic Layered Rare Earth Hydroxide: A Combined Batch Experiments and EXAFS Investigation, Environ. Sci. Technol., 51(2017) 8606–8615.

[14] J. Li, B. Li, N. Shen, L. Chen, Q. Guo, L. Chen, L. He, X. Dai, Z. Chai, S. Wang, Task-Specific Tailored Cationic Polymeric Network with High Base-Resistance for Unprecedented 99TcO4– Cleanup from Alkaline Nuclear Waste, ACS Cent. Sci., 7(2021) 1441–1450.

[15] L. Zhu, D. Sheng, C. Xu, X. Dai, M. A. Silver, J. Li, P. Li, Y. Wang, Y. Wang, L.. Chen, C. Xiao, J.. Chen, R. Zhou, C. Zhang, O. K. Farha, Z. Chai, T. E. Albrecht-Schmitt, S. Wang, Identifying the Recognition Site for Selective Trapping of 99TcO4– in a Hydrolytically Stable and Radiation Resistant Cationic Metal–Organic Framework, J. Am. Chem. Soc., 139(2017) 14873–14876.

[16] N. Shen, Z. Yang, S. Liu, X. Dai, C. Xiao, K. Taylor-Pashow, D. Li, C. Yang, J. Li, Y. Zhang, M. Zhang, R. Zhou, Z. Chai, S. Wang, 99TcO4– removal from legacy defense nuclear waste by an alkaline-stable 2D cationic metal organic framework, Nat. Commun., 11(2020) 5571.

[17] X. Zhang, Y. Guo, N. Xie, R. Guo, Y. Wang, Z. Hu, W. Xu, Y. Ai, J. Gao, J. Wang, Q. Liang, D. Niu, H. Sun, Y. Qi, Ternary NiFeMnOx compounds for adsorption of antimony and subsequent application in energy storage to avoid secondary pollution, Sep. Purif. Technol., 276(2021) 119237.

[18] J.L. Provis, Geopolymers and other alkali activated materials - Why, how, and what?, Mater. Struct., 47(2014) 11-25.

[19] J. L. Provis and S. A. Bernal, Geopolymers and related alkali-activated materials, Annu. Rev. Mater. Sci., 44(2014) 299-327.

[20] V. Cantarel, T. Motooka, I. Yamagishi, Geopolymers and their potential applications in the nuclear waste management field A bibliographical study, (2017)014. Japan https://doi.org/10.11484/jaea-review-2017-014

[21] Y. Huang, M. Han, The influence of α-Al2O3 addition on microstructure, mechanical and formaldehyde adsorption properties of fly ash-based geopolymer products, J. Hazard. Mater., 193(2011) 90–94.

[22] Q. Li, Z. Sun, D. Tao, Y. Xu, P. Li, H. Cui, J. Zhai, Immobilisation of simulated radionuclide 133Cs+ by fly ash-based geopolymer. J. Hazard. Mater., 262(2013) 325–331.

[23] P. He, J. Cui, M. Wang, S. Fu, H. Yang, C. Sun, X. Duan, Z. Yang, D. Jia, Y. Zhou, Interplay between storage temperature, medium and leaching kinetics of hazardous wastes in metakaolin-based geopolymer, J. Hazard. Mater., 384(2020) 121377

[24] D. A. Geddes, X. Ke, S. A. Bernal, M. Hayes, J. L. Provis, Metakaolin-Based Geopolymers for Nuclear Waste Encapsulation. In: Martirena, F., Favier, A., Scrivener, K. (eds) Calcined Clays for Sustainable Concrete, RILEM Bookseries, Springer, Dordrecht, 16(2018).

[25] INTERNATIONAL ATOMIC ENERGY AGENCY, Combined Methods for Liquid Radioactive Waste Treatment, IAEA-TECDOC-1336, IAEA, Vienna (2003).

[26] S. A. Bernal, J. S. J. van Deventer, J. L. Provis, What happens to 5-year-old metakaolin geopolymers? The effect of alkali cation. In: Scrivener, K., Favier, A. (eds) Calcined Clays for Sustainable Concrete. RILEM Bookseries, Springer, Dordrecht, 10(2015).

[27] A. Palomo, A. Fernández-Jiménez, M. Criado, Geopolymers: same basic chemistry, different microstructures, Mater. Constr., 54(275) (2004) 77–91.

[28] A. A. Siyal, M. R. Shamsuddin, M. I. Khan, N. E. Rabat, M. Zulfiqar, Z. Man, J. Siame, K. A. Azizli, A review on geopolymers as emerging materials for the adsorption of heavy metals and dyes. J. Environ. Manage., 224(2018) 324-339.

[29] F. J. López, S. Sugita, M. Tagaya, T. Kobayashi, Metakaolin-Based Geopolymers for Targeted Adsorbents to Heavy Metal Ion Separation. J. Mater. Sci. Chem. Eng., 02(2014) 16–27.

[30] N. Soonthornwiphat, Y. Kobayashi, K. Toda, K. Kuroda, C. R. Islam, T. Otake, Y. Elakneswaran, J. L. Provis, T. Sato, Encapsulation of Sr-loaded titanate spent adsorbents in potassium aluminosilicate geopolymer, J. Nucl. Sci. Technol., 19(2020) 1181-1188.

[31] Q. Tian and K. Sasaki, Application of fly ash-based geopolymer for removal of caesium, strontium and arsenate from aqueous solutions: Kinetic, equilibrium and mechanism analysis. Water Sci. Technol., 79(2019) 21162125.

[32] N. Vandevenne, R. I. Iacobescu, Y. Pontikes, R. Carleer, E. Thijssen, K. Gijbels, S. Schreurs, W. Schroeyers, Incorporating Cs and Sr into blast furnace slag inorganic polymers and their effect on matrix properties. J. Nucl. Mater., 503(2018) 1–12.

[33] X. Niu, Y. Elakneswaran, R. I. Chaerun, J. L. Provis, T. Sato, Adsorption behaviour of simulant radionuclide cations and anions in metakaolin-based geopolymer, J. Hazard. Mater., 429(2022) 128373.

[34] H.F.W. Taylor, Cement Chemistry, 2nd edition, Academic Press Limited, New York (1997).

[35] A.E. Moore, H.F.W. Taylor, Crystal structure of ettringite, Acta Crystallogr., B26(1970) 386-393.

[36] H.F.W. Taylor, Crystal structures of some double hydroxide minerals. Mineralogical Magazine, 39(1973) 377-389.

[37] N. Saikia, S. Kato, T. Kojima, Behavior of B, Cr, Se, As, Pb, Cd, and Mo present in waste leachates generated from combustion residues during the formation of ettringite, Environ. Toxicol. Chem., 25(2006) 1710-1719.

[38] M. Chrysochoou, D. Dermatas, Evaluation of ettringite and hydrocalumite formation for heavy metal immobilisation: Literature review and experimental study, J. Hazard. Mater., 136(2006) 20-33.

[39] J.K. Solem-Tishmack, G.J. McCarthy, B. Docktor, K.E. Eylands, J.S. Thompson, D.J. Hassett, High-calcium coal combustion by-products: Engineering properties, ettringite formation, and potential application in solidification and stabilisation of selenium and boron, Cem Concr Res., 25 (1995) 658-670.

[40] M. Zhang and E. J. Reardon, Removal of B, Cr, Mo, and Se from Wastewater by Incorporation into Hydrocalumite and Ettringite, Environ. Sci. Technol., 37(2007) 2947-2952.

[41] B. Guo, K. Sasaki, T. Hirajima, Characterisation of the intermediate information of selenate-substituted ettringite, Cem. Concr. Res., 99(2017) 30-37.

[42] B. Guo, K. Sasaki, T. Hirajima, Selenite and selenate uptaken in ettringite: Immobilisation mechanisms, coordination chemistry, and insights from structure, Cem. Concr. Res., 100(2017) 166-175.

[43] S. Wang, K. L. Scrivener, Hydration products of alkali-activated slag cement, Cem. Concr. Res., 25(1995) 561-571.

[44] C. Li, H. Sun, L. Li, A review: The comparison between alkali-activated slag (Si+Ca) and metakaolin (Si+Al) cements, Cem. Concr. Res., 40(2010) 1341-1349.

[45] A. Palomo, M. Palacios, Alkali-activated cementitious materials: Alternative matrices for the immobilisation of hazardous wastes: Part II. Stabilisation of chromium and lead, Cem. Concr. Res., 33(2003) 289-295.

[46] P. Chindaprasirt, S. Thaiwitcharoen, S. Kaewpirom, U. Rattanasak, Controlling ettringite formation in FBC fly ash geopolymer concrete, Cem. Concr. Compos., 41(2013) 24-28.

[47] P. Sukmak, P. De. Silva, S. Horpibulsuk, P. Chindaprasirt, Sulphate Resistance of Clay-Portland Cement and Clay High-Calcium Fly Ash Geopolymer, J. Mater. Civ. Eng., 27(2015) 5.

[48] S. Chen, Y. Qi, J. J. Cossa, I. D. S. Dos Santos, Efficient removal of radioactive iodide anions from simulated wastewater by HDTMA-geopolymer, Prog. Nucl. Energy, 177(2019) 103112.

[49] Z. Ji, Y. Pei, Immobilisation efficiency and mechanism of metal cations (Cd2+, Pb2+ and Zn2+) and anions (AsO43- and Cr2O72-) in wastes-based geopolymer, J. Hazard. Mater., 384(2020) 121290.

[50] Q. Tian, K. Sasaki, A novel composite of layered double hydroxide/geopolymer for co-immobilisation of Cs+ and SeO42- from aqueous solution, Sci. Total. Environ., 695(2019) 133799.

[51] P. Ježek, P. Škarpa, T. Lošák, J. Hlušek, M. Jůzl and P. Elzner, Selenium – An Important Antioxidant in Crops Biofortification, Antioxidant Enzyme. InTech., (2012) 343-368.

[52] D.L. Parkhurst, C.A.J. Appelo, User's Guide to PHREEQC (Version 2)—A Computer Program for Speciation, Batch-Reaction, One-Dimensional Transport, and Inverse Geochemical Calculations. U.S. Geological Survey, Water Resources Investigations Report (1999) 99-4259, Washington DC.

[53] C.A.J. Appelo, D.L. Parkhurst, Description of input and examples for PHREEQC version 3—a computer program for speciation, batch-reaction, one-dimensional transport, and inverse geochemical calculations. US geological survey techniques and methods, 6.A43(2013) 497.

[54] L. Divet, R. Randriambololona, Delayed Ettringite Formation: The Effect of Temperature and Basicity on the Interaction of Sulphate and C-S-H Phase, Cem. Concr. Res., 28(1998) 357-363.

[55] R. B. Jewell, R. Rathbone, T. Duvallet, T. L. Robl, Kamyar C. Mahboub, Fabrication and Testing of Low-Energy Calcium Sulfoaluminate-Belite Cements that Utilise Fluidised Bed Combustion By-Products, Coal Combust. Gasific. Prod., 7(2015) 9-18.

[56] G. Renaudin, R. Segni, D. Mentel, J. M. Nedelec, F. Leroux, C. T. Gueho, A Raman Study of the Sulphated Cement Hydrates: Ettringite and Monosulfoaluminate, J. Adv. Concr. Technol., 5(2007) 299-312.

[57] R. I. Chaerun, N. Soonthornwiphat, K. Toda, K. Kuroda, X. Niu, R. Kikuchi, T. Otake, Y. Elakneswaran, J. L. Provis, T. Sato, Retention Mechanism of Cesium in Chabazite Embedded into Metakaolin-Based Alkali Activated Materials, J. Hazard. Mater., 440(2022) 129732.

[58] P.P. Knops-Gerrits, D.E. De Vos, E.J.P. Feijen, P.A. Jacobs, Raman spectroscopy on zeolites, Microporous Mater., 8 (1997) 3-17.

[59] J.K. Solem-Tishmack, G.J. McCarthy, B. Docktor, K.E. Eylands, J.S. Thompson, D.J. Hassett, High-calcium coal combustion by-products: Engineering properties, ettringite formation, and potential application in solidification and stabilisation of selenium and boron, Cem. Concr. Res., 25(1995) 658-670.

[60] M. R. Hartman, S. K. Brady, R. Berliner, M. S. Conradi, The evolution of structural changes in ettringite during thermal decomposition, J. Solid State Chem., 179(2006) 1259-1272.

[61] L. Eklund, I. Persson, Structure and hydrogen bonding of the hydrated selenite and selenate ions in aqueous solution, Dalton Trans. 43(2014) 6315-21.

[62] S. Sharmasarkar, G. F Vance, Selenite–selenate sorption in surface coal mine environment, Adv. Ecol. Res., 7(2002) 87-95.

[63] B. Guo, Q. Tian, T. Oji, L. Wang, K. Sasaki, Effects of Mg compounds in hydroxylated calcined dolomite as an effective and sustainable substitute of lime to precipitate as ettringite for treatment of selenite/selenate in aqueous solution, Colloids Surf. A Physicochem. Eng. Asp., 610(2021) 125782,

[64] M.R. Hartman, R. Berliner, Investigation of the structure of ettringite by time-of-flight neutron powder diffraction techniques, Cem. Concr. Res., 36(2006) 364-370.

[65] G. D. Gatta, U. Hålenius, F. Bosi, L. C. Delgado, M. T. F. Diaz; Minerals in cement chemistry: A single-crystal neutron diffraction study of ettringite, Ca6Al2(SO4)3(OH)12·27H2O. American Mineralogist, 104(2019) 73–78.

[66] Goetz-Neunhoeffer, F., & Neubauer, J, Refined ettringite (Ca6Al2(SO4)3(OH)12·26H2O) structure for quantitative X-ray diffraction analysis. Powder Diffraction, 21(2006) 4-11.

[67] I. Baur and C. A. Johnson, Sorption of Selenite and Selenate to Cement Minerals, Environ. Sci. Technol., 37(2003) 3442-3447.

[68] R. B. Perkins, C. Palmer, Solubility of ettringite (Ca6[Al(OH)6]2(SO4)3·26H2O) at 5–75°C, Geochim. Cosmochim Acta, 63(1999) 1969-1980.

[69] Bootharaju, M. Siddaramappa, Reversible Size Control of Silver Nanoclusters via Ligand-Exchange, Chem. Mater., 27(2015) 4289-4297.

[70] G. H. Woehrle, L. O. Brown, J. E. Hutchison, Thiol-Functionalised, 1.5-nm Gold Nanoparticles through Ligand Exchange Reactions: Scope and Mechanism of Ligand Exchange, J. Am. Chem. Soc., 127(2005) 2172–2183.

[71] N. Takeno, Atlas of Eh-pH diagrams - Intercomparison of thermodynamic databases, Open File Report of GSJ, 419(2005). Geological Survey of Japan, AIST.

# CHAPTER 5

## SURFACE CHEMISTRY AND RADIONUCLIDE ANION IMMOBILISATION POTENTIAL OF PHOSPHORIC ACID-ACTIVATED METAKAOLIN-BASED GEOPOLYMERS

## 5.1 Introduction

The rapid development of contemporary society has brought about remarkable progress in industry and technology, but it has also resulted in a series of significant environmental problems. Among them, the development of the nuclear industry is a prominent example [1, 2, 3]. While the nuclear industry has brought tremendous energy and technological advancements to humanity, it has also produced vast quantities of contaminations, including radionuclides, which are not only released during nuclear accidents [4, 5, 6] but are also generated during normal nuclear facilities operations, posing a significant threat to the natural environment and human health through their diffusion and accumulation in groundwater [7, 8, 9]. At present, an important issue worldwide is how to handle and control the large number of radionuclides generated by the nuclear industry in an efficient, economical and environmentally friendly manner.

Stabilisation/solidification (S/S) technology is widely used for solidifying hazardous waste into a stable, inert, and impermeable material [10, 11, 12]. This process involves mixing the waste with a binder, such as cement, lime, or gypsum, to form a solid block that reduces the environmental threat posed by hazardous waste [13, 14]. Applying S/S technology to nuclear waste disposal has become an essential research topic in recent years. Low to intermediate-level radioactive waste (LLW and ILW) can be stabilised and immobilised using S/S technology [15, 16]. This method has advantages over other disposal methods, such as reducing the volume of waste and increasing its density, making it easier to transport and store [17].

Geopolymer materials are a well-known class of inorganic polymer materials that has gained significant attention due to their low density, excellent thermal and mechanical properties, outstanding fire resistance, excellent chemical resistance, and strong resistance to permeability [18]. Using geopolymer as a potential substitute for Portland cement in nuclear waste management, especially in applying S/S, has gained global attention [19]. Compared to conventional cementitious materials, geopolymer materials have demonstrated superior chemical durability due to their three-dimensional framework structure derived from oxygen-linked aluminium and silicon as well as their higher degree of silicate polymerisation [20].

The common geopolymers that have been extensively studied are alkali-activated aluminosilicate materials (AAMs). The geopolymerisation process involves the depolymerisation, polycondensation, and formation of a gel network of an aluminosilicate precursor when exposed to a highly alkaline solution or activator [21, 22]. AAMs are being explored as a potential solution for the long-term storage of wastewater contaminants, including used absorbent materials such as zeolites, which can encapsulate radionuclides [23]. Due to the large number of tetrahedral aluminium sites, AAMs have a permanent negative framework charge [24, 25]. This surface electrical property makes AAMs of great application in the uptake and adsorption of cationic nuclides [26-30]. $Cs^{+}$ in AAMs would form complexes with zeolites under an alkaline environment and eventually be firmly immobilised in the AAMs [31]. Soonthornwiphat et al. [18] reported that the AAMs have an excellent S/S performance to encapsulate $Sr^{2+}$-loaded titanate ion exchangers. Tian et al. [32] successfully immobilised $SeO_3^{2-}$ and $SeO_4^{2-}$ into AAMs and found that electrostatic interaction is the primary association mode of selenium in geopolymer. However, according to the findings in

our previous study [26] that the permanently negatively charged surface of AAMs restricts the potential for adsorption of anionic radionuclides such as selenium ($^{79}Se$) or iodine ($^{131}I$). Therefore, it raises concerns about the reliability and longevity of AAMs as a solidification method for anionic nuclides, including selenium ($^{79}Se$) or iodine ($^{131}I$).

Acid-activated geopolymers provide an intriguing alternative to AAMs. Among them, phosphoric acid-activated geopolymers (PGPs) are the most well-known and widely used [33]. The acid activators used in PGPs, such as phosphoric acid, have been found to require lower temperatures and emit less $CO_2$ when compared to traditional alkaline activators, such as sodium hydroxide or silicate solutions [34]. Moreover, PGPs exhibit superior mechanical properties in comparison to AAMs [35-37]. Recently, the application of PGPs in the disposal of environmentally hazardous substances is also gaining increasing attention [30]. Liu et al. [38] introduced a new type of porous phosphoric acid-activated metakaolin-based geopolymer foam material and its application in the removal of mixed pollutants (Pb(II), Cd(II), and Ni(II)) from aqueous. Tome et al. [39] reported that phosphoric acid-activated volcanic ash-based geopolymers have the adsorptive potential for anionic (Eriochrome Black T/EBT) and cationic (methylene blue/MB) dyes from water. And in terms of S/S applications, PGPs have also received attention recently. Pu et al. [40] found that acid-activated geopolymers better stabilise $Pb^{2+}$ than cement or alkali-activated geopolymer. However, to our knowledge, the study on the S/S of radionuclides by PGPs is limited, especially of anionic radionuclides such as selenium ($^{79}Se$) or iodine ($^{131}I$). An area that requires significant attention in the field of anionic radionuclide stabilisation and solidification is the surface chemistry and electrical properties of PGPs. While AAMs have been extensively researched

and acknowledged for their permanently negatively charged surface [16], there is a noticeable lack of comprehensive studies in understanding these aspects for PGPs. This knowledge gap poses a significant disadvantage in exploring the potential of PGPs for the immobilisation of anionic radionuclides, highlighting the need for further research in this area.

This study aims to understand the surface chemistry and structure-associated electrostatic properties of PGPs and explore their viability in the field of stabilisation/solidification for $SeO_3^{2-}$, $SeO_4^{2-}$, $I^-$, and $IO_3^{2-}$. Notably, this is the first instance where these specific substances are being considered for S/S implementation utilising PGPs. The surface properties of PGPs were evaluated using a combination of X-ray photoelectron spectroscopy (XPS), zeta potential, X-ray diffraction (XRD), nuclear magnetic resonance spectroscopy (NMR), and inductively coupled plasma optical emission spectroscopy (ICP-OES). The S/S capacity of PGPs towards $SeO_3^{2-}$, $SeO_4^{2-}$, $I^-$ and $IO_3^{2-}$ was evaluated using a combination of XRD, inductively coupled plasma mass spectrometry (ICP-MS), and Fourier-transform infrared spectroscopy (FTIR). By conducting this thorough analysis, a deeper understanding of the surface chemistry of PGPs is attained. Moreover, the findings presented in this study furnish compelling evidence that supports the secure disposal of PGPs, especially those containing radionuclides or other potentially harmful environmental substances.

## 5.2 Experimental

### 5.2.1 Materials

Metakaolin (MK) obtained from Sobueclay (Japan) was used to synthesise PGPs. The chemical composition of metakaolin determined by X-ray fluorescence (XRF) is listed in **Table 5-1**; the molar ratio of $SiO_2$:$Al_2O_3$ of metakaolin is 1.01. An analytical-grade pure commercial phosphoric acid (WAKO (Japan), 85 wt.% $H_3PO_4$), and ultrapure water (TRUSCO, Japan) were used for making a phosphoric acid solution, which was used as an acidic activator for the synthesis of PGPs. $KNO_3$ (KANTO, >99%), KOH (KANTO, >86%), and $HNO_3$ (KANTO, 61%) were used for the adjustment of pH and ionic strength in solutions. In addition, $K_2SeO_3$, $K_2SeO_4$, KI and $KIO_3$ were selected as the simulated radionuclide sources, purchased from WAKO (Japan).

**Table 5-1.** Chemical composition (wt. %) of the metakaolin as determined by X-ray fluorescence.

| Component | Metakaolin |
|---|---|
| $SiO_2$ | 48.59 |
| $Al_2O_3$ | 43.11 |
| $Fe_2O_3$ | 0.54 |
| CaO | 0.21 |
| MgO | 3.66 |
| $Na_2O$ | 2.25 |
| $K_2O$ | 0.13 |
| $TiO_2$ | 1.27 |
| $P_2O_5$ | 1.08 |

| | |
|---|---|
| SO3 | - |
| L.O.I.* | 1.74 |

*: L.O.I. is loss on ignition at 1100℃ for 12h.

### 5.2.2 PGPs synthesis

PGPs were prepared by mechanically mixing stoichiometric amounts of metakaolin with a sufficient quantity of acidic-activated solution giving a solid to liquid mass ratio of 1. Those acidic-activated solutions were prepared by dilution from an 85 wt.% phosphoric acid, and detailed information on PGPs sample compositions is shown in **Table 5-2,** where Si and Al were determined through the molar content of $SiO_2$ and $Al_2O_3$ in metakaolin (**Table 5-1**), and P represented the molar of $H_3PO_4$ from phosphoric acid. To achieve efficient curing while mitigating thermal cracking, a two-stage curing protocol was employed following the acquisition of a homogeneous slurry, as per a prior investigation [41]. This procedure involved an initial pre-curing phase at 40°C for 24 hours, succeeded by a subsequent 24-hour curing phase at 60°C. Afterwards, PGPs were ground to a particle size of less than 150 μm and stored in vacuum bags for further analysis.

**Table 5-2.** The molar ratio of the Si, Al and P in the PGPs, and the concentration and mass fraction of acid activator solutions.

| Samples | Si/Al | P/Al | P/$H_2O$ | $H_3PO_4$ (mM) | $H_3PO_4$ (wt. %) |
|---|---|---|---|---|---|
| PGP1 | 0.956 | 1.025 | 1.042 | 14.659 | 85 |
| PGP2 | 0.956 | 0.821 | 0.391 | 10.305 | 68 |

| | | | | | |
|---|---|---|---|---|---|
| PGP3 | 0.956 | 0.615 | 0.191 | 6.893 | 51 |
| PGP4 | 0.956 | 0.410 | 0.094 | 4.147 | 34 |

### 5.2.3 Surface chemical properties experiments

#### 5.2.3.1 Structural characterisation of PGPs

A Rigaku X-ray diffractometer (MultiFlex, Rigaku, Japan) was used to characterise the synthetic samples with CuKα radiation, scanning from 2θ=5-70° with a scan speed of 6.5° per min and a step size of 0.02°. Solid-state magic angle spinning (MAS) nuclear magnetic resonance (NMR) spectra of the PGPs were acquired using a Bruker 500 MHz spectrometer equipped with an 11.74T magnet. $^{29}$Si MAS NMR spectra were collected at 99.4MHz using a φ3.2mm probe with a pulse width of 1.5 μs (30°), a spinning speed of 5 kHz and a total of 2800 scans were recorded with 20 s recycle delay for each sample. For $^{27}$Al MAS NMR experiments, a φ2.5mm probe operating at 130.4MHz with a pulse width of 5.8 μs (90°), spinning at 30 kHz, was used to record a total of 3600 scans, with a 5 s recycle delay for each sample. Chemical shifts for both $^{29}$Si and $^{27}$Al nuclei were referenced to hexamethylcyclotrisiloxane ($C_6H_{18}O_3Si_3$) and $AlCl_3$ solution (1 mol/L).

#### 5.2.3.2 Zeta potential measurement

A zeta potential & particle size analyser apparatus (ELSZ-1000ZS) was used to measure the zeta potential of the PGPs in neutral (pH = 7) and acidic/alkaline (pH: 2~12) solutions with ionic strength of 10 and 100 mM, and the solid/liquid ratio of suspension was set to 1 g/L.

Moreover, the zeta potential of PGP2 changes with time in $SeO_3^{2-}$, $SeO_4^{2-}$, $I^-$, and $IO_3^-$ solutions were determined. The initial concentrations of anions were 1 mM, and the pH and ionic strength were set as 4 and 10 mM, respectively. Solutions of the same ionic strength and pH without any $SeO_3^{2-}$, $SeO_4^{2-}$, $I^-$, and $IO_3^-$ were used as controls. The zeta potential was measured after immersion of 1, 3, 7, 14, 21, and 28 days. Among the various solutions for examining zeta potential, $KNO_3$ was selected to modulate the ionic strength, whereas KOH and $HNO_3$ were employed to regulate the pH.

### 5.2.3.3 Component changes of PGPs in the aquatic environment

The quantity of P, Si, and Al that dissolved from PGP 1-4 in water, acid, and alkaline solutions was determined using inductively coupled plasma-atomic emission spectroscopy (ICP-OES, SPECTROBLUE, Hitachi, Japan). The ICP-OES analysis covered a wavelength range of 165 nm to 770 nm. The pH values of the solutions were measured using a pH meter from AS ONE Ltd. in Japan, specifically the AS800 model. The solid/liquid ratio of all suspensions was set to 1 g/L, the ionic strength of acidic and alkaline solutions was set to 10 mM by $KNO_3$, and the pH was controlled through KOH and $HNO_3$.

### 5.2.3.4 XPS measurement

X-ray photoelectron spectroscopy (XPS) analysis was performed using a JPS-9200 (JEOL, Japan) for detailed chemical composition characterization of PGPs before and after immersion treatment in water or pH solutions, using X-ray-induced photoelectron spectroscopy. Photoelectron emission was excited by the monochromatic Mg Kα line with a

photon energy of 1253.6 eV. Detailed spectra of every sample were taken through a narrow scan with an energy step of 0.1 eV, and a dwell time of 100 ms. Charging compensation was performed using a neutralizing electronic gun under constant current and voltage. The binding energy axis was adjusted according to the position of the carbon C 1s line.

### 5.2.4 Stabilization/solidification (S/S) and leaching experiment

#### 5.2.4.1 Preparation of solidified wasteform

PGP2 samples were selected as the matrix to solidify $SeO_3^{2-}$, $SeO_4^{2-}$, $I^-$ and $IO_3^-$. The calculated amount of $K_2SeO_3$, $K_2SeO_4$, KI and $KIO_3$ was dissolved in an acid activator solution before mixing with metakaolin to obtain 1 mmol target anions per 100 g of PGPs paste. The fresh mixture was cast into a cylindrical mould with a height of 1.5 cm and an inner diameter of 1.3 cm after stirring, obtaining a 3.6 g (± 0.02g) specimen containing approximately 36 μmol of target anions. These specimens were sealed with parafilm and underwent 2-stage curing as original PGPs.

#### 5.2.4.2 Leaching experiments

Leaching experiments were subsequently conducted after curing, referencing the ANSI/ANS-16.1-2003 standard test (American Nuclear Society, 2004). Each specimen was immersed in an 88 mL deionised water as leachant (the ratio of leachant volume to specimen surface area is 10 mL/cm$^2$) as shown in **Figure 5-1**. The leachant was replaced entirely after cumulative leach times of 2 hours, 9 hours, and 1, 2, 3, 4, 5, 7, 14, 21and 28 days under room temperature from the onset of the test. The leachate was then analysed at each time point to

determine the released $SeO_3^{2-}$, $SeO_4^{2-}$, $I^-$ and $IO_3^-$ from the PGP2 matrix . The specimens were recovered after 28 days of leaching experiment and then ground into powder less than 150 μm for solid analysis after 3 days dry in a 40℃ thermostat.

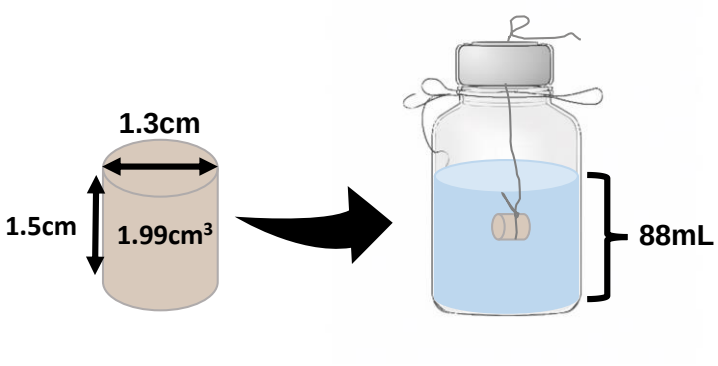


**Figure 5-1.** Schematic of leaching experiments.

### 5.2.4.3 Analytical methods of leaching result

The leachates obtained from the leaching experiments were analysed by inductively coupled plasma-mass spectroscopy (ICP-MS, iCap Q ICP-MS, Thermo Scientific, USA, detection limit 0.01-10ppb). The measurement of $SeO_3^{2-}$ and $SeO_4^{2-}$ was conducted with the application of the Yttrium internal standard method and using ultrapure water as a solvent; all solutions used for ICP-MS measurements were spiked with 1% $HNO_3$ (~60 wt.%) for sample protection. The measurement of $I^-$ and $IO_3^-$ was conducted with the application of the Caesium internal standard method and using 0.5% Tetramethylammonium hydroxide (TMAH) as a solvent; all solutions used for ICP-MS measurements were spiked with 1% $Na_2SO_4$ (1 wt.%) for sample protection. The anions-solidified PGP2 samples before and after the leaching experiment were characterised via Fourier transform infrared (FTIR)

spectroscopy (JASCO670, Japan) at a constant spectral resolution of 4 $cm^{-1}$. Solid samples were recorded in the wavenumber range of 400–2000 $cm^{-1}$ after dilution with KBr and pressing into tablets. In addition, X-ray diffraction (XRD) measurements were conducted using the same method for all solid samples before and after leaching experiments.

## 5.3 Results and discussion

### 5.3.1 Microstructure characterisation

#### 5.3.1.1 XRD

**Figure 5-2** shows the X-ray diffraction pattern of the metakaolin precursor and the PGPs obtained after a 2-stage curing process using different concentrations of phosphoric acid as the activator. The XRD pattern of the metakaolin precursor exhibits a broad hump in the 2θ range of 15-30°, along with minor crystalline phase peaks of mullite and quartz, which are retained in all concentrations of acid-activated PGPs as an inert phase. Upon activation with acidic activators, the broad hump of all samples shifted towards 17-35°, indicating that the PGPs have a more disordered short-range structure with relatively shorter interatomic distances compared to the metakaolin precursors. Among the four types of PGPs, PGP2 exhibits the highest reactivity and the densest structure, as evidenced by the largest relative variation and the fullest hump in the high diffraction angle region. This suggests that a concentration of approximately 10.3 mM may be the optimal concentration for the phosphoric acid-activated activator, consistent with previous findings [44].

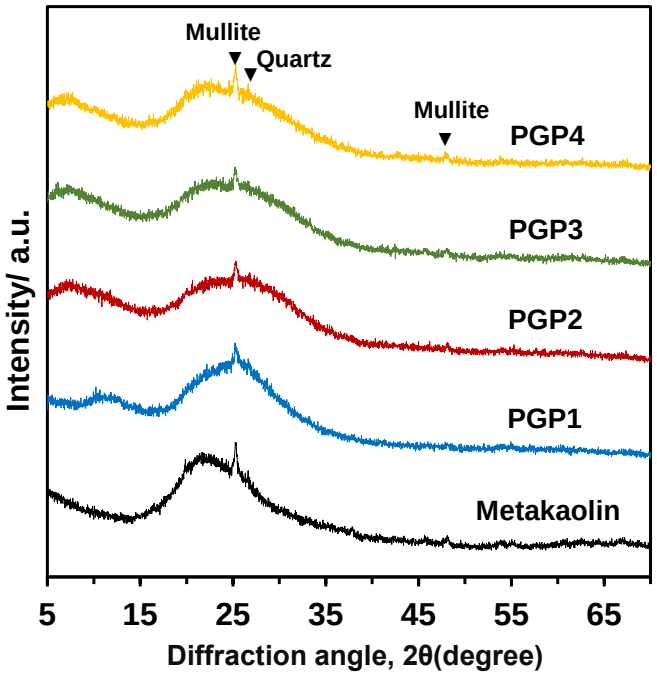


**Figure 5-2.** X-ray diffraction (XRD) patterns of metakaolin and PGPs.

### 5.3.1.2 $^{29}$Si NMR

In cementitious materials, silicon sites are often labelled using the notation $Q^n$(mAl), where Q represents silicon in tetrahedral coordination, and n and m denote the number of tetrahedral atoms and aluminium atoms bonded to the silicon, respectively. The range of values for n and m is from 0 to 4, indicating that the silicon is connected to n other tetrahedral atoms, out of which m are aluminium, through oxygen bridges. Based on this labelling system [40], **Figure 5-3(a)** illustrates the correspondence between the $^{29}$Si nuclei in different chemical environments of cementitious materials and their respective typical ranges of chemical shifts. As the number of bridged oxygen atoms around silicon increases, the chemical shift gradually shifts toward the high field region. This suggests that there is an enhancement of

electromagnetic shielding. Likewise, when more aluminium atoms are substituted around the silicate tetrahedrons, the silicon is exposed to more electromagnetic shielding, causing the $Q^4$(mAl) chemical shift to shift toward the high field.

**Figure 5-3(b-f)** displays the $^{29}$Si NMR spectra along with their corresponding individual Gaussian peaks after the deconvolution process. The main chemical environment of Si in phosphoric acid-activated metakaolin PGPs are reported to include $Q^0$, $Q^1$, $Q^2$(1Al), $Q^3$(1Al), $Q^4$(4Al), $Q^4$(3Al), $Q^4$(2Al), $Q^4$(1Al) and $Q^4$(0Al), which are positioned at chemical shifts approximately around −68 ± 5 ppm, −76 ± 5 ppm, −85 ± 3 ppm, −86 ± 4 ppm, −88 ± 3 ppm, −94 ± 4 ppm, −100 ± 5 ppm, −105 ± 4 ppm, and −115 ± 4 ppm, correspondingly [41]. However, it is important to note that the structural units, such as $Q^4$(4Al), $Q^4$(3Al), $Q^4$(2Al), $Q^4$(1Al) and $Q^4$(0Al), may not necessarily correspond to a single chemical shift peak due to significant overlap between broad resonances in disordered solid phases, particularly for the silicate tetrahedrons. As a result, multiple deconvolution techniques have been utilised to achieve a more accurate fit.

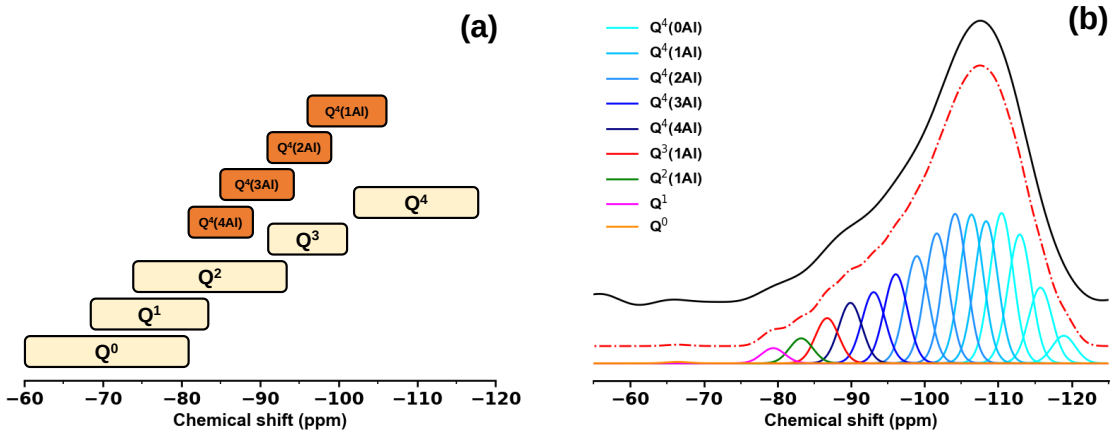

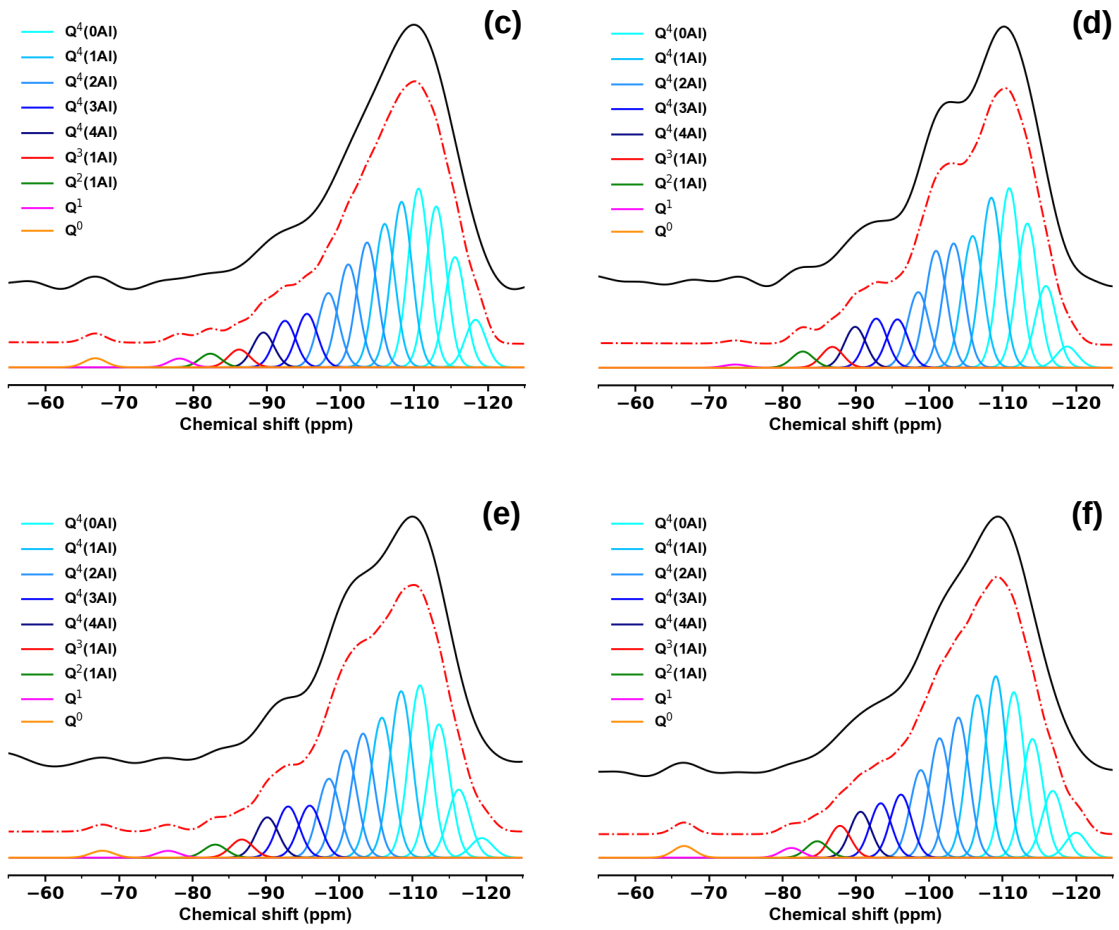


**Figure 5-3.** The typical ranges of the $^{29}$Si chemical shift variation in most classes of solids (a) and deconvolution results of $^{29}$Si NMR spectra for MK and the PGPs after curing: (b) MK, (c)-(f) PGP1, PGP2, PGP3, and PGP4, respectively.

**Figure 5-4** shows the molar fraction of silicon in different chemical environments in the metakaolin and PGPs, which were derived from $^{29}$Si NMR spectra deconvolution results. The $Q^4$(0Al) units are found to be the dominant species for a given PGPs sample, and their proportion increases with the concentration of the acid activator. In contrast, the remaining silicate tetrahedrons decrease as the concentration of the acid activator increases. This is

because higher concentrations of acid activator cause more significant dealumination of metakaolin. This dealumination process will promote the condensation of silicate tetrahedrons, increasing $Q^4$(0Al). It is also noteworthy that the $Q^4$ (1Al) units of all PGPs increase to varying degrees compared to metakaolin. This is because $Q^4$(1Al) is also the product of the dealumination of higher aluminium content silicate tetrahedrons, and higher concentrations of acid activator will further enable the process of dealumination of $Q^4$(1Al), resulting in more $Q^4$(0Al).

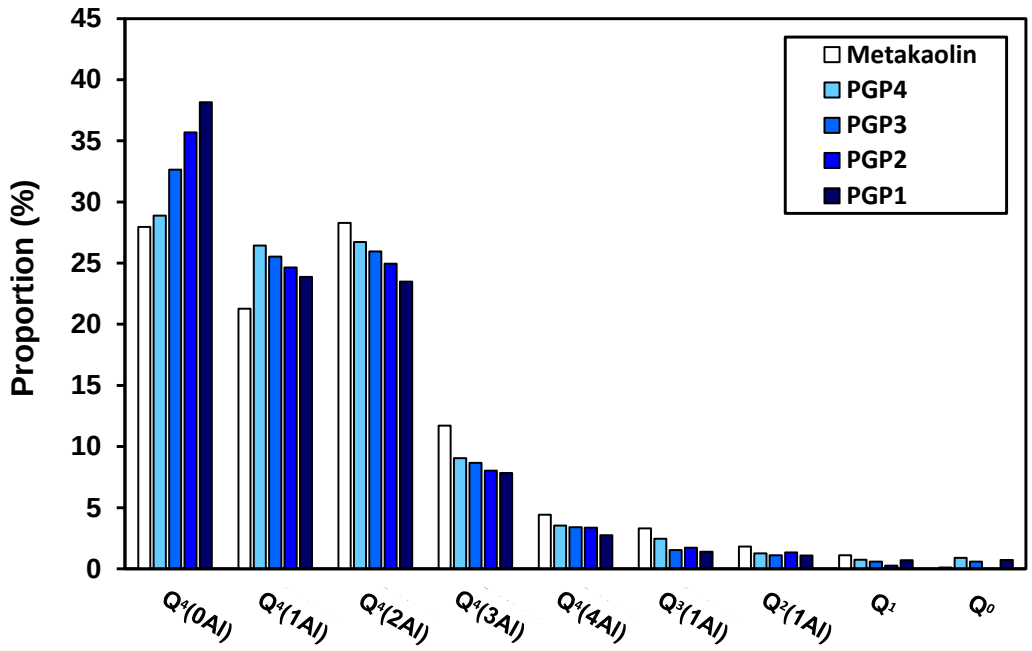


**Figure 5-4.** Molar proportions of Si structural units in MK and PGPs quantified through the $^{29}$Si NMR deconvolved spectra.

### 5.3.1.3 $^{27}$Al NMR

**Figure 5-5(a)** illustrates the primary features of the $^{27}Al$ chemical shift variation observed in most types of porous aluminosilicate solids, where aluminium (Al) typically exists in IV-, V-, and VI-fold coordination structures [46]. As the number of coordination structures around the Al atom increases, the chemical shift gradually shifts to higher fields. However, the chemical shifts of Al with the same coordination number can vary depending on the type of atom connected to Al via a bridging oxygen atom. In general, $Al_x$-OP has a chemical shift closer to the high field range than $Al_x$-OSi/OH because phosphorus (P) is less electronegative than oxygen (O) and silicon (Si). The deconvolution strategy for $^{27}Al$ in the PGPs sample is different from that for $^{29}Si$ because $^{27}Al$ ($S = 5/2$) is a class of quadrupolar nuclei ($S > 1/2$), and quadrupolar interactions must be taken into account in the process of simulating the spectra [45]. As a result, the deconvolution and simulation of $^{27}Al$ NMR spectra in this study were achieved by combining multiple Pearson IV functions [47].

The deconvolution results of $^{27}Al$ NMR spectra for metakaolin and PGPs are shown in **Figure 5-5(b-f)**. The chemical environment of Al in metakaolin is mainly composed of IV- and V-coordinated structures, with a small fraction of VI-coordinated structures. Upon activation with an acid activator, the original VI-coordinated Al species linked to Si/OH in metakaolin disappears, and the V-coordinated Al species decrease significantly. Meanwhile, new IV-, V-, and VI-coordinated Al species linked to -OP are generated. The intensity corresponding to the VI-coordination Al species linked to -OP increases significantly with the increasing concentration of acid activator.

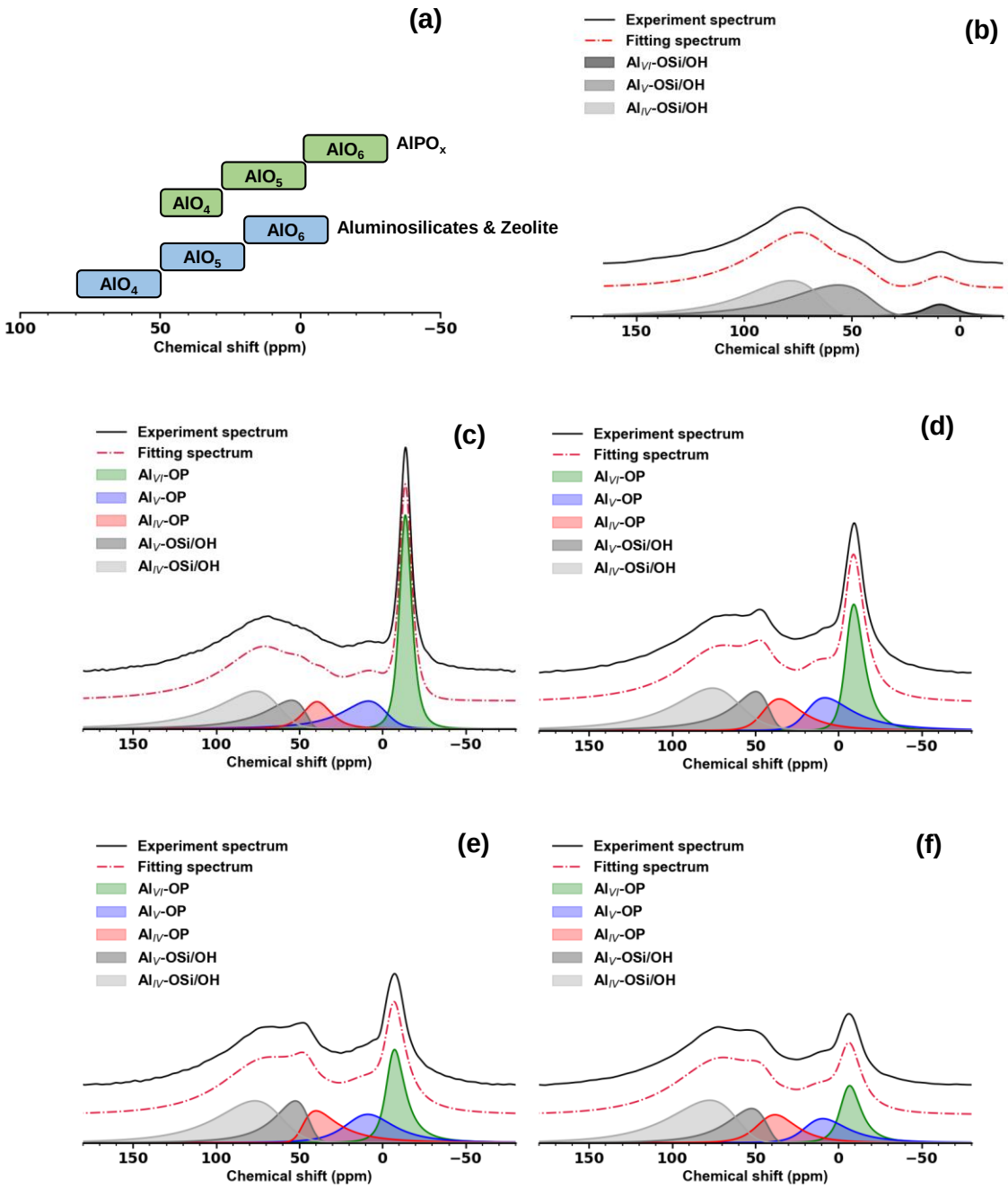


**Figure 5-5.** The typical ranges of the $^{27}$Al chemical shift variation in most classes of solids (a) and deconvolution results of $^{27}$Al NMR spectra for MK and the PGPs after curing. (b) MK, and (c)-(f) PGP1, PGP2, PGP3, and PGP4, respectively.

**Figure 5-6** shows the molar proportion of Al in metakaolin and PGPs for each chemical structural unit based on $^{27}$Al NMR deconvolution. Upon activation of metakaolin to form PGPs, the $Al_{VI}$-OSi/OH component is eliminated, while there also are notable reductions in the $Al_{V}$-OSi/OH and $Al_{IV}$-OSi/OH components. The reduction of the latter two is positively correlated with the concentration of the acid activator. The proportion of $Al_{VI}$-OP, a novel structural unit generated in PGPs, increases significantly with elevated activator concentration. In contrast, the proportion of the other two newly formed structure units, $Al_{IV}$-OP and $Al_{V}$-OP, decreases with higher acid activator concentration. Although PGP4 with the lowest concentration of acidic activator exhibited the lowest percentage of $Al_{V}$-OP of all PGPs, which may be attributed to the insufficient concentration of acid activator, which hinders the effective progress of dealumination and thus the formation of $Al_{V}$-OP to some extent. These findings indicate that higher concentrations of acid activators facilitate the dealumination process of metakaolin but only favour the formation of new structural units of $Al_{VI}$-OP.

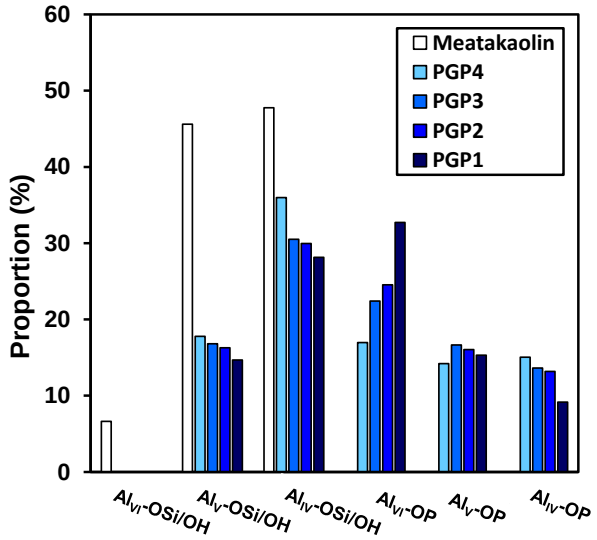

**Figure 5-6.** Molar proportions of Al coordination structural units in MK and PGP 1-4 quantified through the $^{27}$Al NMR deconvolved spectra.

## 5.3.2 Zeta potential

The pH plays a critical role in influencing the surface electrostatic properties of materials. To investigate the zeta potential behavior of PGPs under different pH conditions, PGP powder was immersed in solutions spanning a pH range from acidic to basic (pH: 2~12). The pH and zeta potential values for PGP1 to PGP4 after reaching equilibrium in a neutral solution (pH = 7) are presented in **Table 5-3**. At equilibrium, the pH values exhibited varying degrees of reduction, gradually decreasing with increasing concentrations of the acid activator (PGP4 to PGP1), while the zeta potential showed a corresponding gradual increase. The influence of pH on the zeta potential of PGPs in acidic and basic solutions is depicted in **Figure 5-7.** Similar to the neutral solution (**Table 5-3**), an overall decrease in solution pH was observed after equilibrium, in comparison to the initial pH setting. This decrease can be attributed to the acidic nature of the PGPs activated by the acid activator. The magnitude of pH reduction upon introducing these materials to the solution depended on the concentration of the acid activator. The zeta potential values of PGPs demonstrated an initial increase followed by a subsequent decrease with variations in pH, which was observed in both 10 and 100 mM ionic strength solutions. The zeta potential curve of PGPs in the solution with 100 mM ionic strength appeared flatter compared to that in the 10 mM ionic strength solution. This flattening can be attributed to the formation of a thinner electrical double layer (EDL) on the

surface of PGPs particles in the higher ionic strength solution, resulting in a lower absolute value of zeta potential for the same charge amount [42]. A progressive rightward displacement of the zeta potential peaks was observed across PGP1 to PGP4 in both ionic strength solutions. These peaks exactly correspond to the pH and zeta potential values of PGPs at equilibrium in a neutral solution with an initial pH of 7. This consistency implies that PGPs constantly exhibit the highest positive zeta potential value at the pH where equilibrium is achieved in a neutral environment. The zeta potential will progressively decrease in either direction as the pH deviates from this level.

**Table 5-3.** pH and zeta potential of PGPs at equilibrium in neutral solution.

| | PGP1 | PGP2 | PGP3 | PGP4 |
|---|---|---|---|---|
| pH-10 mM | 3.76 | 4.05 | 4.29 | 4.53 |
| Zeta potential (mV)-10 mM | 40.02 | 36.98 | 33.64 | 25.18 |
| pH-100 mM | 3.66 | 3.98 | 4.24 | 4.41 |
| Zeta potential (mV)-100 mM | 24.95 | 20.08 | 19.55 | 14.88 |

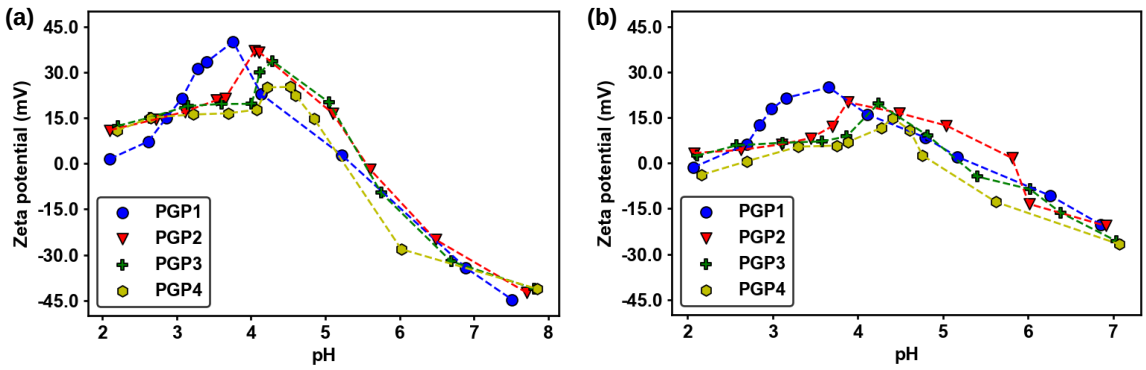


**Figure 5-7.** Zeta potential of PGPs in $NO_3^-$ solutions of ionic strength (a) 10 and (b) 100 mM at various pH values after equilibrium.

The coordination state of Al significantly impacts the surface charge of aluminosilicate materials in their surface structure. For example, the surface is negatively charged in zeolites and AAMs where IV-coordinated Al dominates [48][49]. This is because the tetrahedral $Al_{IV}$ sites always provide Brønsted acidity, resulting in a negatively charged surface [50]. In contrast, octahedral $Al_{VI}$ sites exhibit an amphoteric nature. In acidic environments, they can provide Brønsted basicity and a positive charge after binding to protons, whereas in alkaline environments, they can provide Brønsted acidity and a negatively charged surface [51]. **Figure 5-8** shows the zeta potential of PGPs as a function of the $Al_{VI}/Al_{IV}$ ratio determined using $^{27}Al$ NMR analysis in a neutral solution. The surface charge of the PGPs sample is positively correlated with the $Al_{VI}/Al_{IV}$ ratio in its structure, which can be well explained by the above theories.

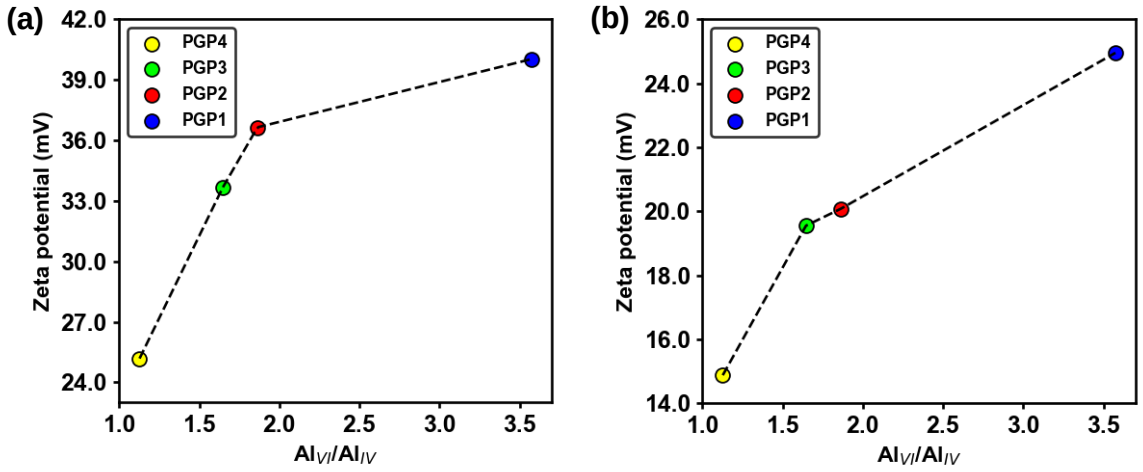


**Figure 5-8.** Zeta potential of PGPs in neutral solution with ionic strengths of (a) 10 mM and (b) 100 mM as a function of $Al_{VI}$ / $Al_{IV}$ molar ratio.

**Figure 5-9** presents the time-dependent zeta potential of PGP2 in four different anion solutions. Following a day of immersion, only the zeta potential of PGP2 in $SeO_4^{2-}$ exhibited a significant decrease compared to the control group. Subsequently, the zeta potentials gradually decreased to varying extents, with a noticeable distinctions observed after 7 days, demonstrating a significant electrostatic attraction of PGP to all anions. The equilibrium was achieved approximately after 14 days, with only a slight decrease observed at 28 days. The reduction in zeta potential after reaching equilibrium followed the order of $SeO_4^{2-}$>$SeO_3^{2-}$>$I^-$>$IO_3^-$. The charge density plays a crucial role in the variation of zeta potential upon adsorption onto colloidal surfaces. Even among ions with the same valence, those with larger ionic size and lower charge density exhibit a relatively limited influence on the zeta potential [43]. While the ionic size of $SeO_4^{2-}$ and $SeO_3^{2-}$ are comparable, the latter acquires protons in acidic surroundings, forming $HSeO_3^-$, thus exhibiting a lower charge

density than $SeO_4^{2-}$. On the other hand, the charge density of $IO_3^-$ with oxygen atoms is considerably lower than that of $I^-$, resulted in a change in the relatively low zeta potential.

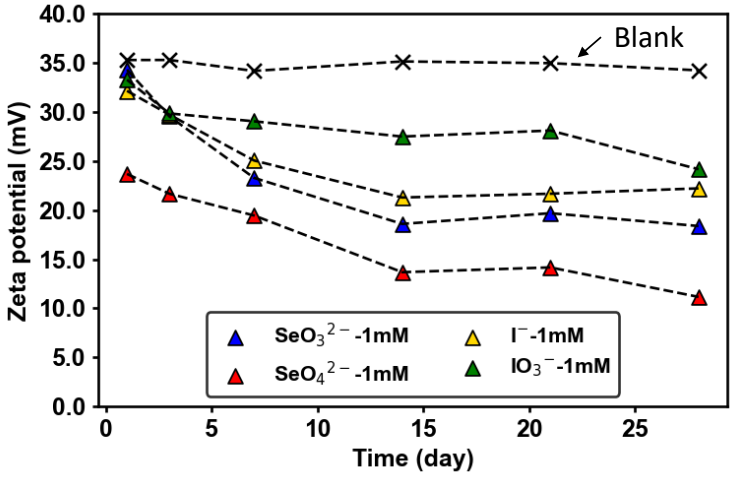


**Figure 5-9.** Zeta potential of PGP2 in anionic solutions of 1 mM concentration with the time change (All solutions have a pH of approximately 3.6 ± 0.2).

## 5.3.3 Surface changes in the aqueous environment

### 5.3.3.1 Component changes

To study the surface behaviours of the PGPs in the aqueous environment, the change in the surface composition of the PGPs after being immersed in water was investigated. **Figure 5-10(a)** presents the percentage and relative proportions of Al, Si, and P in the raw materials. In all PGPs, the proportions of Al and Si remain consistent, given that metakaolin is the source. However, the proportion of P declines as the concentration of acid activator decreases. The composition of the ground PGPs powder is depicted in **Figure 5-10(b)**, the surface of the PGPs shows a higher Si content and lower P and Al content with decreasing concentration

of acid activator, except for PGP1, which has the second-lowest Al content after PGP4. In comparison to the raw material, as determined by the experimental design composition (Fig. 10(a)), it is evident that all PGPs, with the exception of PGP4, exhibit reduced levels of Al and increased levels of P on their surfaces. This can be attributed to the dealumination and penetration of P during the geopolymerisation process, which resulted in a significant number of defective sites in the original Si-O-Al structure. During the grinding process, these sites were easily fractured, thus becoming the surface of the obtained powder. Upon water immersion (**Figure 5-10(c)**), significant amounts of Al and P leached from the surface of the PGPs, while little Si was detected in the leachate. This indicates the inability of the acid activator to dissolve Si in metakaolin and the presence of large amounts of extra-framework Al (EFAL) and free $PO_4^{3-}$ on the surface of the PGPs. Furthermore, the analysis of surface Al, P, and Si contents after water immersion reveals that the relative Al and P content on the surface of all PGPs is similar after water immersion (**Figure 5-10(d)**), which may be attributed to the preference of Al and P for the formation of Al-O-P in the structure [41]. Moreover, the Si content exhibits a rising trend from PGP2 to PGP4, with PGP1 displaying comparable Si content to that of PGP4. This can be explained by the fact that a suitable concentration acid activator (PGP2) can facilitate the geopolymerisation process, resulting in more Al-O-P units forming within the structure. In contrast, excessive concentration of acid activator (PGP1) may promote a rapid dealumination process and the accumulation of $Al^{3+}$ around the metakaolin particles, causing an impediment to the reaction. Therefore, combining the XRD and NMR analysis results, PGP2 was selected as the sample in this context for further study.

When PGP2 was immersed in an acidic environment, the leaching of Al increased significantly as the pH decreased (**Figure 5-10(e)**). Conversely, in an alkaline environment, the leaching of Al remained consistently low and was independent of pH, with any fluctuations presumably due to $Al^{3+}$ precipitation from the basic pH.. Correspondingly, as demonstrated in **Figure 5-10(f)**, the concentrations of Si, Al, and P on the surface of PGP2 exhibited distinct trends when exposed to an acidic solution at different pH levels. Specifically, as solution pH decreased, the proportion of Si increased gradually, while the proportion of Al and P decreased alongside. In contrast, the the individual compositions remained stable after immersion in an alkaline solution.

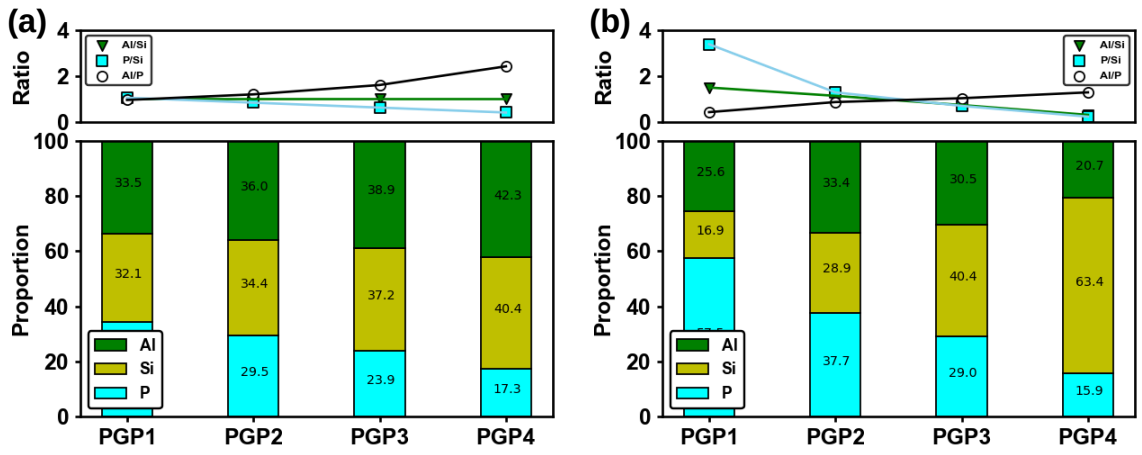

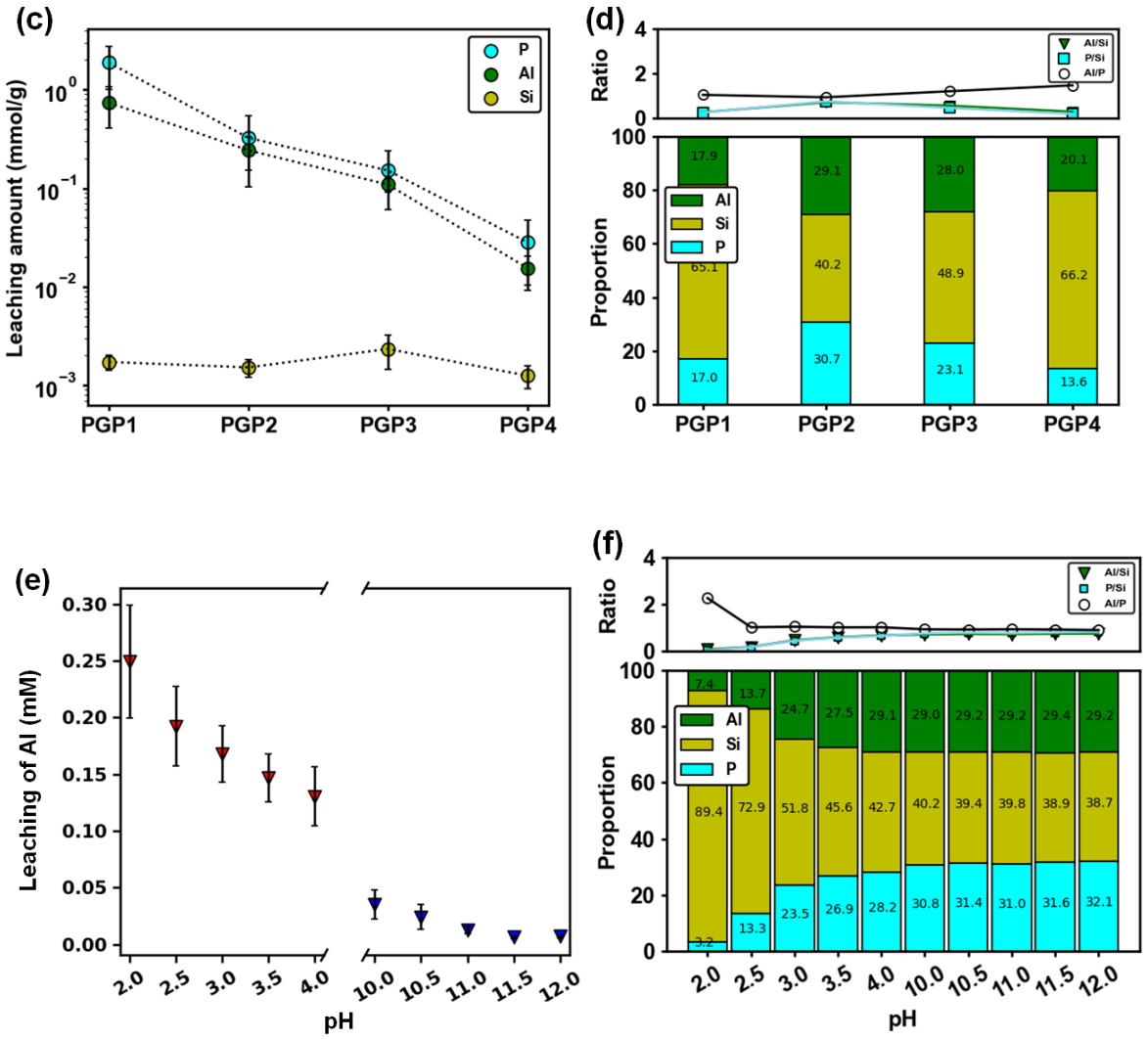


**Figure 5-10.** Proportion and the relative molar ratio of Al, Si and P in (a) raw materials, (b) PGPs before water immersion, (c) PGPs after water immersion. (d) Leaching of Al, Si and P from PGPs into the washing water. (e) Proportion and the relative molar ratio of Al, Si and P in the PGP2 sample with pH variation, and (f) the leaching of Al in the corresponding pH solution.

### 5.3.3.2 XPS spectroscopy analysis

X-ray photoelectron spectroscopy (XPS) was employed to examine the alterations in surface chemistry of PGP2 samples following their immersion in aqueous solutions with varying pH. The resulting XPS spectra changes of Al 2p, Si 2p, O 1s, and P 2p of PGP2 samples in acidic and alkaline solutions are shown in **Figure 5-11(a)** and **(b)**, respectively, to the progressive pH modification. In acidic solutions (**Figure 5-11(a)**), the intensity of Al 2p and P 2p decreases gradually with decreasing pH, which is attributed to the dissolution and leaching of Al and P from the surface of PGP2 in acidic conditions (**Figure 5-10**). Furthermore, as pH levels decrease, the binding energies of Si 2p and O 1s displays a gradual increase. This trend can be attributed to the dissolution of Al and P from the surface structure of PGP2, resulting in a higher electron cloud density around Si and O atoms. In alkaline solutions (**Figure 5-11(b)**), no significant changes in chemical composition or structure are observed from any XPS spectra with increasing pH. The results are in line with prior compositional analyses (**Figure 5-10(f)**) and suggest that PGP2 can maintain a more stable surface chemical structure in an alkaline environment than in an acidic environment.

To fulfil a more comprehensive analysis of the changes in the surface chemical structure of PGP2 under different pH conditions, high-resolution X-ray photoelectron spectroscopy (XPS) spectra at three initial pH values (pH 2, pH 7, and pH 12) were deconvoluted through Gaussian amp function and compared (**Figure 5-11(c)**). Furthermore, a quantification of the different chemical states of the PGP2 sample was conducted, and the results are presented in **Table 5-4**. The Al 2p spectra of PGP2 exhibit two peaks located at 75.15 and 76 eV,

respectively. As established in previous studies [52, 53], the peak at 75.16 eV is attributed to $AlPO_4$ linkages, while the peak at 76 eV corresponds to Al-O-Si bonds. In neutral and alkaline solutions, no significant difference in the Al 2p contributes to both chemical environments. However, in acidic solutions, both peaks are significantly weakened, but the relative intensity of the Al-O-Si peak is dominant. These results indicate that the Al-O-P bond in AlPO4 is more vulnerable to breakage in acidic environments than the Al-O-Si bond. Consequently, the dealumination of the PGP2 surface is primarily caused by the breakage of the Al-O-P bond.

The Si 2p spectra can be deconvoluted into three components. The peak at a binding energy of 102 eV is associated with Si-O-Al [51], while the peaks at around 103.1 and 104 eV are attributed to Si-O-P and Si-O-Si, respectively [54, 55]. The presence of these three stable peaks in neutral and alkaline environments indicates the relative stability of the chemical environment and composition of Si on the PGP2 surface, similar to the behaviour observed for Al. However, in an acidic environment, the Si 2p peak of Si-O-P disappears, leaving only a faint Si-O-Al peak. This suggests that the dealumination of the PGP2 surface in an acidic environment is more plausible to occur through the removal of P-linked Al from Si-O-P-Al, rather than Si-O-Al.

The O 1s spectra of PGP2 can be decomposed into 4 main components. The peak at 531 eV can be attributed to P-O-P bonds from the network structure or P=O bonds from the $PO_4^{3-}$ functional groups [55, 56]. The binding energy peaks at 532.1 and 533 eV correspond to bridging oxygen in Si-O-Al and Si-O-Si, respectively [51, 57]. The peak at 534 eV

corresponds to the O 1s binding energy of terminal Si (Si-OH) groups [58].The O 1s peaks of Si-O-Si in the PGP2 surface exhibit relatively stable content in both neutral and alkaline environments, while an increase in acidic environments is due to dealumination. Correspondingly, the O 1s contributing to Al-O-Si decrease significantly in acidic environments while remaining almost constant in neutral and alkaline environments. Although the O 1s peak corresponding to P-O-P (P=O) is relatively weak, a reduction can still be observed in acidic environments. The O 1s peak corresponding to Si-OH gradually decreases from low to high pH, which can be attributed to the decreasing of Si-OH at the defective sites or terminal Si resulting from broken P-O-Si and Al-O-Si. The $Si\text{-}O^-$ at these fracture points have a strong affinity to accept protons from the acidic environment to form Si-OH. While in an alkaline environment, hydroxyl radical ions in the solution react with the Si-OH on the surface of PGP2, which is a common reaction observed in silicate materials in alkaline environments [59]. This reaction leads to a weakening of the O 1s XPS peak intensity of Si-OH. Notably, as the intensity of the O 1s peak corresponding to Si-OH decreases, a new peak appears at a binding energy of around 534.5 eV, which has been previously identified as O 1s in $Si\text{-}O^-$ [60]. This result also provides evidence that the Si-OH groups on the surface of PGP2 undergo deprotonation to form $Si\text{-}O^-$ in an alkaline environment.

In the P 2p spectra, only one component can be discerned on the PGP2 surface in natural and alkaline environments. This component is likely a mixture of Si-O-P bonds, Al-O-P bonds, and variations in the content of O-P-O and P=O bonds [61]. In such cases, P exists in a crosslinking-type chemical environment, connecting Al and Si in a tetra-coordinated phosphorous [62]. Consequently, it becomes difficult to distinguish the individual

contributions of each bond. However, in the acidic environment, although the intensity of the XPS peak of P 2p is relatively low, a shift of binding energy can still be observed. After deconvolution, a new peak is obtained at approximately 136.18 eV, which is believed to represent the component of terminal-type P. This type of P is only linked on one side with Al or a tiny portion of Si after the breakage of the Al-O-P bond in an acidic environment.

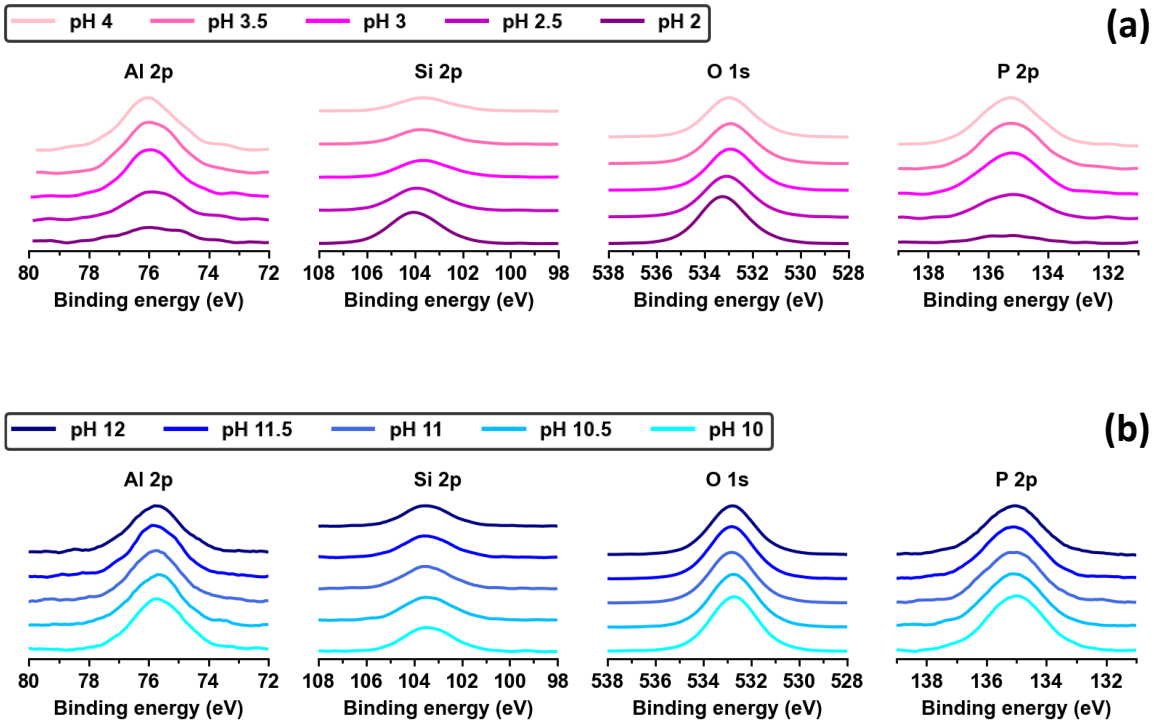

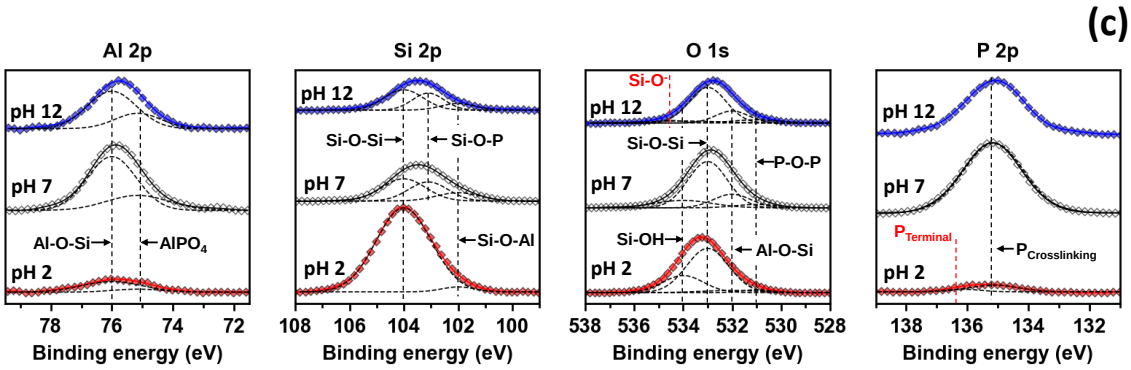


**Figure 5-11.** XPS survey spectra of PGP2 after the immersion in (a) acidic solution and (b) alkaline solution. High-resolution XPS analysis of PGP2 after immersion in water and original pH 2 and 14 solutions: Al 2p, Si 2p, O 1s and P 2p.

**Table 5-4.** X-ray photoelectron spectroscopy of functional groups of PGP2 sample.

| Peak name | Functional group | Binging energy (eV) | Proportion (%) pH 2 | Proportion (%) pH 7 | Proportion (%) pH 12 |
|---|---|---|---|---|---|
| Al 2p | $AlPO_4$ | 75.15 | 18.82 | 26.26 | 27.89 |
| | Al-O-Si | 76 | 81.18 | 73.74 | 72.11 |
| Si 2p | Si-O-Al | 102 | 5.32 | 17.16 | 15.03 |
| | Si-O-P | 103.1 | - | 36.02 | 34.44 |
| | Si-O-Si | 104 | 94.68 | 46.82 | 50.53 |
| O 1s | $P\text{-}O^-$ (P=0) | 531 | 2.97 | 4.98 | 7.40 |
| | Al-O-Si | 532.1 | 4.68 | 17.55 | 19.08 |
| | Si-O-Si | 533 | 67.25 | 62.76 | 63.15 |
| | Si-OH | 534 | 25.10 | 14.71 | 7.13 |
| | $Si\text{-}O^-$ | 534.5 | - | - | 3.24 |
| P 2p | Crosslinking-P | 135.12 | 77.54 | 100 | 100 |
| | Bridging-P | 136.18 | 22.46 | - | - |

### 5.3.4 Evaluation of S/S capacity for anions

The leaching of $SeO_3^{2-}$, $SeO_4^{2-}$, $I^-$ and $IO_3^-$ from PGP2 is shown in **Figure 5-12.** All anions were leached consistently from PGP2-based samples and reached leaching extents of 2.14%, 3.04%, 3.55% and 4.23% for $SeO_3^{2-}$, $SeO_4^{2-}$, $I^-$ and $IO_3^-$ respectively after 28 days. It is evident that PGP exhibit high capability in stabilising Se oxyanions compared to $I^-$ and $IO_3^-$, which perform a lower total leaching amount and a flatter upward curve. Taking electrostatic effect into account, this result is consistent with previous speculations based on zeta potential (**Figure 5-9**). However, the high solidification capacity of PGP2 for $SeO_3^{2-}$ compared to $SeO_4^{2-}$ appears to contradict the zeta potential results (**Figure 5-12(a)**). It should be noted that $SeO_3^{2-}$ in PGP is typically present in the form of $HSeO_3^-$ due to the acidic environment [63]. Therefore, despite having a greater amount of electrostatic attraction, its impact on the zeta potential of the PGP surface is not as strong as that of $SeO_4^{2-}$. On the other hand, it is noteworthy that the PGPs sample containing $I^-$ after the 28-day leaching experiment showed a brownish-yellow substance with a distinctly irritating odour (**Figure 5-12(b)**), which was considered to be KI. Thus, the high solidification ability of PGP for $I^-$ is also favoured by the precipitation of KI in addition to ionic electrostatic attraction, which shows a more pronounced effect on the zeta potential of PGPs than $IO_3^-$ (**Figure 5-9**).

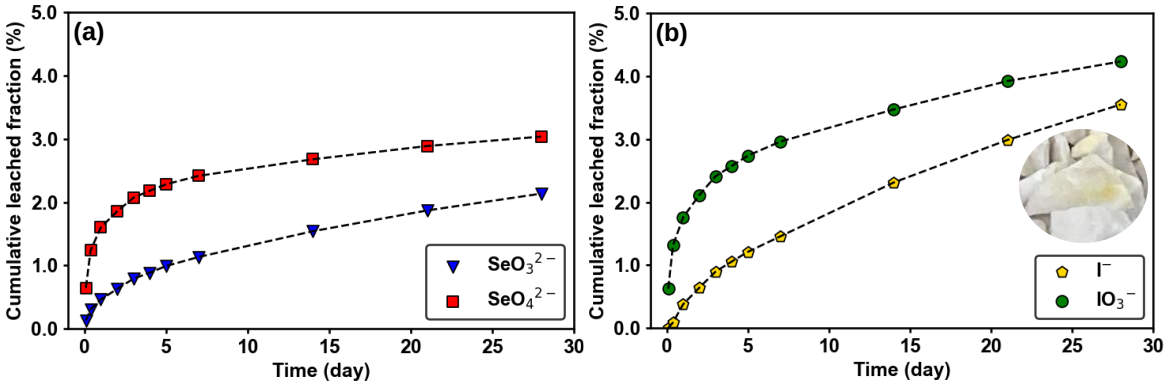


**Figure 5-12.** Cumulative fraction of (a) Se oxyanions ($SeO_3^{2-}$ and $SeO_4^{2-}$), and (b) $I^-$ and $IO_3^-$ leaching from PGP2 for 28 days.

**Table 5-5** compares previous studies on solidifying $SeO_3^{2-}$, $SeO_4^{2-}$, $I^-$ and $IO_3^-$ into the alkaline-activated materials. In a study by Tian et al. [32], $Na_2SiO_3$ and NaOH were used as alkali activators to activate geopolymer materials to solidify Se oxyanions. After an 18-hour leaching procedure, it was determined that the $Na_2SiO_3$-activated geopolymer exhibited superior efficiency in solidifying $SeO_3^{2-}$ and $SeO_4^{2-}$, as compared to NaOH-activated geopolymers, even when enhanced with calcined hydrotalcite (CHT). The former resulted in a leaching percentage of 10% and 18%, respectively. The ability of alkali-activated geopolymer to solidify $I^-$ was ineffective, as over 80% of $I^-$ was leached out during a 21-day leaching process [64]. In addition, due to the lack of studies and data on the immobilisation of $IO_3^-$ by alkali-activated geopolymers, the capacity of typical alkali-absorbent ettringite and layered double hydroxides (LDHs) to immobilise $IO_3^-$ is compared here [65, 66]. Although both ettringite and LDH have demonstrated some capacity for immobilisation, a considerable amount of $IO_3^-$ was still observed to leach out after the leaching process. By comparison, the PGP studied here exhibits a much better capacity for solidification and immobilisation for all

four anions. To the best of our knowledge, this study showcases the highest level of effectiveness compared to all published reports on the solidification capacity of alkaline-activated metakaolin geopolymer substrates for $SeO_3^{2-}$, $SeO_4^{2-}$, $I^-$ and $IO_3^-$.

**Table 5-5.** Leaching of four anionic radionuclides $SeO_3^{2-}$, $SeO_3^{2-}$, $I^-$ and $IO_3^-$ from alkaline-activated materials in literature: alkali-activated geopolymer matrices for Se oxyanions and $I^-$, and other adsorbents for $IO_3^-$, compared with employment of PGPs.

| Condition | $SeO_3^{2-}$ | $SeO_4^{2-}$ | $I^-$ | $IO_3^-$ | reference |
|---|---|---|---|---|---|
| S/S in $Na_2SiO_3$-based GPs | 10% (18 h) | 18% (18 h) | | | [32] |
| S/S in the NaOH-based GPs with calcined hydrotalcite (CHT) | 50% (18 h) | 60% (18 h) | | | [32] |
| S/S in the alkaline-activated metakaolin-based GP | | | >80% (21 days) | | [64] |
| Iodate substituted ettringite | | | | 31% (35 days) | [65] |
| Iodate doped Mg/Al LDHs | | | | 21% (21 days) | [66] |
| S/S in phosphoric acid activated metakaolin-based geopolymer | 2.14% (28 days) | 3.04% (28 days) | 3.55% (28 days) | 4.23% (28 days) | This study |

To study the structural changes occurring during the solidification of anions and the leaching procedure in the PGP2 samples, X-ray diffraction (XRD) was employed. **Figure 5-13(a)** displays the XRD patterns of the original PGP2 sample and the PGP2 samples that underwent solidification with anions. The results indicate that the XRD pattern of the PGP2 sample

remains unchanged with the anion solidification after the 2-stage curing process, displaying the same broad hump in the 2θ range of 15°-35° as the original PGP2 sample. The XRD patterns of the PGP2 samples solidifying anions after 28 days of leaching experiments are shown in **Figure 5-13(b)**. It is obvious that after 28 days of the leaching process, the PGP2 samples with solidified anions still maintain the same XRD pattern as previously. These results indicate that the crystalline structure of PGP2 did not undergo any changes after solidifying the anions and was able to maintain its structural stability even after 28 days of leaching.

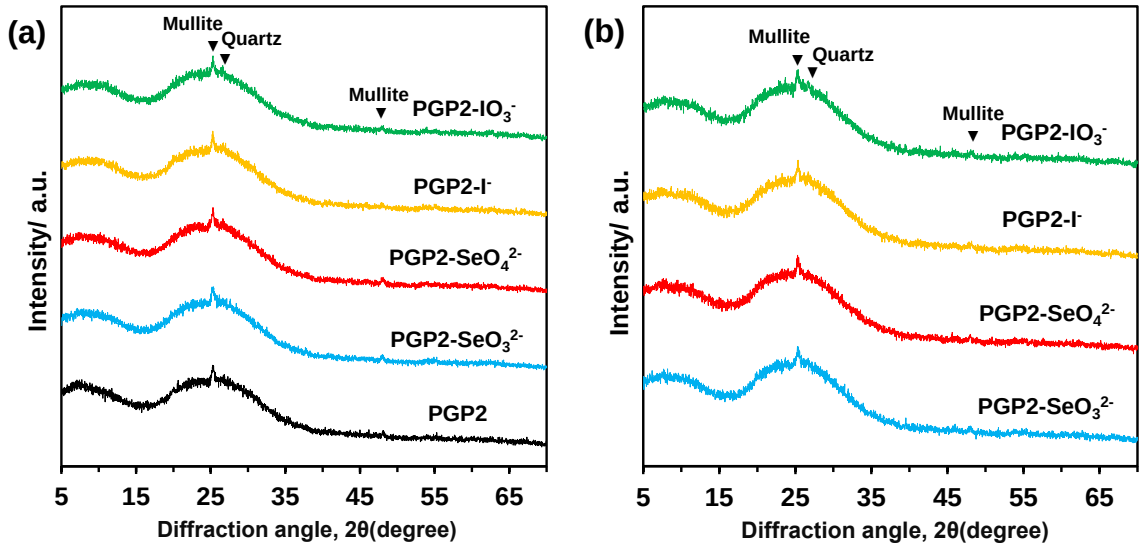


**Figure 5-13**. XRD pattern of pure PGP2 and PGP2 samples incorporated with anions of $SeO_3^{2-}$, $SeO_4^{2-}$, $I^-$ and $IO_3^-$ (a) before and (b) after leaching.

The PGP2 samples with incorporated anions before and after leaching were characterised by FTIR spectroscopy (**Figure 5-14**). The assignments of PGP2 samples absorption peak are determined according to previous studies [41, 67, 68, 69, 70, 71, 72]. The absorption peaks

located at the wavenumber of 1600–1700 $cm^{-1}$ are due to the bending vibration of the OH groups. The peaks at 900-1200 $cm^{-1}$ and 720 $cm^{-1}$ are assigned to the asymmetric and symmetric stretching of Si–O–Si and Al–O–Si, respectively. The peaks at 912 $cm^{-1}$, 800 $cm^{-1}$, 630 $cm^{-1}$ and 450 $cm^{-1}$ are assigned to the stretching and bending vibration of Si-O-P, Si-O-Si, O-P-O, and Si-O, respectively. Moreover, it can be found that there is a faint peak of $CO_3^{2-}$ vibration mode at 1405 $cm^{-1}$. This is because phosphoric acid-activated geopolymers expose active hydroxyl groups on their surfaces during the geopolymerisation (**Figure 5-3**), which can easily absorb carbon dioxide from the air and produce carbonation, disappearing after 28 days of leaching. Notably, all vibration modes of the PGP2 remained unaltered after incorporating anions (**Figure 5-14(a)**). Both the intensities and frequencies remained nearly constant, indicating that the PGP2 matrix retained their structural integrity even after anion incorporation. No new chemical linkages were observed that could have suggested a chemical connection between the PGP2 matrix and the anions. Furthermore, consistent FTIR spectra were observed for all PGP2 samples before and after leaching, indicating that the PGP2 maintained its structural stability even after 28 days of leaching (**Figure 5-14(b)**).

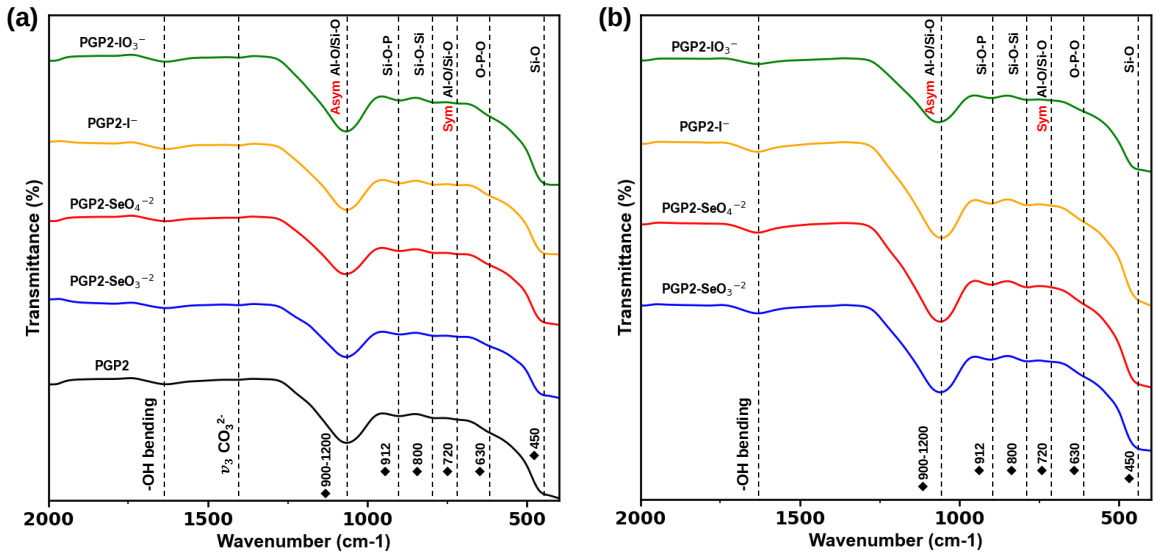


**Figure 5-14.** FTIR spectra of PGP2 samples (a) before and (b) after leaching.

## 5.4 Conclusion

The surface chemistry and structure-related electrostatic properties of phosphoric acid activated metakaolin-based geopolymers (PGPs) and their potential in stabilisation/solidification (S/S) applications have been studied and evaluated through zeta potential, microstructure characterisation, immersion behaviour and leaching experiment. The conclusions could be drawn as follows.

1) PGPs develop $Al_{VI}$-OP and $Al_{IV}$-OP structural units after undergoing the geopolymerisation reaction, whose ratio controls the surface electrostatic properties of PGPs. Increasing concentrations of acid activators lead to a higher ratio of these units, resulting in more sites of positive charge. An optimal concentration of approximately 10.3 mM of the phosphoric acid activator is recommended when activating metakaolin. This

concentration effectively supports the geopolymerisation process without inducing excessive dealumination, which could hinder the reaction.

2) The surfaces of PGPs demonstrate a zeta potential that initially increases and then decreases as pH levels rise. Typically, the zeta potential reaches its peak value at the equilibrium pH in neutral solutions. Within a certain equilibrium pH range of about 2-5, the surfaces of PGPs carry a positive charge and possess electrostatic adsorption capabilities for anions such as $SeO_3^{2-}$, $SeO_4^{2-}$, $I^-$ and $IO_3^-$.

3) When PGPs come into contact with an acidic aqueous environment, the surface structure of PGPs experiences preferential fracture of the $AlPO_4$ units, which contributes to the dealumination process. This phenomenon becomes more prominent as the pH decreases, leading to a decreased ratio of $Al_{VI}$-OP and $Al_{IV}$-OP and subsequently causing a decline in the positive electrical properties of the PGPs surface. Conversely, PGPs show a relatively stable structure in an alkaline aqueous environment. However, a large number of Si-OH structural units in the surface structure, along with VI-coordination Al, which exhibits Brønsted acidity in an alkaline environment, lose their protons and generate negative charges. This process intensifies with pH, leading to an increase in the negative charge of the PGPs surface.

4) The immobilisation of $SeO_3^{2-}$, $SeO_3^{2-}$, $I^-$ and $IO_3^-$ anions within the PGPs matrix is highly effective, without any significant changes in the matrix structure observed after solidification of these anions, even after 28 days of leaching experiments. This effective immobilisation is primarily attributed to the electrostatic attraction between the anions

and the positively charged structural unit, $Al_{VI}$-OP, located at the PGPs matrix interface. Remarkably, this association leads to a significant enhancement in the retention of the anions, compared to previous studies that utilised different matrix.

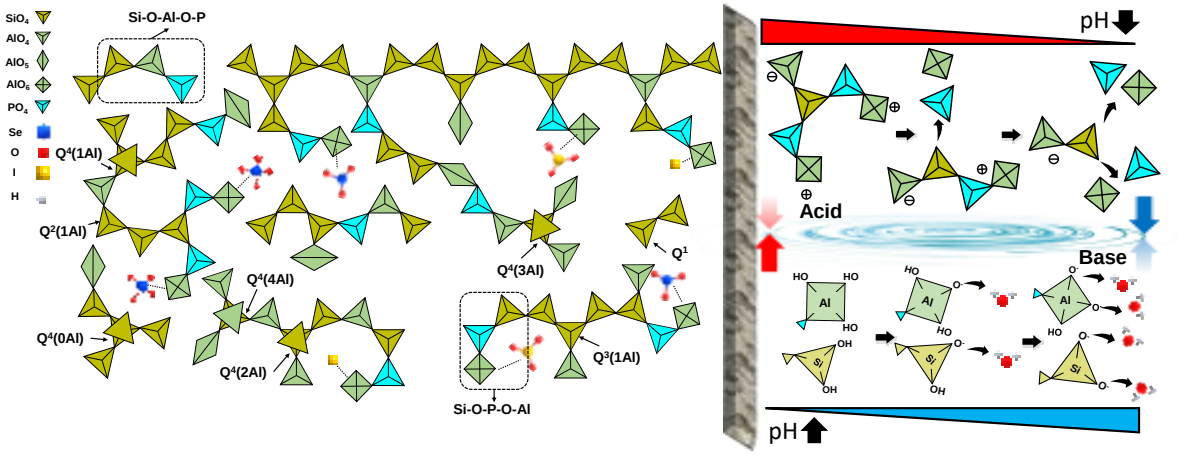


**Figure 5-15.** Schematic illustration of the anion-immobilisation in PGPs and surface behaviour of PGPs in acidic/alkaline aquatic environments.

## References

[1] I. N. Kessides, The future of the nuclear industry reconsidered: Risks, uncertainties, and continued promise, Energy Policy, 48(2012) 185-208.

[2] D. Kaczorowski, J.Ph. Vernot, Wear problems in nuclear industry, Tribol. Int., 39(2006) 1286-1293.

[3] I. G. McKinley, J. M. West, S. M. L. Hardie, A Risk Management Perspective on Climate Change: Lessons Learned from the Nuclear Industry, Environ. Manage., 69(2022) 835–846.

[4] TEPCO, 2013. Basic Policy for the Contaminated Water Issue at the TEPCO's Fukushima Daiichi Nuclear Power Station.

[5] C. de Boer, I. Catsburg, A Report: The Impact of Nuclear Accidents on Attitudes Toward Nuclear Energy, The Public Opinion Quarterly, 52(1988) 254-261.

[6] T. Ohba, K. Tanigawa, L. Liutsko, Evacuation after a nuclear accident: Critical reviews of past nuclear accidents and proposal for future planning, Environ. Int., 148(2021) 106379.

[7] H. Sekimoto, H. Nakamura, N. Takagi, Toxicity of radioactive wastes discharged from nuclear energy centre in the future equilibrium state, Ann. Nucl. Energy, 23(1996), 663-668.

[8] L.A. Kszos, A.J. Stewart, Review of Lithium in the Aquatic Environment: Distribution in the United States, Toxicity and Case Example of Groundwater Contamination, Ecotoxicology, 12(2003), 439–447.

[9] D. I. Kaplan, M. E. Denham, S. Zhang, C. Yeager, C. Xu, K. A. Schwehr, H. P. Li, Y. F. Ho, D. Wellman, P. H. Santschi, Radioiodine Biogeochemistry and Prevalence in Groundwater, Critical Reviews in Environmental Science and Technology, 44(2013) 2287-2335.

[10] R. Pojasek, Stablilization, solidification of hazardous wastes, Environ. Sci. Technol., 12(1978) 382-386.

[11] J. R. Conner, S. L. Hoeffner, The History of Stabilization/Solidification Technology, Environ. Sci. Technol., 28(1998) 325-396.

[12] C. C. Wiles, A review of solidification/stabilisation technology, J. Hazard. Mater., 14(1987) 5-21.

[13] J. Zhang, P. L Bishop, Stabilization/solidification (S/S) of mercury-containing wastes using reactivated carbon and Portland cement, J. Hazard. Mater., 92(2002) 199-212.

[14] S. A. A. Tajudin, M.A.M. Azmi, A.T.A. Nabila, Stabilization/Solidification Remediation Method for Contaminated Soil: A Review, IOP Conf. Ser.: Mater. Sci. Eng., 136(2016) 27-29.

[15] S.B. Eskander, S.M. Abdel Aziz, H. El-Didamony, M.I. Sayed, Immobilization of low and intermediate level of organic radioactive wastes in cement matrices, J. Hazard. Mater., 190(2011) 969-979.

[16] S. Kearney, A. S. Yorkshire, D. A. Geddes, T. Hanein, S. Nelson, J. L. Provis, B. Walkley, Chapter 25 - Cement-based stabilisation/solidification of radioactive waste, Low Carbon Stabilization and Solidification of Hazardous Wastes, 2022 407-431.

[17] M. I. Ojovan, H. J. Steinmetz, Approaches to Disposal of Nuclear Waste, Energies, 15(2022) 7804.

[18] P. Duxson, A. Fernández-Jiménez, J. L. Provis, G. C. Lukey, A. Palomo & J. S. J. van Deventer, Geopolymer technology: the current state of the art, J. Mater. Sci., 42(2007) 2917–2933.

[19] V. Cantarel, T. Motooka, I. Yamagishi, Geopolymers and their potential applications in the nuclear waste management field A bibliographical study (JAEA-Review--2017-014). Japan.

[20] R.S. Krishna, J. Mishra, M. Zribi, F. Adeniyi, S. Saha, S. Baklouti, F. U. A. Shaikh, H.S. Gökçe, A review on developments of environmentally friendly geopolymer technology, Materialia, 20(2021) 101212.

[21] J.L. Provis, Geopolymers and other alkali activated materials - Why, how, and what?, Mater. Struct. 47(2014) 11-25.

[22] J. L. Provis and S. A. Bernal, Geopolymers and related alkali-activated materials, Annu. Rev. Mater. Sci., 44(2014) 299-327.

[23] TEPCO, n.d. Contaminated Water Treatment. (2023).

[24] S. A. Bernal, J. S. J. van Deventer, J. L. Provis. (2015). What happens to 5-year-old metakaolin geopolymers? The effect of alkali cation. In: Scrivener, K., Favier, A. (eds) Calcined Clays for Sustainable Concrete. RILEM Bookseries, vol 10. Springer, Dordrecht.

[25] A. Palomo, A. Fernández-Jiménez, M. Criado, Geopolymers: same basic chemistry, different microstructures, Mater. Constr., 54(275) (2004), 77–91.

[26] X. Niu, Y. Elakneswaran, R. I. Chaerun, J. L. Provis, T. Sato, Adsorption behaviour of simulant radionuclide cations and anions in metakaolin-based geopolymer, J. Hazard. Mater., 429(2022) 128373.

[27] Q. Tian and K. Sasaki, Application of fly ash-based geopolymer for removal of caesium, strontium and arsenate from aqueous solutions: Kinetic, equilibrium and mechanism analysis. Water Sci. Technol. 79(2019) 21162125

[28] N. Soonthornwiphat, Y. Kobayashi, K. Toda, K. Kuroda, C. R. Islam, T. Otake, Y. Elakneswaran, J. L. Provis, T. Sato, Encapsulation of Sr-loaded titanate spent adsorbents in potassium aluminosilicate geopolymer, J. Nucl. Sci. Technol., 19(2020) 1181-1188.

[29] N. Vandevenne, R. I. Iacobescu, Y. Pontikes, R. Carleer, E. Thijssen, K. Gijbels, S. Schreurs, W. Schroeyers, Incorporating Cs and Sr into blast furnace slag inorganic polymers and their effect on matrices properties. J. Nucl. Mater. 503(2018) 1–12.

[30] Q. Tian, Yi. Bai, Yi. Pan, C. Chen, S. Yao, K. Sasaki, H. Zhang, Application of Geopolymer in Stabilization/Solidification of Hazardous Pollutants: A Review, Molecules, 27(2022) 4570.

[31] R. I. Chaerun, N. Soonthornwiphat, K. Toda, K. Kuroda, X. Niu, R. Kikuchi, T. Otake, Y. Elakneswaran, J. L. Provis, T. Sato, Retention Mechanism of Cesium in Chabazite Embedded into Metakaolin-Based Alkali Activated Materials, J. Hazard. Mater., 440(2022) 129732.

[32] Q. Tian, B. Guo, K. Sasaki, Immobilization mechanism of Se oxyanions in geopolymer: Effects of alkaline activators and calcined hydrotalcite additive, J. Hazard. Mater., 387(2020) 121994.

[33] J. Davidovits, Geopolymer, Chemistry and Applications, (2008).

[34] M. Fawer, M. Concannon, W. Rieber, Life cycle inventories for the production of sodium silicates, Int. J. Life Cycle Assess., 4(1999) 207-212.

[35] H.K. Tchakouté, C.H. Rüscher, Mechanical and microstructural properties of metakaolin-based geopolymer cements from sodium waterglass and phosphoric acid solution as hardeners: a comparative study, Appl. Clay Sci., 140(2017) 81-87.

[36] Y.S. Wang, J.G. Dai, Z. Ding, W.T. Xu, Phosphate-based geopolymer: formation mechanism and thermal stability. Mater. Lett., 190(2017) 209-212.

[37] Y.S. Wang, Y. Alrefaei, J.G. Dai, Silico-aluminophosphate and alkali-aluminosilicate geopolymers: a comparative review, Front. Mater., 6(2019) 106.

[38] Y. Liu, Y. Meng, X. Qiu, F. Zhou, H. Wang, S. Zhou, C. Yan, Novel porous phosphoric acid-based geopolymer foams for adsorption of Pb(II), Cd(II) and Ni(II) mixtures: Behavior and mechanism, Ceram. Int., 49(2023) 7030-7039.

[39] S. Tome, D. T. Hermann, V. O. Shikuku, S. Otieno, Synthesis, characterisation and application of acid and alkaline activated volcanic ash-based geopolymers for adsorptive remotion of cationic and anionic dyes from water, Ceram. Int., 47(2021) 20965-20973.

[40] S. Pu, Z. Zhu, W. Song, H. Wang, W. Huo, J. Zhang, A novel acidic phosphoric-based geopolymer binder for lead solidification/stabilisation, J. Hazard. Mater., 415(2021) 125659.

[41] H. Lin, H. Liu, Y. Li, X. Kong, Properties and reaction mechanism of phosphoric acid activated metakaolin geopolymer at varied curing temperatures, Cem. Concr. Res., 144(2021) 106425.

[42] M. Takeya, A. Ubaidah, M. Shimokawara, H. Okano, T. Nawa, Y. Elakneswaran, Crude oil/brine/rock interface in low salinity waterflooding: Experiments, triple-layer surface complexation model, and DLVO theory, J. Pet. Sci. Eng., 188(2020) 106913.

[43] E. E. Saka, C. Güler, The effects of electrolyte concentration, ion species and pH on the zeta potential and electrokinetic charge density of montmorillonite, Clay Minerals, 41(2006) 853-861.

[44] H. K. Tchakouté, C. H. Rüscher, E. Kamseu, F. Andreola, C. Leonelli, Influence of the molar concentration of phosphoric acid solution on the properties of metakaolin-phosphate-based geopolymer cements, Appl. Clay Sci., 147(2017) 184-194.

[45] B. Walkley, J.L. Provis, Solid-state nuclear magnetic resonance spectroscopy of cements, Mater. Today Adv., 1(2019) 100007.

[46] F. Taulelle, B. Bouchevreaua, C. Martineaua, NMR crystallography driven structure determination: nanoporous materials, Cryst. Eng. Comm., 15(2013) 8613-8622.

[47] R. M. Mironenko, O. B. Belskaya, V. P. Talsi, V. A. Likholobov, Quadrupolar magic angle spinning NMR spectra fitted using the Pearson IV function, Solid State Nucl. Magn. Reson., 63–64(2014) 37-41.

[48] X. Yi, K. Liu, W. Chen, J. Li, S. Xu, C. Li, Y. Xiao, H. Liu, X. Guo, S. Liu, A. Zhen, Origin and Structural Characteristics of Tri-coordinated Extra-framework Aluminum Species in Dealuminated Zeolites, J. Am. Chem. Soc., 140(2018) 10764–10774.

[49] D. Zhang, D. Wang, Z. Liu, F. Xie, Rheology, agglomerate structure, and particle shape of fresh geopolymer pastes with different NaOH activators content. Constr. Build. Mater., 187(2018) 674–680.

[50] M.-G Barthés-Labrousse, Acid–base characterisation of flat oxide-covered metal surfaces, Vacuum, 67(2002) 358-392.

[51] Y. Yang, J. Tang, H. Song, Y. Yang, Z. Gu, J. Fu, Y. Liu, M. Zhang, Z. Qiao, C. Yu, Dendritic Mesoporous Silica Nanoparticle Adjuvants Modified with Binuclear Aluminum Complex: Coordination Chemistry Dictates Adjuvanticity, Angew. Chem., 59(2020) 19610–19617.

[52] Y. Kameshima, A. Yasumori, K. Okada, XPS and X-ray AES (XAES) Study of Various Aluminate Compounds, Hyomen Kagaku, 21(2000) 481-487.

[53] N. Komatsu, T. Satoh, M. Honjo, T. Futatuki, K. Masumoto, C. Kimura, H. Aoki, Influence of inserting AlN between AlSiON and 4H–SiC interface for the MIS structure, Applied Surface Science, 257(2011) 8307-8310.

[54] Ph. Massiot, M.A. Centeno, I. Carrizosa, J.A. Odriozola, Thermal evolution of sol–gel-obtained phosphosilicate solids (SiPO), J. Non. Cryst. Solids, 292(2001) 158-166.

[55] J. Xiang, R. Zhu, Q. Chen, G. Lv, Y. Yang, A novel montmorillonite-based soil amendment for Cd/REEs immobilisation and nutrients sustained release, Appl. Clay Sci., 221(2022).

[56] L. Todan, E.M. Anghel, P. Osiceanu, R.V.F. Turcu, I. Atkinson, S. Simon, M. Zaharescu, Structural characterisation of some sol–gel derived phosphosilicate glasses, J. Mol. Struct., 1086(2015) 161-171.

[57] S. Wang, T. Nguyen, H. Peng, S. Wu, D. Parry, A. Urban, L. Huang, Sodium removal from bauxite desilication product (sodalite) aided by chelating effects of inorganic and organic acids, J. Environ. Manage., 338(2023) 117837.

[58] M. Todea, V. Simon, M. Muresan-Pop, A. Vulpoi, M.M. Rusu, A. Simion, M. Vasilescu, G. Damian, D.M. Petrisor, S. Simon, Silica-based microspheres with aluminum-iron oxide shell for diagnosis and cancer treatment, J. Mol. Struct., 1246(2021) 131149.

[59] Y. Elakneswaran, T. Nawa, K. Kurumisawa, Electrokinetic potential of hydrated cement in relation to adsorption of chlorides, Cem. Concr. Res., 39(2009) 340-344.

[60] K. Wu, L. Song, Y. Hu, H. Lu, B. K. Kandola, E. Kandare, Synthesis and characterisation of a functional polyhedral oligomeric silsesquioxane and its flame retardancy in epoxy resin, Prog. Org. Coat., 65(2009), 490-497.

[61] Ph. Massiot, M. A. Centeno, M. Gouriou, M. I. Domínguez, J. A. Odriozola, Sol–gel obtained silicophosphates as materials to retain caesium at high temperatures, J. Mater. Chem., 13(2003) 67-74.

[62] A. Majjane, A. Chahine, M. Et-tabirou, B. Echchahed, T. Do, P. M. Breen, X-ray photoelectron spectroscopy (XPS) and FTIR studies of vanadium barium phosphate glasses, Mater. Chem. Phys., 143(2014) 779-787.

[63] M. Kang, F. Chen, S. Wu, Y. Yang, C. Bruggeman, L. Charlet, Effect of pH on Aqueous Se(IV) Reduction by Pyrite, Environ. Sci. Technol. 45(2011) 2704–2710.

[64] O. Toshihiko, K. Naofumi, T. Kazuya, T. Kohei, U. Satoshi, I. Ryohei, K. Tatsuki, T. Ayaka, K. Daniel, S. Peter, Sorption and solidification of iodide, 21st EGU General Assembly, EGU2019, Proceedings from the conference held 7-12 April 2019 in Vienna, Austria, id.12383. 2019EGUGA.2112383O

[65] N. M. Avalos, T. Varga, S. T. Mergelsberg, J. A. Silverstein, S. A. Saslow, Behavior of iodate substituted ettringite during aqueous leaching, Applied Geochemistry, 125(2021) 104863.

[66] F. L. Theiss, G. A. Ayoko, R. L. Frost, Leaching of iodide (I−) and iodate (IO3−) anions from synthetic layered double hydroxide materials, J Colloid Interf Sci., 478(2016) 311-315.

[67] C. A. Rees, J. L. Provis, G. C. Lukey, J. S. J. v. Deventer, In Situ ATR-FTIR Study of the Early Stages of Fly Ash Geopolymer Gel Formation, Langmuir, 23(2007), 9076–9082.

[68] C. A. Rees, J. L. Provis, G. C. Lukey, J. S. J. v. Deventer, Attenuated Total Reflectance Fourier Transform Infrared Analysis of Fly Ash Geopolymer Gel Aging, Langmuir, 23(2007), 8170–8179.

[69] Q. Tian, K. Sasaki, A novel composite of layered double hydroxide/geopolymer for co-immobilisation of $Cs^{+}$ and $SeO_4^{2-}$ from aqueous solution, Sci. Total Environ., 695 (2019), 133799.

[70] W. K. W. Lee and J. S. J. v. Deventer, Use of Infrared Spectroscopy to Study Geopolymerization of Heterogeneous Amorphous Aluminosilicates, Langmuir, 19(2003) 8726–8734.

[71] M. Criado, A. F. Jiménez, A. Palomo, Alkali activation of fly ash: Effect of the $SiO_2/Na_2O$ ratio: Part I: FTIR study, Microporous Mesoporous Mat., 106(2007) 180-191.

[72] W.K.W. Lee, J.S.J. Van Deventer, Effects of anions on the formation of aluminosilicate gel in geopolymers, Ind. Eng. Chem Res., 41 (2002) 4550-4558.

# CHAPTER 6

## CONCLUSIONS AND FUTURE WORKS

## 6.1 Introduction

This thesis presents a comprehensive study on the immobilisation and adsorption of radionuclides using geopolymer materials in the process of nuclear waste disposal. The primary objectives of this research are to gain a deep understanding of the mechanisms and capabilities of geopolymer materials in immobilising and adsorbing cationic and anionic radionuclides from nuclear waste. Additionally, the study aims to develop new materials based on geopolymer substances that can enhance the broad and reliable immobilisation and adsorption capabilities of radionuclides. There are several factors that affect the immobilisation of radionuclides by geopolymers, with the surface properties of the geopolymer being the dominant factor. From a materials engineering perspective, the main factors controlling the surface properties of geopolymers include different aluminosilicate precursors, alkaline or acidic activators, and different curing conditions. Additionally, external factors such as the nature of the radionuclide and the chemical environment in which the geopolymer is in service can also cause variations in the curing and adsorption capacity.

This work includes the following main sections: (i) An overview of the literature review, synthesis methods, and basic properties of geopolymer materials (described in Chapter 2). (ii) An overview of the chemical properties and the common treatments of radionuclides (described in Chapter 2). (iii) A study of the immobilisation capacity of alkali-activated geopolymer materials, the in-depth understanding of mechanism, and a developed thermodynamically based cationic radionuclides ion-exchange model (described in Chapter 3). (iv) Screening of suitable admixtures and maintenance conditions for the introduction of

in-situ ettringite during the geopolymerisation of alkali-activated geopolymers to develop anionic radionuclides uptake ability while retaining cationic radionuclides immobilisation capacity (described in Chapter 4). and (v) A study of surface chemistry and electrostatic properties of phosphoric acid-activated metakaolin-base geopolymer to determine their immobilisation capacity for anionic radionuclides (described in Chapter 5).

## 6.2 Conclusions

### 6.2.1 Adsorption of radionuclides by alkali-activated geopolymer

In Chapter 3, the geopolymer with alkali activation of the metakaolin was determined to have a final formulation of 1:1:13 composition of $K_2O$:$SiO_2$:$H_2O$, exhibiting a remarkable ability to absorb cationic radionuclides such as $Cs^+$, $Sr^{2+}$, and $Co^{2+}$. Nevertheless, these geopolymer materials do not possess the direct capacity to uptake anions such as $I^-$, $IO_3^-$, $SeO_3^{2-}$, and $SeO_4^{2-}$. Noteworthy findings from this study reveal that the framework of the geopolymers maintains a permanent negative charge when immersed in an aqueous solution. Ion exchange emerges as the primary mechanism responsible for the uptake of radionuclide cations. Specifically, a one-to-one exchange was observed between $Cs^+$ and $K^+$, while both one-to-two and one-to-one exchanges were feasible in the cases of $Sr^{2+}$ and $Co^{2+}$. Furthermore, the incorporation of $Co^{2+}$ was facilitated by the formation of cobalt blue ($CoAl_2O_4$). To accurately predict the binding behaviour of $Cs^+$ and $Sr^{2+}$ at low concentrations, thermodynamic modeling was conducted based on an ion exchange mechanism. However, for improved predictions at high concentrations of $Sr^{2+}$ and $Co^{2+}$, the model requires

modification, such as incorporating precipitation and non-charge balanced ion exchange mechanisms.

### 6.2.2 In-situ ettringite enhanced anionic radionuclide immobilisation

In Chapter 4, a modified geopolymer containing in situ ettringite was successfully synthesized by introducing gypsum and ground blast furnace slag (Gyp 10wt% + 3S). This modification greatly enhances the geopolymer's ability to uptake Se oxyanions, as ettringite demonstrates a high affinity for Se oxyanion adsorption. The study reveals that the generated ettringite, whether in the in-situ form or through co-precipitation, effectively interacts with the geopolymer, which carries a permanent negative charge, due to its positively charged surface. This interaction compensates for the partial negative charge and maintains the geopolymer's basic structure and cation uptake capacity following ettringite synthesis. In terms of Se oxyanion immobilisation, synthetic ettringite can immobilize both $SeO_3^{2-}$ and $SeO_4^{2-}$ through co-precipitation, while only $SeO_3^{2-}$ can be uptaken through the binding process. The binding process primarily involves ion exchange with $SO_4^{2-}$ at low concentrations (< 1 mmol/L), while at higher concentrations (> 1 mmol/L), the dominant mechanism shifts to ligand exchange with Ca-OH2. In the case of in-situ ettringite, its uptake mechanism for $SeO_3^{2-}$ is partially shielded by electrostatic interaction and hydrogen bonding with the geopolymer matrix. Despite these modifications, the modified geopolymer retains its capacity to adsorb cationic radionuclides such as $Cs^+$ and $Sr^{2+}$, and it exhibits a significant uptake capacity for $SeO_3^{2-}$ through ion exchange as the controlling mechanism. Moreover, thermodynamic modeling based on an ion exchange mechanism proves to be accurate in

predicting the uptake behaviour of both synthetic ettringite and modified geopolymers for $SeO_3^{2-}$ at low concentrations (< 1 mmol/L).

### 6.2.3 Surface chemical properties and anions immobilisation of PGPs

In Chapter 5, the surface chemistry and structure-related electrostatic properties of phosphoric acid activated metakaolin-based geopolymers (PGPs) were investigated for their potential in stabilization/solidification (S/S) applications. The evaluation included zeta potential measurements, microstructure characterization, immersion behaviour analysis, and leaching experiments. The zeta potential of PGPs surfaces exhibited an initial increase followed by a decrease as pH levels rose, with the maximum value observed at neutral pH. Within a specific pH range, the surfaces of PGPs carried a positive charge and demonstrated electrostatic adsorption capabilities for anions such as $SeO_3^{2-}$, $SeO_4^{2-}$, $I^-$, and $IO_3^-$. The geopolymerization reaction of PGPs resulted in the development of $Al_{VI}$-OP and $Al_{IV}$-OP structural units, with the ratio of these units influencing the surface electrostatic properties. Increasing concentrations of acid activators led to a higher ratio of these units, resulting in a higher zeta potential in neutral aqueous environments. A phosphoric acid activator concentration of around 10.3 mM was found to be optimal, facilitating the geopolymerization process without causing excessive dealumination. In acidic aqueous environments, the $AlPO_4$ units in the PGPs surface structure preferentially fractured, contributing to the dealumination process. This effect became more pronounced as the pH decreased, leading to a reduced ratio of $Al_{VI}$-OP and $Al_{IV}$-OP and a decrease in the positive electrical properties of the PGPs surface. Conversely, in alkaline aqueous environments, a large number of Si-OH structural

units and VI-coordination Al lost protons, generating negative charges and increasing the negative charge of the PGPs surface. The immobilisation of $SeO_3^{2-}$, $SeO_4^{2-}$, $I^-$, and $IO_3^-$ anions within the PGPs matrix was highly effective, with no significant changes in the matrix structure observed even after 28 days of leaching experiments. This effective immobilisation was primarily attributed to the electrostatic attraction between the anions and the positively charged structural unit, $Al_{VI}$-OP, located at the PGPs matrix interface. Importantly, this association resulted in a significant enhancement in anion retention compared to previous studies using different types of matrices.

## 6.3 Suggestions for future works

### 6.3.1 Further development of geopolymer in radionuclides immobilisation

Previous studies have shown that geopolymer, as a substitute for Portland cement, exhibits adsorption and immobilisation capabilities for cationic radionuclides ($Cs^+$, $Sr^{2+}$, and $Co^{2+}$), as well as for the modified cationic radionuclides ($SeO_3^{2-}$). Based on this, further exploration of geopolymer materials for the disposal of nuclear waste is carried out. There are two specific directions:

1) Research on the adsorption and immobilisation of radioactive nuclides in geopolymer with varying porosity (specific surface area) based on computer-aided material design, 3D printing technology, and other techniques (foaming agents or organic solution porous membrane plates). Compared to densely packed block materials and finely powdered materials after solidification, porous geopolymer materials have a

continuous structure, higher mechanical strength, and sufficient specific surface area, making them suitable for the adsorption and immobilisation of radioactive nuclides in various waste disposal scenarios. However, there are apparent technical challenges to be addressed: how to adjust the material composition to make it suitable for 3D printing or achieve good contact and effects with foaming agents. Additionally, a suitable set of equipment needs to be designed for material printing and design. Ultimately, the obtained porous materials should have higher adsorption capacity and stability compared to traditional high-density block products.

2) Application of geopolymer materials in the solidification of organic waste. During the operation of nuclear power, decommissioning of nuclear facilities, and application of nuclear technology, a large amount of organic radioactive waste, especially organic liquid waste, inevitably accumulates. The hydration process of traditional cementitious materials is affected by this organic waste, leading to a decrease in strength and solidification capability. In contrast, geopolymer materials can effectively immobilize this organic waste during the hydration process without compromising the structure. Therefore, geopolymer materials are highly promising for the solidification of organic waste. However, the development of solidification for organic liquid waste has been slow, especially in the absence of previous research on the application of water-hardened gel materials as guidance. The solidification capacity, stability, and safety of the process need to be systematically studied and analyzed. Gel materials corresponding to different functional groups of organic liquid waste should be further developed. Direct geological disposal of solidified organic

liquid waste can conserve energy, minimize secondary pollution, and possess significant application value.

### 6.3.2 Application of other inorganic materials in radionuclides treatment

Geological disposal of nuclear waste generally involves isolating radioactive waste in deep underground repositories, where the waste is encapsulated in buffer materials. After several decades or even hundreds of years, the surface-contacting buffer materials will evolve into stable mineral materials under the influence of thermodynamics and kinetics. The commonly used Portland cement typically transforms into a C-A-S-H structure, while geopolymer materials transform into more stable zeolites. Therefore, exploring and researching different inorganic materials as buffer materials, as well as their stability and durability, are of significant importance for the sustainable development of nuclear fuel backend disposal.

Subsequent research can include the synthesis, manufacturing, and mechanism investigation of different types of zeolites, various types of cement (including their mineral components: C-S-H, AFt, AFm, etc.), and other high-performance mineral adsorbents such as layered double hydroxides (LDH), which are naturally occurring or artificially synthesized minerals. In addition, for a wide range of nuclides, including difficult-to-adsorb anionic nuclides such as $SeO_3^{2-}$, $SeO_4^{2-}$, $I^-$, and $IO_3^-$, which cannot be effectively adsorbed by alkali-activated geopolymers, there is a need to conduct research on the synthesis of high-performance ceramic adsorbents based on aluminosilicate material design.

### 6.3.3 Machine learning based adsorption model informatisation

Adsorption energy is a key parameter for evaluating the adsorption performance during the adsorption process and can be estimated or calculated using various methods. Currently, density functional theory (DFT) is widely accepted in computational chemistry for calculating the energy difference between the pre- and post-adsorption states. However, for complex molecular structures, precise theoretical calculations require significant computational resources. In recent years, machine learning (ML) has emerged as a powerful tool to establish targeted adsorption models that address the challenges in describing and predicting adsorption reaction performance. By combining existing databases and necessary experimental results in subsequent research, effective predictive models for material design and adsorption energy can be established using a variety of machine learning algorithms. This research is of significant importance in reducing the need for extensive experimentation, conserving resources, and facilitating the long-term disposal of nuclear waste.

# Supporting Information

## 1. Thermodynamic ion exchange model and its fitting method

### Python-written best $Log_k$ fitting code template

The following Python-IPhreeqcCOM template code simplifies the search for the best fitting $Log_k$ values between the results obtained from Phreeqc and experimental data. The search is automated using the least squares method, which gradually narrows down the range of values based on the parameters provided.

Initially, the experimental data is imported into the process, and the $Log_k$ value is determined based on the provided boundary conditions. Next, the phreeqc module is utilised to calculate the leaching of $SO_4^{2-}$. A range of Se initial concentration-$SO_4^{2-}$ leaching curves corresponding to different $Log_k$ values is obtained, and the closeness of these curves to the experimental data is evaluated using the Root Mean Squared Error (RMSE). The least squares method is then applied to determine the best-fitting $Log_k$ value within the given range, which corresponds to the smallest RMSE.

### The code:

```
from win32com.client import Dispatch

import pandas as pd

import numpy as np
```

```
from scipy.stats import pearsonr
import matplotlib.pyplot as plt

# Creating PHREEQC objects
def GetResult(input_string, db_path = 'WATEQ4F.DAT'):
  dbase = Dispatch('IPhreeqcCOM.Object')
  dbase.LoadDatabase(db_path)
  dbase.RunString(input_string)
  output = dbase.GetSelectedOutputArray()
  return output

# Calculate the RMSE between two arrays
def calculate_rmse(a, b):
  return np.sqrt(np.mean((a - b)**2))

# Create a function that compares two sets of data
def calculate_correlation(a, b):
    corr, _ = pearsonr(a, b)
    return corr

# Calculate RMSE from log_k
def get_fit(K_fitting, Con, SO4_leaching_ex, SeO3_binding_ex):
                            # Make sure experimental data has been imported
  SeO3_binding_f=[]
  SO4_leaching_f=[]
  for Se_con in Con:
    input_str = f'''
      Phase
                            Ettringite   # In order to simulate the pH change and
                              #SO42- environment in the experiment
        Ca6Al2(SO4)3(OH)12:26H2O + 12H+ = 2Al+++ + 6Ca++ + 38H2O + 3SO4--
        log_k 57.730
```

```
   delta_h -389.36
SOLUTION 1
  units  mmol/kgw
  Temp 20
  ph  7 charge
  water   1
  Se(4) {Se_con}
EQUILIBRIUM_PHASES 1
  Ettringite 0 0.000797 #Indicates the amount of
  Save solution 1   #ettringite in the system at 1
  End                    #mol/L
EXCHANGE_MASTER_SPECIES
  Xg Xg+2

EXCHANGE_SPECIES
  Xg+2 = Xg+2
  log_k = 0

  Xg+2 + SO4-2 = XgSO4
  log_k = 0

  XgSO4 + SeO3-2 = XgSeO3 + SO4-2
  -gamma 3.5 0.015
  log_k = {K_fitting}

USE SOLUTION 1
EXCHANGE 1
  XgSO4 4e-5     #ettringite contains 0.004 mol/kg of
CALCULATE_VALUES   #exchangeable SO42-
SeO3(binding)
-start
10 m_Se = MOL("XgSeO3") *1000
```

```
    100 SAVE m_Se
    -end
    SO4(leaching)
    -start
    10 m_S = (4e-5-MOL("XgSO4")) *1000
    100 SAVE m_S
    -end

    SELECTED_OUTPUT
     -reset false
    -calculate_values SeO3(binding)
    -calculate_values SO4(leaching)

  '''
  output = GetResult(input_str)
  XgSeO3, SO4 = output[1]
  SeO3_binding_f.append(XgSeO3)
  SO4_leaching_f.append(SO4)

 fit = calculate_rmse(SO4_leaching_ex, SO4_leaching_f)
 return fit

#setting parameters  #Arbitrary starting conditions and boundaries can be set
min_fit = 1
K_fitting=0
best_fit=0
left = 0
right = 20
epsilon = 0.0001

# Loop calculation of fit
while right - left > epsilon:
```

```
    mid = (left + right) / 2
    fit = get_fit(mid)
    if fit < min_fit:
        min_fit = fit
        K_fitting = mid
    if fit < get_fit(mid+epsilon):
        right = mid
    else:
        left = mid

best_K_fitting = K_fitting
best_fit = get_fit(best_K_fitting)

plt.plot(x, y)
```

## 2. $SeO_3^{2-}$ redox state

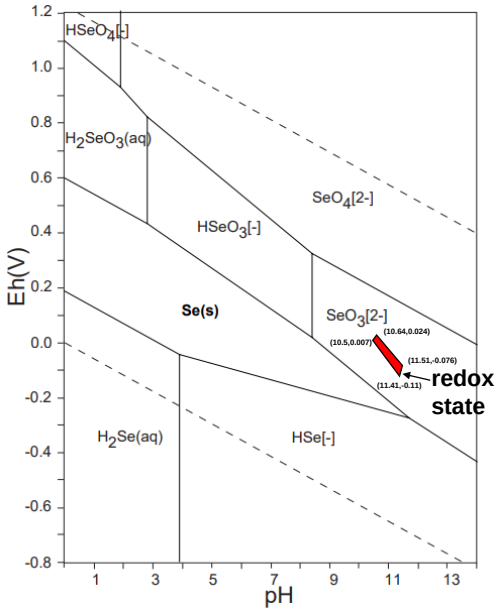


**Fig. S4-1.** Eh-pH diagram at 298.15 K, $10^5$ Pa [71]. The redox state of $SeO_3^{2-}$ in this study is marked in the red area.